UK Dementia Research Institute

CARDIFF UNIVERSITY
PRIFYSGOL CAERDYDD

Unravelling the molecular basis of the association of genetic variation in the *clusterin* gene with risk of Alzheimer's disease

Thesis submitted for the Degree of
Doctor of Philosophy (Medicine)

October 2023

Ioana Aurora Veteleanu

Abstract

Background: Genome-wide association studies (GWAS) identified *clusterin* (*CLU*) as the third most significant genetic risk factor for Alzheimer's disease (AD), while biomarker studies found clusterin to be significantly elevated in AD. The work in this thesis aimed to address the incompletely understood association between intronic SNPs in *CLU* and risk for AD through relating genotypes at *CLU* single nucleotide polymorphisms (SNPs) to plasma clusterin levels and measuring secreted and intracellular clusterin in induced pluripotent stem cell (iPSC)-derived astrocytes.

Methods: To quantify clusterin levels in human biofluids, a panel of monoclonal antibodies was generated through hybridoma technology. A sandwich ELISA was developed and characterised, and clusterin was measured in plasma and CSF from subjects with AD and healthy individuals. To study the effects of SNPs in *CLU* on clusterin synthesis, five iPSC lines carrying different genotypes at genome-wide significant (GWS) SNPs were differentiated into astrocytes, and intracellular and secreted clusterin was measured at mRNA and protein levels.

Results: Monoclonal antibodies specifically bound human clusterin in serum and a sensitive ELISA was set up (Chapter 2). Clusterin was significantly elevated in plasma from subjects with AD or Down Syndrome compared to healthy controls, and no significant change was observed in CSF (Chapter 3). Using an endophenotype-GWAS approach, no SNPs were found to be significantly associated with changes in plasma clusterin protein levels (Chapter 4). In iPSC-derived astrocytes, intracellular clusterin was significantly elevated at the gene and protein level in rs11136000 C/C carriers (Chapter 5).

Conclusions: Increased clusterin levels in AD compared to control were not influenced by *CLU* GWS SNPs, and may reflect other aspects of AD pathology observed in the periphery. However, these SNPs might have functional effects particularly in the brain, as intracellular clusterin isoforms from astrocytes were found to be significantly elevated in carriers of risk alleles. This work provides insight into the mechanistic role of SNPs in *CLU* in modulating AD risk by altering clusterin secretion.

Abbreviations

Aβ	Amyloid beta
AD	Alzheimer's disease
ANOVA	Analysis of variance
APC	Astrocyte precursor cell
APOE	Apolipoprotein E
APP	Amyloid precursor protein
BBB	Blood brain barrier
BIN1	Bridging integrator 1
BSA	Bovine serum albumin
CLU	Clusterin
CNTF	Ciliary neurotrophic factor
CNS	Central nervous system
CR1	Complement receptor 1
CSF	Cerebrospinal fluid
EGF	Epidermal growth factor
DMEM	Dulbecco's Modified Eagle Medium
DS	Down Syndrome
EDTA	Ethylenediaminetetraacetic acid
ELISA	Enzyme-linked immunosorbent assay
EOAD	Early-onset Alzheimer's disease
eQTL	Expression quantitative trait locus
ER	Endoplasmic reticulum
FACS	Fluorescence activated cell sorting

FBS	Foetal bovine serum
FGF	Fibroblast growth factor
GFAP	Glial fibrillary acidic protein
GWAS	Genome-wide association study
GWS	Genome-wide significant
HRP	Horseradish peroxidase
ICC	Immunocytochemistry
IHC	Immunohistochemistry
iPSC	Induced pluripotent stem cell
LD	Linkage disequilibrium
LIF	Leukaemia inhibitory factor
LOAD	Late-onset Alzheimer's disease
LPS	Lipopolysaccharide
LRP2	Low-density lipoprotein-related protein 2 receptor
mAb	Monoclonal antibody
MAC	Membrane attack complex
MAF	Minor allele frequency
MCI	Mild cognitive impairment
mitoCLU	Mitochondrial clusterin
MMSE	Mini mental state examination
mRNA	Messenger RNA
nCLU	Intracellular clusterin
NFκB	Nuclear factor kappa-light-chain-enhancer of activated B cells
NfL	Neurofilament light
NHS	Normal human serum

NPC	Neural progenitor cell
OR	Odds ratio
PBMC	Peripheral blood mononuclear cell
PBS	Phosphate buffered saline
PET	Positron emission tomography
PFA	Paraformaldehyde
PLXNA4	Plexin A4
PRS	Polygenic risk score
PS1, PS2	Presenilin 1, 2
PTK2B	Protein tyrosine kinase 2 beta
ROC	Receiver operator characteristic curve
RT	Room temperature
RT-qPCR	Reverse transcription quantitative polymerase chain reaction
sCLU	Secreted clusterin
SDS-PAGE	Sodium dodecyl sulphate polyacrylamide gel electrophoresis
SNP	Single nucleotide polymorphism
TREM2	Triggering receptor expressed on myeloid cells 2

Table of contents

Acknowledgements

I was very fortunate to complete my PhD at the Dementia Research Institute in Cardiff, surrounded by many great scientists who contributed to the success of this project. First, I would like to express my gratitude to Prof. Paul Morgan, who gave me the opportunity to join his group for my PhD, always offered advice and solutions whenever I had questions, and allowed me to contribute my own ideas throughout the project. I would like to thank Dr Rebecca Sims, who was always keen to share her expertise in genetics with me and took the time to guide me through the complex genetic aspects of Alzheimer's disease. I would also like to thank Dr Wioleta Zelek, who was not only a very supportive teacher in the lab, but is also a wonderful friend. I was incredibly lucky to have you as a supervisor when I started my PhD during a pandemic, and I will always appreciate everything you did to help me.

Special thanks to Drs Rob Byrne, Sarah Carpanini, and Nikoleta Daskoulidou for their invaluable advice and useful tips for my work with stem cells. You are all excellent teachers and I really enjoyed working with you. I would also like to thank Jincy Winston for always sharing your knowledge and troubleshooting with me, and generally making work in the stem cell lab amazing for everyone. A big thank you to Sam Keat, not only for his support throughout this PhD, but also for always being keen to help with any bioinformatics questions.

I would like to also thank my mum, who has always been extremely supportive and encouraging, especially during lockdowns.

Last but not least, I would like to acknowledge the financial support from Alzheimer's Research UK, who funded this project and made all the work possible. I have certainly learnt a lot as a scientist by completing this project.

CHAPTER 1: Introduction

1.1 Alzheimer's disease

Alzheimer's disease (AD), a progressive neurodegenerative disease, is the most common cause of dementia, with a prevalence of 13% in people over the age of 65. First described in 1906 by Alois Alzheimer as "a peculiar severe disease process of the cerebral cortex" following examination of a 50-year-old woman exhibiting paranoia, aggression, confusion, sleep and memory disturbances, AD is now recognised as a severely debilitating disorder with enormous burden on carers and the national health service. As a clinical syndrome characterised by decline in memory, attention, executive and visuospatial functions and changes in personality, dementia leads to severe impairment in performing daily life activities within 5 years of diagnosis. AD should not be confused with mild cognitive impairment (MCI), characterised by mild forgetfulness and slowing of cognitive function that do not significantly affect a person's daily life, and is frequently seen in the elderly. MCI often precedes AD, when patients begin to experience early signs of AD and a decline in their mini mental state examination (MMSE) score. The prevalence of AD is estimated to rise worldwide due to an increasing aging population and might exceed 130 million cases by 2050 (Nichols et al, 2022). Following decades of research into therapies targeting amyloid beta (Aβ), two antibodies against Aβ (aducanumab and lecanemab) that showed modest effects on slowing disease progression have recently been approved for clinical use (Sevigny et al, 2016; van Dyck et al, 2023). Although this is an important advancement toward improving AD patients' lives, safer and more effective treatments are still needed.

In post-mortem tissue, AD pathology consists mainly of the deposition of Aβ plaques extracellularly and accumulation of the hyperphosphorylated form of the protein tau intracellularly (Hardy & Selkoe, 2002). The amyloid precursor protein (APP) pathway mediates the proteolytic processing of Aβ in the brain: sequential cleavage of APP occurs via two crucial enzymes, β-secretase and γ-secretase, leading to $A\beta_{40}$ and $A\beta_{42}$ release into the extracellular space (Steiner & Haass, 2000). Numerous studies have shown that $A\beta_{42}$ accumulates and aggregates more rapidly than shorter Aβ peptides due to its hydrophobic nature, accelerating AD pathogenesis; these findings underpin "the amyloid beta hypothesis of AD" (Fryer & Holtzman, 2005). The earliest event

proposed to occur in the pathogenesis of AD is the deposition of $A\beta_{42}$ aggregates as senile plaques, which can occur more than a decade before the onset of cognitive impairment (Jack et al, 2013). Initially, no disturbances of synaptic networks occur, but as Aβ levels rise, more plaques are deposited and increase in size as they attract further amyloid deposition. This causes damage to neuronal terminals, exacerbating glutamate release, which reaches toxic concentrations and promotes synaptic loss in the hippocampus (Cummings et al, 2015). At this stage, symptoms tend to be rather non-specific, including memory impairment and confusion, making it difficult to establish a clear diagnosis. Currently, AD is diagnosed using positron emission tomography (PET) imaging of amyloid plaque deposition in the brain and/or measures of $A\beta_{42}/A\beta_{40}$ ratios in cerebrospinal fluid (CSF); however, no clinical test has complete accuracy since amyloid plaques are commonly found in brains of aged individuals who did not show signs of dementia antemortem (Zolochevska et al, 2018). This highlights the urgent need for biomarkers in correctly diagnosing subjects affected by AD before the onset of symptoms to enable the implementation of better clinical trial inclusion criteria, as well as monitoring disease progression.

1.2 Genetic component of Alzheimer's disease

Alzheimer's disease appears to be a multifactorial disease with pathological and etiological complexity. Most cases (>90%) occur sporadically late in life, and are referred to as late onset AD (LOAD); however, a few causative genes have been linked to the relatively small proportion of patients with familial AD (fAD): *APP*, presenilin 1 and 2 (*PSEN1, PSEN2*). Approximately 1-2% of AD patients have rare mutations in these genes; they develop AD at an early age and show a faster rate of progression, together with less common neurological symptoms not normally associated with sporadic AD (Bateman et al, 2012). An association between AD and Down Syndrome (DS), a condition caused by the presence of an extra chromosome 21 encoding the *APP* gene, was first identified in 1948: the extra gene results in elevated levels of Aβ in the brains of subjects with DS (Jervis, 1948). DS occurs in 1 per 1000 live births and is characterised by intellectual disability, followed by a transition to dementia by the age of 50. As an entirely genetic and relatively common form of dementia, DS has been studied in the search for *APP* roles in AD.

In LOAD, many genetic risk factors have been identified that together account for 68 – 79% heritability, rising to over 90% for early onset AD (EOAD), a type of spontaneous AD that manifests before the age of 65 (Sims et al, 2020). Among these, apolipoprotein E (*APOE*) is the strongest genetic risk factor, confirmed by numerous clinical, pathological, and genome-wide association studies (GWAS). In humans, *APOE* can be found as three polymorphic alleles at a single locus on chromosome 19, due to two mutations (rs7412 Cys/Arg^{112}; rs429358 Cys/Arg^{158}) leading to the production of three major isoforms with different lipid-binding abilities: ApoE2 (Cys^{112}, Cys^{158}), ApoE3 (Cys^{112}, Arg^{158}), ApoE4 (Arg^{112}, Arg^{158}) (Mahley & Rall, 2000). The ε3 allele is carried by approximately 70% of the population, while the ε4 allele is three times more common in AD patients. Carrying a single ε4 copy increases one's risk for AD by 3.7-fold, and having two copies increases the risk by 12-fold; hence, ε4 is present in 65-80% of AD patients (Farrer et al, 1997). Inheritance of the ε2 allele is protective and has been found to suppress disease-associated changes in astrocytes, microglia, oligodendrocytes, and endothelial cells, due to a reduction in co-expression of proteins associated with inflammatory responses, synaptic transmission, and translational modifications (Dai et al, 2018).

1.3 Clusterin – genetics in AD

Besides *APOE*, 75 other significant genomic risk loci to AD have emerged to date, including single nucleotide polymorphisms (SNPs) in genes encoding proteins implicated in immune function, such as *bridging integrator 1* (*BIN1*), *triggering receptor expressed on myeloid cells 2* (*TREM2*), and *complement receptor 1* (*CR1*) (Bellenguez et al, 2022). In 2009, two large GWAS identified *CLU* (encoding clusterin, also called apolipoprotein J) as a genetic locus implicated in AD, now considered the third strongest genetic risk factor for AD (Lambert et al, 2009; Harold et al, 2009). A further two-stage GWAS conducted by Lambert and colleagues in 2013 on 74,046 AD and control subjects of European ancestry confirmed that SNPs in *CLU* reached genome wide significance in their association with AD. More recently, a very large meta-analysis of case-control studies was performed by Jansen et al (2019) on 71,880 AD and AD/dementia by proxy cases and 383,378 controls, identifying loci in *CLU* significantly associated with AD risk. Kunkle et al (2019) performed a three stage meta-analysis on the consortium used by Lambert et al in 2013, with additional non-

Hispanic white subjects, totalling 35,274 clinical and autopsy documented AD cases and 59,163 controls. This study confirmed the association between genetic variation in *CLU* and AD risk, with multiple signals near the *CLU* locus significantly associated with altering LOAD risk. The largest GWAS to date combined data from multiple European datasets (111,326 cases and 677,663 controls) and identified 75 loci associated with AD risk, 42 of them new (Bellenguez et al, 2022). With regards to *CLU*, this was once again confirmed as a significant locus, with rs11787077 (a SNP in high linkage disequilibrium with previously identified SNPs in *CLU*) shown to be a significant expression quantitative trait locus (eQTL) for clusterin expression in the brain, where the minor protective T allele is associated with increased clusterin levels in the brain. A summary of AD-associated SNPs in *CLU* identified since 2009 is listed in Table 1.1. By analysing chromatin interaction data from spleen and liver, Jansen et al (2019) reported a physical interaction between *CLU* and protein tyrosine kinase 2 beta (*PTK2B*), itself a GWAS hit, which are both highly expressed in brain tissue. This may indicate a joint effect of these two genes on AD pathogenesis, as PTK2B was shown to be a modulator of tau toxicity in Drosophila eyes (Dourlen et al, 2017). Additionally, rs73223431 in *PTK2B* is a significant AD GWAS hit (Schwartzentruber et al, 2021; Bellenguez et al, 2022).

Table 1.1. Summary of LOAD-associated SNPs in *CLU* identified through GWAS. MAF=minor allele frequency; OR=odds ratio. MAF, OR and p values are reported for the cohort used for this study.

Study identifying the SNP	Lead variant	Major allele	Minor allele	MAF AD	MAF control	OR	P value
Harold et al (2009); Lambert et al (2009); Hollingworth et al (2011)	rs11136000	C	T	0.3659	0.4087	0.835	0.02359
Lambert et al (2009)	rs9331888	C	G	0.2909	0.2808	1.051	0.568
Lambert et al (2009); Jun et al (2015); Zhu et al (2019)	rs2279590	C	T	0.3837	0.4224	0.8515	0.04237
Naj et al (2011); Wightman et al (2020)	rs1532278	C	T	0.361	0.4075	0.8213	0.01354
Lambert et al (2013); Kunkle et al (2019); deRojas et al (2021)	rs9331896	T	C	0.3716	0.4155	0.8317	0.02043
Marioni et al (2018); Jansen et al (2019)	rs4236673	G	A	0.367	0.4087	0.8391	0.02762
Schwartzentruber et al (2021)	rs867230	A	C	0.3754	0.4155	0.8453	0.03438
Bellenguez et al (2022)	rs11787077	C	T	0.367	0.4087	0.8391	0.02762

CLU is a single copy gene comprising 9 exons located at the p21-12 locus on chromosome 8, spanning approximately 18,115 base pairs. Although the majority of mutations in AD patients are found in intronic regions, some rare mutations have also been identified in exons 5-8 of the clusterin β-chain and were found to influence the secretory trafficking of clusterin in vitro (Bettens et al, 2015). Among 36 SNPs identified by Lambert et al (2009), all in non-coding regions of the *CLU* gene, 3 were significantly associated with altered AD risk (rs11136000, rs9331888, rs2279590) and were shown to be in a linkage disequilibrium (LD) block. These findings were replicated by Harold et al (2009) and other smaller studies in Caucasian cohorts (Seshadri et al, 2010; Jun et al, 2010), establishing rs11136000 as the major risk SNP implicated in LOAD. Located in intron 3 of *CLU*, rs11136000 has a major C allele carried by 88% of Caucasians that confers an increased risk of 1.16-fold for AD compared to the minor T allele, associated with decreased risk for AD and better cognitive performance. In the pre-AD stage, C allele carriers displayed faster cognitive decline and poorer memory scores associated with the transition from MCI to AD in comparison with T allele carriers (Mengel-From et al, 2011; Lin et al, 2012). With regards to clusterin protein expression, several studies showed no effect of rs11136000 genotype on plasma clusterin concentrations (Mullan et al, 2013; Haight et al, 2018), while others found an increase in clusterin associated with the protective allele in control subjects only (Schürmann et al, 2011). An increase in *CLU* mRNA was found in the blood of AD patients, but this was not affected by rs11136000 genotype (Thambisetty et al, 2010). The minor T allele at rs11136000 was associated with increased expression of clusterin in brain tissue (frontal, occipital, and temporal cortex tissue, hippocampus and interlobar white matter), and decreased levels of Aβ measured by PET (Tan et al, 2021). Ling et al (2012) also found an increase in brain *CLU* mRNA levels in AD compared to controls, and an association between the T allele at rs11136000 and increased levels of *CLU* mRNA transcript of intracellular but not secreted clusterin, suggesting that this SNP in *CLU* might modulate intracellular clusterin (nCLU) only. Moreover, Zhou et al (2014) found that the C allele of rs11136000 was associated with higher CSF tau levels in AD patients carrying the *APOE*ε4 allele, suggesting that clusterin may interact with other AD related proteins in addition to Aβ. More recently, a SNP in high LD with rs11136000 (r^2=0.99), rs11787077, was identified as the most significant signal in a large GWAS (Bellenguez et al, 2022). Data from brain single nuclei epigenetic annotations showed that the *CLU*

SNP rs11787077 overlapped with an astrocyte specific enhancer and super-enhancer, suggesting that effects of some SNPs in *CLU* might be cell type specific (Nott et al, 2019).

Another *CLU* SNP associated with AD risk, rs9331888, was initially mapped to exon 1 of the *CLU* gene, and its G risk allele has been shown to reduce the levels of clusterin mRNA (in peripheral blood mononuclear cells) and protein (in plasma) in AD and to a greater extent in controls (Xing et al, 2012). However, more recent annotations placed rs9331888 within an intron of the NM_001831.3 transcript and not in exon 1, raising questions about this SNP's role in regulating alternative splicing of *CLU*. The SNP rs2279590 is located in intron 7 within a regulatory region that may regulate *CLU* expression (Padhy et al, 2017). Deletion of a genomic region flanking rs2279590 in HEK293 cells led to a decrease in *CLU* expression, suggesting that this SNP lies within an enhancer element (Padhy et al, 2017). Although the functional consequences of the above described alleles are still unclear, it is evident that *CLU* is a key genetic risk factor for LOAD, and that further investigation could provide meaningful insights into unravelling the molecular basis of neurodegeneration.

Unlike *APOE*, where missense mutations directly affect ApoE protein structure and function, AD-associated variants in *CLU* are intronic SNPs unlikely to influence protein structure. Nevertheless, SNPs within *CLU* and other AD related genes interact with each other throughout life, making it difficult to establish a particular SNP as protective or risk without considering other SNPs. Common AD-associated variants, including those in *CLU*, often confer a small risk compared to rare variants linked to higher disease risk, and cannot fully explain the entire genetic component of AD. The effect can, however, be estimated by generating a polygenic risk score (PRS) – the sum of risk alleles an individual carries, weighted by their effect sizes to determine an individual's risk of AD. Bellenguez et al (2022) explored the effects of 83 variants at 75 loci identified in their GWAS on progression to AD from normal cognition or MCI by constructing a PRS and testing its predictive power when data were adjusted for age, sex, and *APOE* genotype. They found that a person's odds for getting AD were increased by 5% for each risk variant carried, while inheriting 18-20 risk variants increased their risk as much as one *APOE* ε4 allele. While large genetic studies are extremely powerful in identifying and characterising new genetic variants predisposing

to AD, a deeper and more thorough understanding of the mechanisms behind the impact of intronic SNPs on risk is still needed.

1.4 Clusterin – protein biochemistry and function

The *CLU* gene is transcribed into at least 2 distinct mRNA isoforms. The majority of mature, secreted clusterin is derived from the mRNA transcript NM_001831.3 (Prochnow et al, 2013). This mRNA isoform is translated into a 449 amino acid pre-protein that contains an endoplasmic reticulum (ER) signalling peptide within exon 2, and two nuclear localization signals in exons 3 and 8-9. Following translation, the pre-protein undergoes posttranslational modifications in the ER, where the 22 amino acid leader sequence is cleaved to yield an immature 50 kDa pro-protein. Next, the pro-protein is modified in the ER by phosphorylation and N-linked glycosylation at 6 asparagine residues, converting it to a 60 kDa precursor that is translocated to the Golgi apparatus. Here, carbohydrate moieties are attached to the clusterin precursor protein, resulting in the 80 kDa antiparallel heterodimer known as secreted clusterin (sCLU), cleaved into the individual clusterin subunits: the α and β chains (each 40 kDa) linked by five disulphide bonds (Figure 1.1) (Rohne et al, 2015). Clusterin is prone to self-aggregation and forms high molecular weight dimers and tetramers depending on the pH of the environment (Poon et al, 2002), making it difficult to crystallise for structural analysis. Stewart et al (2007) found that almost 60% of the secondary structure of clusterin is composed of α-helices, while its tertiary structure appears disorganised, allowing the exposure of molten globule domains which can form many hydrophobic interactions with intracellular and extracellular components (Bailey et al, 2001).

The second *CLU* mRNA lacks exon 2 and begins translation at exon 3, thereby avoiding the initial ER processing but retaining the nuclear localization sequences. This encodes an unglycosylated, single chain clusterin protein isoform of approximately 45-50 kDa, known as nuclear or intracellular clusterin (nCLU) (Leskov et al, 2003). Although these early studies suggested that nCLU was the product of a distinct mRNA transcript, it is now speculated that secreted clusterin and intracellular clusterin arise from the same transcript, and that stress-induced non-canonical translation leads to incomplete glycosylation or cleavage, allowing immature clusterin to escape the secretory pathway. More recently, Herring et al (2019) found a non-

glycosylated 45 kDa clusterin isoform localised in the mitochondria (mitoCLU) of rodent cortical tissue, where translation started at exon 2. This finding was replicated in transfected human cells, with predominant expression of mitoCLU in the mitochondria of primary neurons and astrocytes. Since mitoCLU does not express a mitochondrial targeting sequence, the mechanism of clusterin translocation to the mitochondria and its role in mitochondrial function remains to be explored.

Figure 1.1. Clusterin synthesis. Clusterin is transcribed from exon 2 within the *CLU* gene for the secretory pathway, or exon 3 for the intracellular pathway which escapes ER processing and remains in the nucleus. Through ER modifications, the pre-protein is cleaved into a 50 kDa immature protein, then phosphorylated and N-linked glycated, followed by the α and β subunits being joined by 5 disulphide bonds in the Golgi apparatus. The mature protein is then secreted to fulfil many roles throughout the body. Figure created in BioRender.

Clusterin was initially discovered in 1983 in ram rete testis fluid as a high molecular weight protein capable of “clustering” Sertoli cells; more recently, clusterin expression has been found in almost all tissues and fluids, including liver, lung, spleen, heart, reproductive tissues, and brain (Blaschuk et al, 1983). Over the years, clusterin has

been rediscovered as an abundant protein in human serum composed of two 40 kDa chains called SP-40,40 (Murphy et al, 1988), as a plasma inhibitor of complement cytolysis (CLI, Jenne and Schopp, 1989), and as a high density lipoprotein in human plasma termed apolipoprotein J (de Silva et al, 1990); gene sequencing revealed that these were all the same protein (Wong et al, 1993). Clusterin is now described as a multifunctional glycoprotein implicated in many intracellular and extracellular pathways (cholesterol transport, inhibition of the complement system, extracellular chaperone, regulation of cell survival and death) and able to interact with a wide range of receptors and ligands. Cancer research has provided many insights into the functions of clusterin in disease, focusing particularly on cell death and apoptosis pathways. Clusterin is overexpressed in breast, ovarian, and prostate cancers, promoting tumorigenesis and rendering cells resistant to chemotherapy (Peng et al, 2019). Specifically, sCLU was found to be the protein isoform responsible for increased chemoresistance and tumour aggressiveness via interactions with the pro-apoptotic protein BAX which stimulates pore formation in the mitochondrial membrane, causing release of proapoptotic proteins (Jun et al, 2011) (Figure 1.1). In prostate cancer, clusterin participates in the ubiquitination of inhibitor kappa B (IkB), promoting the translocation of NF-kB to the nucleus and upregulation of NF-kB genes; in ovarian cancer, clusterin promotes angiogenesis and chemoresistance (Fu et al, 2013). Knockdown of *CLU* in cancer cell lines led to increased tumour cell response to chemotherapy and death (Redondo et al, 2007). In the heart, clusterin plays a protective role following cardiac damage, with increased clusterin plasma levels frequently observed in heart transplant patients who recover well (Hollander et al, 2014). Clusterin is expressed in damaged arteries in the early stage of atherosclerosis, where it removes cholesterol from macrophage-foam cells (Gelissen et al, 1998). It is considered a sensitive biosensor of oxidative stress, having numerous stress-response sites in the *CLU* promoter, and shown to protect cardiomyocytes from H_2O_2-induced apoptosis (Jun et al, 2011). Oxidative stress has been observed during both normal and pathological aging in the brain, however whether an increase in brain clusterin levels protects by reducing reactive oxygen species induced neuronal damage remains to be explored.

1.5 Role of clusterin in the brain and implications for AD

As a very hydrophobic protein composed mainly of coil-coiled α-helices able to bind proteins with exposed hydrophobic regions, clusterin has been regarded as a chaperone in the brain and elsewhere. Molecular chaperones are involved in a wide range of biological processes concerning protein folding, translocation, regulation of signal transduction, or degradation of misfolded proteins, properties that hinted to a potential involvement of clusterin in AD. Indeed, within the Aβ cascade, disturbances of Aβ homeostasis can be influenced by chaperones for amyloidogenic proteins, such as apolipoproteins. After ApoE, clusterin is the second most abundant apolipoprotein in the brain, with many roles in lipid transport, metabolism, and cholesterol efflux. It is primarily produced by astrocytes, followed by neurons, and displays a regional and cell-type specific pattern of expression in the brain, with highest levels found in the hippocampus, followed by frontal cortex tissue and striatum (Kang et al, 2016). Soluble clusterin levels were increased together with Aβ42 and tau in brain areas susceptible to AD; however, the clusterin:Aβ ratio was lowest in regions with high plaque pathology (Miners et al, 2017; Shepherd et al, 2020). Clusterin interacts with hydrophobic patches on $A\beta_{1\text{-}42}$ oligomers and binds with high affinity to amphiphatic α-helical regions on misfolded or aggregated Aβ. Upon binding, clusterin inhibits fibrillogenesis by primary and secondary nucleation mechanisms, reducing the number of nuclei available for further fibril growth (Beeg et al, 2016). This process is highly dependent on the clusterin:Aβ molar ratio, such that a 1:10 ratio allows clusterin to bind high numbers of Aβ peptides and reduce their cytotoxicity, while a 1:500 ratio has an opposing effect, exacerbating amyloid formation (Yerbury et al, 2007). Treatment of human astrocytes with Aβ led to a decrease in sCLU, however an increase in nCLU was observed, along with vacuoles containing fibrillary Aβ forms, suggesting clusterin participates in internalisation of Aβ and therefore its clearance (Nuutinen et al, 2007). Treatment of iPSC derived neurons with Aβ25-35 for 48 hours led to an increase in nCLU, but no change was observed in levels of sCLU (Robbins et al, 2018). Moreover, an in vivo study by Qi et al (2018) showed that injection of a synthetic clusterin peptide into the lateral ventricles of 5xFAD mice for 2 weeks reduced Aβ deposition in the brain, decreased soluble Aβ levels and rescued cognitive deficits tested in Morris water maze. Adeno-associated viral vector delivery of clusterin into the lateral ventricles of 2-day old APP/PS1 mice to overexpress clusterin in astrocytes led to

fewer amyloid plaques in the cortex and hippocampus compared to GFP injection after 8 months (Wojtas et al, 2020). When *Clu*$^{+/-}$ mice were crossed with APP/PS1 mice, higher levels of fibrillar amyloid were observed in the cortex and hippocampus compared to *Clu*$^{+/+}$ (Wojtas et al, 2020). However, in PDAPP mice crossed with *Clu*$^{-/-}$ mice, clusterin deficiency led to a reduction in fibrillar amyloid and decreased neuritic dystrophy by 12 months, although levels of amyloid deposition in the brain were similar to those of *Clu*$^{+/+}$ mice (DeMattos et al, 2002). These findings highlight a potential dual role of clusterin in the fibrillogenesis, deposition and proteolysis of Aβ in vivo.

Within the brain, Aβ is produced predominantly in endosomes and its release from neurons is influenced by synaptic activity both pre- and postsynaptically (Cirrito et al, 2008). Clusterin colocalised with Aβ plaques around synapses in the AD brain, with highest levels of clusterin in *APOEε4* carriers (Jackson et al, 2019). Clusterin is responsible for mediating Aβ transport across the blood brain barrier via low-density lipoprotein-related protein 2 receptor (LRP2), found exclusively on ependymal cells, and internalization in microglia via TREM2. A novel high affinity receptor for clusterin, Plexin A4 (PLXNA4), was found to be expressed throughout all regions of the brain with a significant reduction in AD brains, despite elevated clusterin levels in CSF (Kang et al, 2016). Reduction or knockout of *PLXNA4* in mice led to impairments in learning and memory in a contextual fear-conditioning paradigm; although the mechanism of interaction between PLXNA4 and CLU is unknown, these data suggest that PLXNA4 might modulate *CLU* levels in the brain (Kang et al, 2016).

Apart from Aβ, clusterin interacts with other proteins involved in the pathogenesis of AD as an extracellular molecular chaperone. Tau, a microtubule stabilising protein found in neurons, becomes hyperphosphorylated at different sites, detaches from microtubules and self-aggregates, compromising neuronal integrity throughout disease progression. Tau (total tau, pTau-181, pTau-217, pTau-231) has been established as a reliable AD plasma biomarker, capable of distinguishing AD from control with an area under the curve of 0.83 for pTau-217 alone (Palmqvist et al, 2021). Although tau is an intracellular component, hyperphosphorylated tau can be exocytosed and spread in a prion-like fashion. When injected into hippocampi of rats, clusterin promotes tau phosphorylation (Martin-Rehrmann et al, 2005), and nCLU is upregulated in the brain of Tg4510 tau transgenic mice (Zhou et al, 2014).

An additional important role of clusterin has been described in immunomodulation. Clusterin is a complement lysis inhibitor, inhibiting the formation of the membrane attack complex, a structure that generates pores in the membrane of the targeted cell, causing its lysis (Jenne and Tschopp, 1989). This could be a potential mechanism by which clusterin protects brain cells from damage.

1.6 Plasma clusterin – an emerging biomarker in AD

To be diagnosed with AD, an individual must undergo clinical examination involving cognitive assessments, blood tests for the measurement of proteins related to AD, and brain scans that can identify damage to the areas prone to erosion as the disease progresses (McKhann et al, 2011). Symptoms of mild cognitive impairment are common among the elderly, with a certain degree of forgetfulness being regarded as normal. However, confusion, significant memory loss, and personality changes need to be addressed by a clinician to establish a correct diagnosis. Biomarkers are defined as laboratory measurements of changes that reflect the activity of a disease process, ideally at an early stage of the disease. In AD, biomarkers are used with the purpose of increasing accuracy of diagnosis as well as predicting the progression from MCI to AD, and currently involve the measurement of Aβ and tau, the two proteins most widely involved in the progression of the disease, in cerebrospinal fluid and plasma (Blennow & Zetterberg, 2018).

Clusterin has been evaluated as a potential AD biomarker in numerous studies (Hardy et al, 2011), many of which showed that MCI and AD patients had significantly elevated plasma or CSF clusterin levels compared to non-demented controls. When coupled with genetic data identifying SNPs in *CLU*, this can provide a more reliable association between clusterin levels and cognitive status and a more consistent method of tracking disease progression. Other studies found little or no evidence that clusterin is elevated in AD compared to control, concluding that clusterin is not a viable biomarker in AD. When interpreting results, it should be noted that several factors might contribute to discrepancies seen among studies, including the type of assay used for the quantification of clusterin (enzyme-linked immunosorbent assays (ELISA), multiplex assays, mass spectrometry, Western blot), ethnicity of the subjects, study sample size, and the type of neurological assessment used to diagnose AD. Validated ELISA kits of variable quality that purport to measure clusterin protein levels in human biological

fluids are commercially available and have been widely used across different laboratories.

In a study involving an Irish cohort of AD patients, MCI patients, and controls, Mullan et al (2013) found a statistically significant increase in clusterin plasma levels in AD and MCI compared to controls, as well as MCI versus AD ($p<0.001$). No relationship was identified between rs11136000 genotype and plasma clusterin levels. Jongbloed et al (2015) found MCI patients had significantly higher clusterin plasma levels than controls and AD, which negatively correlated with cognitive function over a period of 3 years. Although plasma and CSF clusterin levels correlated, there was no significant difference between CSF clusterin levels among the three groups. In a prospective study on a Chinese and Taiwanese population, Hsu et al (2017) found that AD patients in the highest tertile of plasma clusterin levels and *APOEε4* carrier patients had significantly higher clusterin levels than controls and lower MMSE scores over a follow-up period of two years. In a case-control study involving AD patients, MCI patients, and controls, Hakobyan et al (2016) reported significantly higher clusterin plasma levels in AD versus controls, and in MCI patients who did not subsequently convert to AD within a year compared to MCI patients who did convert who. Deming et al (2016) reported that AD patients had significantly higher CSF but not plasma clusterin levels compared to controls (24.74 µg/ml vs 19.92 µg/ml), suggesting that CSF clusterin would be a more relevant biomarker than plasma clusterin.

Other studies found no significant differences between either plasma or CSF clusterin levels in AD patients compared to control, and weak or no associations between cognitive scores, *CLU* genotype and clusterin levels (Silajdzic et al, 2012; Thambisetty et al, 2010; Dukic et al, 2016; Schürmann et al, 2011; Xing et al, 2012). Moreover, commercial ELISA kits used in these studies, usually on EDTA plasma stored at -80°C, gave widely different quantified clusterin levels in plasma. Even the same assay used by different researchers resulted in very different mean values in control plasma samples: 33.3 µg/ml, 82.2 µg/ml, 167 µg/ml, respectively (Silajdzic et al (2012), Thambisetty et al (2010), and Xing et al (2012)). Another commercial assay used by several groups also gave high variability in control plasma clusterin levels: 161.5 µg/ml, 178.6 µg/ml, 243.8 µg/ml, and 255 µg/ml respectively (Schürmann et al (2011), Mullan et al (2013), Hsu et al (2017), Haight et al (2018)). This poor performance

highlights the need for a reliable and reproducible immunoassay for measurement of plasma clusterin that would aid in early diagnosis of AD.

1.7 Astrocytes – roles of glia in the brain and AD pathology

The central nervous system (CNS) is made up of many different cell types, each of which can be further classified based on their location, function, or morphology. Within the entire brain, recent estimates have placed the number of neurons at 86 billion, and close to 50 billion for glia (von Bartheld, Bahney and Herculano-Houzel, 2016). While neurons have been at the centre of neurodegenerative disease research for decades, the roles of glia and other cells in disease are now increasingly recognised. Astrocytes are the most abundant glial cell type in the brain and are responsible for a variety of roles, many of which support the normal functioning of neuronal activity. Astrocytes maintain blood-brain barrier (BBB) integrity by wrapping their endfeet around endothelial cells and pericytes; provide structural support during neuronal development; are actively involved in synapse formation by increasing the number of dendritic spines on neurons and synapse refinement by releasing signals instructing synaptic pruning; express receptors for neurotransmitters and mediate synaptic activity by recycling neurotransmitters and controlling K^+ levels; secrete numerous cytokines, chemokines and neurotrophic factors (Figure 1.2). In the hippocampus, a brain region often affected by Alzheimer's disease, the number of neurons was significantly decreased in patients with AD (110 million) compared to healthy controls (270 million) and asymptomatic subjects with brain AD pathology (220 million), with no significant differences observed in glial cell numbers between AD and control (Andrade-Moraes et al, 2013). A significant reduction (22%) in the number of neurons was also observed in the cerebral cortex (grey matter only) of AD patients compared to controls, accompanied by a significant increase (45%) in non-neuronal cells (Andrade-Moraes et al, 2013).

In normal physiology, astrocytes are structurally and functionally diverse, generally classified as fibrous (with long thin fibre-like processes, found in the white matter) or protoplasmic (short-branched, in contact with synapses and blood vessels, found in the grey matter). Their cytoskeleton is made up of many interlaced filamentous structures, such as glial fibrillary acidic protein (GFAP) and vimentin (Potokar et al, 2020). In response to pathological conditions, astrocytes undergo morphological

changes, sometimes triggered by activated microglia. Astrogliosis, a process where astrocytes change their appearance from stellate to rounder, more enlarged cells and switch their profile from neuroprotective to neurotoxic, often accompanies AD as seen in immunostaining of brain tissue for GFAP. Reactive astrocytes extend their processes and surround Aβ plaques (Kato et al, 1998). While they can engulf $A\beta_{42}$ fibrils and transport them to lysosomes, primary mouse astrocytes are slow at phagocytosis, as large amounts of Aβ were still present inside the cells even after 12 days (Sollvander et al, 2016). Unlike microglia, which phagocytose Aβ efficiently, astrocytes do not degrade these aggregates completely, perhaps due to the low acidity of the lysosomes engulfing them, leaving behind N-terminally truncated Aβ forms that may be later secreted (Sollvander et al, 2016).

Another particularly important role of astrocytes, highly relevant to this project, is their secretory nature, notably, they secrete lipoproteins ApoE and ApoJ (clusterin), involved in cholesterol uptake and transport, as well as Aβ clearance from the brain parenchyma. Zwain et al (1994) first showed that astrocytes secrete clusterin in vitro. As described in Section 1.5, clusterin is a chaperone for Aβ and aids in its uptake and clearance provided that Aβ levels do not overwhelm clusterin-mediated clearance mechanisms. Astrocytes thus represent the most appropriate cell type to study the effects of SNPs in *CLU* on clusterin production. A summary of the roles of astrocytes is graphically displayed in Figure 1.2.

1.8 Induced pluripotent stem cells as a model of neurodegenerative diseases

AD is a complex disease involving changes in numerous cellular processes and pathways regulating cell homeostasis, with microglia and astrocytes implicated in AD pathology as much as neurons. This makes disease modelling extremely challenging, since mouse models are genetically modified to develop AD pathology, while post-mortem brain tissue can only inform on end-stage disease. In vitro systems are useful for studying molecular pathways and cell-cell interactions; however, certain cell types, such as brain cells, are difficult to obtain and maintain in vitro. Induced pluripotent stem cells (iPSCs) are a good alternative, as they can not only be differentiated into almost any cell type, but also edited genetically to study effects of mutations. iPSCs can be reprogrammed from somatic cells in a relatively short time, proliferate

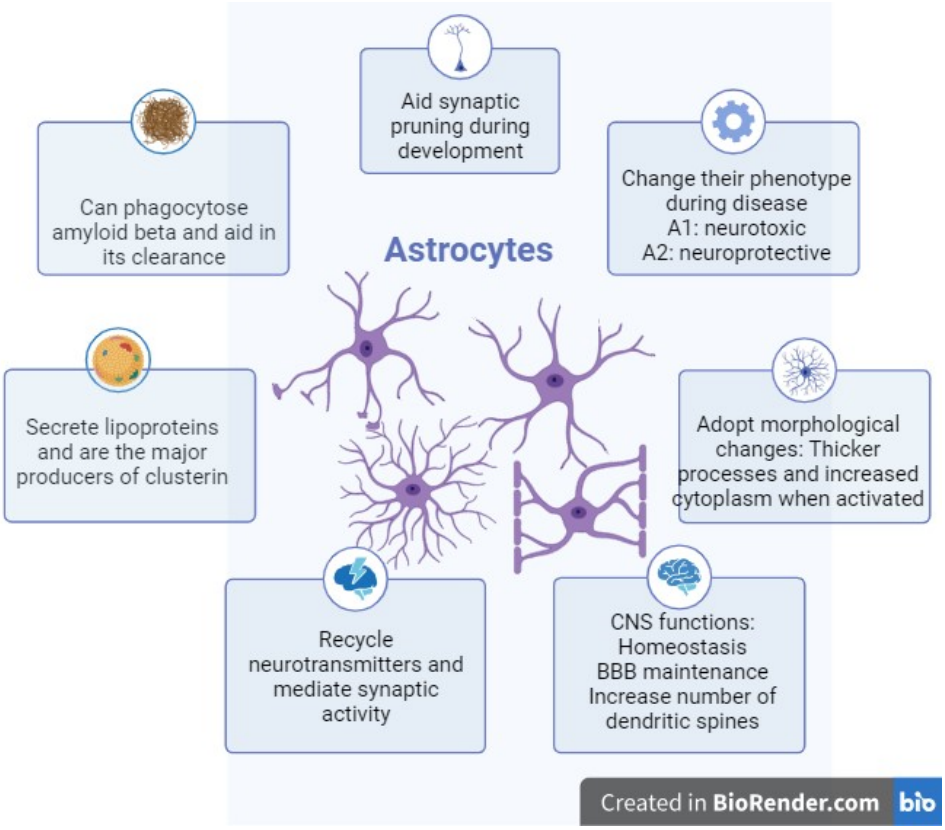

Figure 1.2. Roles of astrocytes in homeostasis and disease. Figure created in BioRender.

indefinitely, and can be banked in large numbers, making them an excellent resource for studying disease at the cell level. Due to advances in iPSC technology, reprogramming of peripheral blood mononuclear cells (PBMCs) or skin fibroblasts into iPSCs now uses non-integrating viral vectors to express pluripotency genes (*SOX2, OCT3/4, KLF4, c-MYC*) without integration into the genome (Fusaki et al, 2009). iPSCs can then be used to obtain brain cells, including different types of neurons, by culturing the cells in the presence of growth factors and inhibitors of pathways that govern expression of genes that are normally active during development of each cell type.

Due to an incomplete understanding of gliogenesis during brain development, differentiation of astrocytes from iPSCs is more complex and of longer duration compared to differentiation of neurons. Numerous protocols have been published using methods developed in research labs and several commercial kits have been made available (Table 1.2). In most cases, differentiation of astrocytes involves a neural precursor cell (NPC) intermediate; therefore, iPSCs are first exposed to SMAD inhibitors, a well-known method for obtaining NPCs. These cells can then be directed

either toward the neuronal or astrocytic lineage, the latter being accomplished by exposing the cells to leukaemia inhibitory factor (LIF) to allow those with high gliogenic potential to proliferate. Since CD44 positive cells are more likely to commit to the astrocytic lineage (Liu et al, 2004), these cells can be isolated by fluorescence activated cell sorting (FACS). The final stages of the differentiation involve expanding the astrocyte progenitors in the presence of epidermal growth factor (EGF) and fibroblast growth factor (FGF), followed by terminal differentiation using ciliary neurotrophic factor (CNTF).

Table 1.2. Protocols for differentiating iPSCs into astrocytes. EB = embryoid body; EGF = epidermal growth factor; FGF = fibroblast growth factor; BDNF = brain derived neurotrophic factor; GDNF = glial derived neurotrophic factor; IGF-1 = insulin-like growth factor 1; cAMP = cyclic adenosine monophosphate; LIF = leukaemia inhibitory factor; FBS = foetal bovine serum; CNTF = ciliary neurotrophic factor; BMP = bone morphogenic protein.

Publication/Source	**Starting point**	**Neural induction**	**Gliogenesis**	**Terminal differentiation**
Perriot et al (2021)	Spheres, then rosettes	SB431542, Noggin, FGF2, Laminin	LIF + EGF	CNTF
Serio et al (2013)	Neurospheres	SB431542, dorsomorphin, N-acetylcysteine	LIF + EGF; EGF + FGF	CNTF
Krencik et al (2011)	Neurospheres	BDNF, GDNF, IGF-1, cAMP	CNTF, LIF, FBS	
Shaltouki et al (2013)	EBs	StemPro medium	FGF (1 day)	CNTF, BMP, FGF ± FBS
TCW et al (2017) - commercial medium for NPCs	EBs iPSC	LDN, SB431542 StemCell Technologies Neural induction medium	ScienCell medium	

1.9 Aims

The hypothesis underlying this project is that SNPs in *CLU* associated with AD risk influence levels of clusterin protein in plasma and CSF, and that changes in clusterin levels are responsible for progression to AD. This project therefore has several aims

centred around dissecting the molecular mechanisms underlying predisposition to AD caused by genetic variants in *CLU*:

1) Establish specific antibodies and a robust assay to detect and measure clusterin in human biofluids and tissues with high sensitivity and specificity;
2) Measure clusterin levels in plasma and CSF from subjects with AD or DS compared to healthy controls;
3) Test whether GWS SNPs in *CLU* influence plasma clusterin levels;
4) Explore clusterin synthesis and secretion in iPSC-derived astrocytes from donors homozygous for the major or minor allele at rs11136000 and rs11787077.

CHAPTER 2: Development of a robust assay to measure clusterin levels in human biological fluids

2.1 Introduction

Clusterin is expressed in almost every tissue in the human body and is abundant in serum/plasma (144.5 – 485.9 µg/ml), allowing quantitative measurements to be made in biofluids. A sandwich ELISA is a type of immunoassay involving an antibody (immunoglobulin, mAb or polyAb) against the target adsorbing to the surface of the immunoplate, the antigen added to the plate at a suitable dilution of the biological fluid in an appropriate sample diluent, and a second mAb or polyAb specific for the antigen being added to detect the antigen captured by the first mAb. A few commercial clusterin sandwich ELISA kits are available for research purposes, although they are costly, which restricts their use to a limited number of samples. This chapter will describe the specific reagents produced to set up an ELISA and the validation steps implemented to meet the first aim of the study. In order for an ELISA to be validated as a sensitive and reliable assay, it must meet certain criteria: the detection limit must be clearly distinguished from the background signal given by the negative control sample (high signal to noise ratio); the antibodies used must be specific for the antigen to be measured in a complex biological fluid; the assay should be able to accurately measure levels of antigen in a sample spiked with a known concentration of antigen; and should prove reliable when a sample measured in replicate across at least three separate experiments falls within a range of values not exceeding 10% variation (intra- and inter-assay coefficients of variation below 10%). To accomplish this, it is crucial that the antibodies used specifically bind clusterin to avoid non-specific signal and inaccurate measurements. mAbs used in ELISA can be either monoclonal, recognising a single epitope on the antigen, or polyclonal, recognising multiple epitopes. It is preferred that monoclonal antibodies are used in ELISA for better specificity and sensitivity, although a monoclonal antibody used to capture the antigen paired with a polyclonal antibody (polyAb) to detect this is also often used. Although polyAb can be more rapidly produced at lower costs, they may cross-react with antigens from a different species, vary in composition between batches, and include large quantities of non-specific antibodies. Hybridoma technology is an *in vitro* mAb production technique where B cells expressing antibodies from a mouse immunised against the antigen are fused with myeloma cells to yield hybridoma cells. These cells

can grow continuously in culture, and their tissue culture (TC) supernatant is harvested over a period of weeks for the purification of the desired antibody. This ensures uniform production of the same antibody that can be bulk purified and stored appropriately for use in numerous assays. This technique will be employed in this study to obtain mAbs against human clusterin for establishing a sandwich ELISA capable of measuring levels of clusterin in human biological fluids.

Pure proteins are essential for the quantification of the protein of interest in a complex biofluid as they can be used to create a standard curve on known concentrations. In this study, proteins were purified using immunoaffinity chromatography – an isolation technique that allows a specific antigen to be purified by reversibly binding to an antibody coupled to a chromatographic matrix, while unbound sample components are washed away. This is a highly efficient, one-step purification method that can result in high yields of purified native protein. Occasionally, proteins are purified together with other proteins, due to hydrophobic interactions or a high affinity for each other in blood. Additional purification "polishing" steps are therefore necessary to ensure the protein of interest is of high purity (>90%). These include gel filtration, ion exchange chromatography, and separating the protein of interest from the contaminant by immobilising the contaminant on a column packed with antibodies against it. Once the protein's identity and purity are confirmed, and the protein is proven to be specifically recognised by mAbs in Western blot (WB) and ELISA, this can be used for setting up the highly specific immunoassay.

This chapter will describe the techniques used to purify clusterin from human serum, the process of obtaining mAbs using hybridoma technology, and the development of a sensitive and robust sandwich ELISA using the reagents generated.

2.2. Methods

2.2.1. Protein purification by affinity chromatography

2.2.1.1 Serum/plasma preparation

To purify proteins by affinity chromatography, normal human serum or plasma was used as a source of protein. After blood donation, blood was allowed to coagulate at room temperature (RT) for 1 hour and overnight on ice. Blood was centrifuged for 20 minutes (mins) at 2500 rpm at 4°C, serum collected and stored at -80°C until further use. Immediately prior to purification, serum was thawed and filtered through a 0.2 µm

filter. To obtain plasma, blood was centrifuged for 20 mins at 2500 rpm at 4°C immediately after collection, serum collected and EDTA was added at a final concentration of 5 mM. Plasma was frozen at -80°C and filtered through a 0.2 µm filter before use.

2.2.1.2. Buffers used in the purification system

Buffers used during the purification process were prepared fresh and stored at 4°C. Table 2.1 details the composition of buffers used in affinity chromatography. All reagents were obtained from Fisher Scientific UK or Sigma Aldrich and were of analytical grade.

Table 2.1. Affinity purification buffers

Buffer	Composition
Wash/Equilibration buffer	10 mM Tris, 150 mM NaCl, 0.001% w/v NaN_3, pH 7.4
Elution buffer	0.1 M Glycine, pH 2.5
Neutralisation buffer	10 mM Tris, 150 mM NaCl, pH 9
Dialysis buffer	PBS (8.2 mM Na_2HPO_4, 1.5 mM KH_2PO_4, 137 mM NaCl, pH 7.4); or HBS (0.01 M HEPES, 0.5 M NaCl, 135 mM $CaCl_2$, 1 mM $MgCl_2$ pH 7.4)
Column storage buffer	0.001% w/v NaN_3 in PBS (affinity columns); 20% EtOH in ddH_2O (protein G)

2.2.1.3. Affinity columns

To purify clusterin from human serum, HiTrap NHS activated Sepharose High Performance columns (1 or 5 ml, GE Healthcare, HiTrap NHS-activated HP, #17-0716-01, #17-0717-01) were used with the in-house anti-clusterin monoclonal antibodies (mAbs; MBI40 or 2D5) immobilised according to the manufacturer's instructions. For each column, ~7 mg antibody for 1 ml columns and ~25 mg antibody for 5 ml columns were used; coupling efficiency was determined by measuring the amount of unbound antibody that was eluted after washing the column and was usually >90%. Columns were stored at 4°C in storage buffer and washed with elution buffer before first use to remove any unbound antibody.

2.2.2. Purification protocol

Proteins were affinity purified from 25 – 100 ml human serum/plasma or hybridoma cell supernatant using the AKTA Pure 01 system (GE Healthcare #WIN-QET7M352MJ). The column was washed and equilibrated with 5 column volumes (CV) of wash buffer, and serum or plasma was then applied through the column at a flow rate of 1 – 2 ml/min. The column was washed with wash buffer until the UV reading stabilised at ~0 mA, indicating any residual proteins had been removed. Bound protein was eluted into 1 ml fractionation tubes containing 100 µl neutralisation buffer by applying 5 CV elution buffer at 5 ml/min. The column was re-equilibrated with storage buffer and stored at 4°C. Clusterin was purified from human serum or plasma as described above, dialysed in PBS and stored at -80°C. Polishing steps (gel filtration, ion exchange chromatography) were applied to obtain clusterin of high purity and are described in sections 2.2.4.1 and 2.2.4.2.

2.2.3. Dialysis, concentration, and storage of purified proteins

Protein concentration of peak fractions (indicated by high UV peaks on the AKTA system) were determined using Nanodrop (Labtech International Model, #ND1000) by applying 2 µl of sample after a blank reading of protein storage buffer was taken. Protein concentration was calculated by applying Beer-Lambert's Law: protein concentration (mg/ml) = A280/protein extinction coefficient (clusterin = 1.03). Fractionation tubes containing eluted protein were pooled together and dialysed in PBS using 30 kDa cut-off dialysis tubing (Medicell International Ltd, London, UK), with constant stirring overnight at 4°C. Protein samples were then concentrated using 30 kDa cut-off concentrator tubes (ThermoFisher, #88522) and protein concentration determined using the Bradford assay. Bovine serum albumin (BSA, ThermoFisher, #23235) was used to construct an 11-point standard curve starting at 1 mg/ml and serially diluting 25 µl 1:2 in PBS in a 96 well plate. One well was left blank (PBS only). Sample (50 µl) was used neat and serially diluted 1:2 in PBS. Bradford reagent (Pierce Coomassie Plus, #23238) was added to each well (25 µl) and absorbance was read at 595 nm using a microplate reader (Labtech International, Infinite F50, #30190077). A standard curve was plotted using GraphPad Prism 5, absorbance readings of samples interpolated on the curve, and concentrations calculated by multiplying the

obtained values by the dilution factor. Proteins were stored on ice at 4°C short term (<2 weeks) or -80°C long term.

2.2.4. Protein purification polishing steps

2.2.4.1. Gel filtration

Gel filtration, a technique involving separation of molecules based on their molecular weight as they pass through a column with a porous matrix gel medium, was employed to separate clusterin from IgG contaminants. Proteins of high molecular weight pass through the column faster because they are excluded from the porous bead matrix and thus elute earlier than smaller proteins. Clusterin eluted from the affinity column was concentrated using a 30 kDa protein concentrator tube and loaded onto a gel filtration column (GE Healthcare, Superdex 200, #1-2552-46) preequilibrated with PBS at 0.3 ml/min flow rate. PBS was then applied through the column at 0.3 ml/min (20 ml) flow rate and eluted protein collected in 1 ml fractionation tubes. Fractionations were then assessed for protein content by Nanodrop and checked for purity by SDS-PAGE as described below.

2.2.4.2. Ion exchange chromatography

Ion exchange chromatography, a technique that separates molecules based on their charge using a salt gradient, was used to remove minor contaminants. Purified clusterin (after affinity and gel filtration) was dialysed into a low salt buffer (0.1 M NaCl, 10 mM Tris) and applied to an ion exchange column (ThermoFisher Scientific, Mono Q column, Poros 50 HQ #1-2552-46) equilibrated with the same buffer using the AKTA Pure 01 system (GE Healthcare). A linear NaCl gradient elution was applied from 0.1 M to 1 M NaCl at 5 ml/min, and 1 ml fractions were collected during the elution.

2.2.4.3. Protein A and protein G bead trapping of IgG

Additional polishing steps were followed to remove IgG contaminants, including a protein G column used to trap the IgG while clusterin would freely flow through the column. Protein G is isolated from Staphylococcus aureus and binds IgG with high affinity in various sources of IgG, such as serum and cell supernatants. Clusterin in PBS was applied to the protein G column preequilibrated with binding buffer (Table 2.1), and the flow-through collected, concentrated using 30 kDa protein concentrator

tubes (ThermoFisher, #88522) and purity checked using SDS-PAGE. Protein A beads were used to capture the IgG contaminant which, like protein G, bind IgG with high affinity in various sources. Affinity purified and gel filtered clusterin were pooled and incubated with protein A beads at a 5:1 ratio for 1 hour at room temperature (RT) with gentle agitation. After the incubation period, the sample was centrifuged at 1000 rpm for 1 minute, supernatant collected and subjected to SDS-PAGE and Coomassie blue staining to verify purity.

2.2.5. SDS-PAGE and Western blotting

2.2.5.1. SDS-PAGE and Coomassie stain

To assess the purity of proteins, sodium dodecyl sulphate polyacrylamide gel electrophoresis (SDS-PAGE) was used with Coomassie staining of the gel to visualise proteins. The buffers and reagents used are described in Table 2.2. Gels were poured in-house using 1.5 mm gel casting cassettes (Fisher Scientific, #11559156) and stored at 4°C in PBS-soaked tissue. Protein samples (2 µg protein diluted in 25 µl PBS) were prepared by diluting 1:5 in either non-reducing (NR) or reducing (R) loading dye and heated to 100°C for 10 mins. Molecular weight markers (ThermoFisher, PageRuler Plus prestained protein ladder, #26620) were loaded onto the gel for accurate determination of protein size. Gels were run using a mini gel tank (Invitrogen) filled with running buffer at 100 mV for 1 hour. The gel was then stained using the Quick Coomassie Blue stain (Generon, #NB-45-00078-1L) for 15 min, and destained with distilled H_2O for 4 hours.

Table 2.2. Buffers used in SDS-PAGE

Buffer/Reagent	Composition
Non-reducing loading buffer	0.1 M Tris, 10% w/v glycerol, 2% w/v SDS, bromophenol blue, pH 6.8
Reducing loading buffer	NR loading buffer with 5% v/v β-mercaptoethanol
Stacking buffer	0.5 M Tris, 0.4% SDS, pH 6.8
Separating buffer	1.5 M Tris, 0.4% SDS, pH 8.8
Running buffer	20x Bolt MES SDS running buffer (ThermoFisher #B0002) diluted to 1x in ddH_2O
2.5% stacking gel	600 µl stacking buffer, 157 µl 40% acrylamide/bis, 1.69 ml ddH_2O, 2.5 µl TEMED, 25 µl 10% ammonium persulphate
7.5% separating gel	1.875 ml separating buffer, 1.4 ml 40% acrylamide/bis, 4.1 ml ddH_2O, 7.5 µl TEMED, 75 µl 10% ammonium persulphate

2.2.5.2. Western Blotting

Western blotting was performed to assess the specificity of the mAbs produced in recognising clusterin in human plasma. The buffers and reagents used in Western blots are described in Table 2.3. Following SDS-PAGE (described in section 2.2.5.1), the gel was equilibrated in transfer buffer, placed on nitrocellulose membrane of the same dimensions, and sandwiched between sheets of filter paper pre-soaked in transfer buffer. The blotting cassette was inserted into the apparatus filled with transfer buffer such that the gel would face the anode side, according to the manufacturer's instructions (Bio-Rad, #1703930). The proteins were then transferred onto the nitrocellulose membrane at 100V for 1h. The transfer efficiency was assessed by Ponceau staining of the membrane for 5 – 10 mins, which stained the separated proteins and allowed distinct lanes to be separated by cutting them with a scalpel blade for incubation with different antibodies. The blots were then destained in ddH_2O and blocked with 20 ml blocking buffer for 1h at RT with gentle agitation of the tubes. The blots were incubated with a primary antibody (2 µg/ml) or buffer only as a negative control overnight at 4°C with gentle agitation. After washing the blots three times every 5 mins at RT, blots were incubated with a horseradish peroxidase (HRP)-conjugated secondary antibody (1 in 10000 dilution, Jackson ImmunoResearch #715-035-151) for 40 mins at RT. The blots were washed three times, soaked in 500 µl ECL Western Blotting Reagent (Cytiva #GERPN2106), and bands visualised by autoradiography.

Table 2.3. Buffers and reagents used in Western blotting

Buffer/Reagent	**Composition**
Transfer buffer	25 mM Tris, 191 mM Glycine, 20% methanol in ddH_2O
Wash buffer	0.05% Tween-20 in PBS
Blocking buffer	5% BSA in wash buffer

2.2.6. Hybridoma technology

2.2.6.1. Animals

Wild-type (WT) mice used in this study to generate mAb against clusterin were obtained from breeding colonies in the Biomedical Services Unit (Cardiff University) and were housed in a barrier housing facility under a 12 h normal light-dark cycle, with ad libitum access to food and water.

2.2.6.2. Mouse immunisation and screening for antibody production

To obtain antibodies against human clusterin, three WT mice were immunised with human clusterin by a licensed experimenter (Dr Wioleta Zelek). Purified clusterin was diluted in PBS and mixed with an equal volume of complete Freund's adjuvant until thoroughly emulsified. The animals then received approximately 250 µl of emulsion (20 – 50 µg protein per mouse) via subcutaneous injections. After 4 weeks, mice received a second injection of clusterin (20 – 50 µg antigen) emulsified in incomplete Freund's adjuvant. One week later, blood was collected in EDTA coated tubes by tail vessel microsampling, plasma harvested and screened for antibody production using a direct ELISA with immobilised clusterin as described in section 2.2.7.3. Briefly, plates were coated with 0.5 µg/ml purified clusterin in 50 µl coating buffer/well, blocked with 100 µl blocking buffer, washed and 100 µl mouse plasma diluted 1:1000 in 1% BSA in PBST was added to the first well of each row in duplicate. Fifty µl of each plasma sample were then serially diluted 1:2 in wells containing 1% BSA in PBST and incubated for 1 hour at 37°C. Plasma from a non-immunised mouse was used as a negative control, and a commercial mAb against human clusterin (J84, #3713-6-250 Mabtech) was used as a positive control. Wells containing only 1% BSA in PBST were used to determine the assay's background absorbance. The plate was washed three times with PBST and 50 µl donkey anti-mouse HRP conjugated secondary antibody was added to each well at 1:1000 dilution for 1 hour at 37°C. The plate was washed three times and 50 µl OPD substrate (Sigma Fast) diluted in 20 ml ddH_2O was added to each well until colour developed, followed by addition of 50 µl 5% H_2SO_4 to each well to stop the reaction. Absorbance was read immediately at 492 nm using a spectrophotometer and results plotted as sigmoidal dose-response curves. The mouse expressing the highest mAb titre was selected for the fusion.

2.2.6.3. Tissue culture reagents

Tissue culture was performed under sterile conditions, in a fume hood, using sterile tissue culture plates and flasks. All reagents were obtained from Gibco (Invitrogen, UK) and plastics were obtained from ThermoFisher. Cells were maintained in a humidified incubator at 37°C in 5% CO_2 95% O_2. Medium was pre-warmed to 37°C before addition to cells. Table 2.4 shows the types of medium used and their composition.

Table 2.4. Cell culture media and reagents

Medium	Components
Basic medium	RPMI 1640 medium
F15 medium	Basic medium supplemented with 15% foetal bovine serum (FBS), 3A (1% penicillin, 1% streptomycin, 2 mM L-glutamine, 1 mM sodium pyruvate), and 0.001% β-mercaptoethanol
HAT-F15 medium	F15 medium supplemented with 0.1 mM hypoxanthine, 0.4 µM aminopterin, 16 µM thymidine
HT-F15 medium	F15 medium supplemented with 0.1 mM hypoxanthine, 16 µM thymidine
Low IgG medium	Basic medium supplemented with 10% ultra-low foetal calf serum (FCS), 3A, and 0.001% β-mercaptoethanol
Integra flask medium	Basic medium supplemented with 3A and 0.001% β-mercaptoethanol
Freezing medium	10% w/v DMSO in FBS

2.2.6.4. Mouse peritoneal macrophage preparation

Mice were sacrificed using a Schedule 1 method by a licensed experimenter (Dr Wioleta Zelek) and their abdomen rinsed with 70% ethanol. Cold basic medium (10 ml) was injected into the peritoneal cavity using a 21-gauge needle, flushed several times to dissociate macrophages, and slowly withdrawn to harvest macrophages. These were then centrifuged at 1500 rpm for 5 minutes and resuspended in HAT- or HT-F15 medium before they were added to cell culture plates. For each fusion (10 x 96-well plates), one mouse was sacrificed during each re-cloning step (detailed in Section 2.2.6.6).

2.2.6.5. SP2 and spleen cell fusion protocol

Generation of hybridoma cell lines is an essential step in ensuring constant and uniform production of mAbs. Two of the three immunised mice producing antibodies against clusterin received a third injection intraperitonially of purified clusterin in PBS two days before being sacrificed and their spleens harvested aseptically. Murine myeloma cells (SP2) grown in T75 flasks in 20 ml F15 medium were mixed with B cells (dissociated by perfusing the spleen from each immunised animal with cold basic

medium several times using a 19-gauge needle) at a 2:1 ratio in a TC hood. Cells were washed with pre-warmed basic medium and centrifuged at 1800 rpm for 5 minutes. The pellet was allowed to dry and 1 ml pre-warmed PEG-1500 was then added dropwise while gently agitating the cells. The cells were allowed to rest for 30 seconds before 50 ml pre-warmed basic medium was slowly added. Fused cells were washed by centrifugation, resuspended in 50 ml pre-warmed HAT-F15 medium and 50 µl/well added to ten 96-well plates pre-seeded with 50 µl feeder cells/well (mouse macrophages harvested from the peritoneal cavity on the same day) and placed in a 37°C incubator (5% CO_2) for two weeks. After the incubation period, wells were inspected under the microscope for visible cell growth and screened for antibody production by direct ELISA as described above, except 50 µl cell supernatant was used undiluted and wells were replenished with 50 µl fresh F15-HAT medium.

2.2.6.6. Hybridoma re-cloning

Following screening in ELISA, wells displaying strong optical densities and with healthy cells in the well were selected for re-cloning, a process intended to ensure the antibodies generated are monoclonal by allowing a single clone in each well to grow and expand. Twenty clones per fusion were selected, cells scraped off the bottom of the well and 50 µl split into top 6 wells of a 96 well plate containing freshly harvested peritoneal macrophages in 50 µl HAT-F15 medium per well, followed by 10 µl taken out of the first wells and serially diluted down the plate. Plates were returned to the incubator for 10 days and visually inspected for cell growth under the microscope on day 10. After 10 days, clones were screened for mAb production by direct ELISA as described above and 20 clones from each fusion (usually the lowest row with strong ELISA signal) were selected for a second re-cloning. The re-cloning process was repeated as above with HT-F15 medium. Cells were incubated at 37°C for one week, after which a third re-cloning was performed following the steps in the second re-cloning. Finally, a fourth and fifth re-cloning were performed one week apart using F15 medium. One week after the fifth re-cloning, clones were expanded to 6 well-plates (one clone/well), and the ones found to give strong signal in ELISA further expanded to T75 flasks when sufficient density was reached. Low IgG medium was used to aid in the purification of monoclonal antibodies generated. Each hybridoma was frozen in 1 ml freezing medium and stored in liquid nitrogen for future use.

2.2.6.7. Antibody isotyping

To determine the class and subclass of each monoclonal antibody produced, isotyping was performed on TC supernatant from each clone during the fifth re-cloning. Four ELISA plates were coated with 2 µg/ml rat anti-mouse either IgG1, IgG2a, IgG2b, or IgM (BioLegend, #406602, #406712, #406702, #406502) in 50 µl coating buffer overnight at 4°C. The plates were washed three times with PBST and 100 µl blocking buffer (2% BSA in PBST) was added to each well for 1 hour at 37°C, followed by three PBST washes. TC supernatant from each hybridoma well was added in duplicated to each plate (50 µl/well), together with mouse IgG1 (at 10 ng/ml), IgG2a (at 10 ng/ml), IgG2b (at 20 ng/ml), and IgM (at 20 ng/ml) in positive control wells on each plate. Plates were incubated for 1 hour at 37°C, washed three times with PBST and donkey anti-mouse IgG-HRP at 1:1000 was added to plates isotyping IgG classes, or goat anti-mouse IgG/IgM-HRP at 1:1000 to the plate isotyping IgM for 1 hour at 37°C. Finally, plates were washed three times and 50 µl TMB substrate was added to each well until colour developed, and the reaction was stopped by the addition of 50 µl 5% sulfuric acid to each well. Absorbance was read at 450 nm using a spectrophotometer and isotype confirmed for each clone.

2.2.6.8. Seeding and maintenance of Integra flasks

For large scale production of antibodies (1-2 mg/ml in harvested medium), bioreactors were used (CELLine AD 1000 #90025). In these flasks, cells are grown in the lower chamber in 15 ml low IgG medium, while the upper chamber is filled with Integra flask medium, which provides nutrients and waste elimination through a semipermeable membrane. The culture was set up for anti-clusterin antibodies by filling the upper chamber of Integra flasks with 1000 ml medium, and inoculating the lower chamber with at least 10 million viable hybridoma cells in 15 ml low IgG medium. Flasks were incubated at 37°C (5% CO_2, 95% O_2) for fourteen days, followed by weekly harvesting and fresh medium (~25ml) exchange. Harvested TC supernatant was stored at 4°C until antibodies were purified.

2.2.6.9. Antibody purification

Hybridoma cells producing mAbs against clusterin, each growing in T75 flasks or Integra flasks in low IgG FBS medium, had 20 ml of supernatant harvested twice a week and replaced with fresh pre-warmed 20 ml medium/flask. After two weeks,

approximately 180 ml supernatant from each clone was filtered through a 0.22 µm filter and run over a 5 ml HiTrap NHS activated protein G column (Cytiva, #17040501) as described in section 2.1.4. All mAb tested in direct ELISA and WB were purified using the same method, with column washing between each mAb. Purified antibodies were dialysed in PBS overnight at 4°C using 30 kDa cut-off cellulose dialysis membranes. Antibody concentrations were determined by their absorbance at 280 nm using NanoDrop, and antibodies with concentrations below 1 mg/ml were concentrated using 10 kDa concentrator tubes. The mAbs were stored at -20°C until further use. Their purity was assessed by SDS-PAGE followed by Coomassie staining of the gels as previously described.

2.2.6.10. Testing antibody specificity by WB

Antibodies against human clusterin obtained through hybridoma technology were tested in WB using human plasma (1:300) and pure clusterin (1 µg protein/lane) to determine their specificity for clusterin. WB was performed as described in section 2.2.5.2. The blots (except for lanes reserved for secondary antibody incubation only) were incubated with a primary antibody against clusterin (J29 Mabtech #3173-5-250 at 2 µg/ml, or in house generated hybridoma TC supernatants diluted 1:4 in blocking buffer) overnight at 4°C with constant agitation. After washing, blots were incubated with HRP-conjugated donkey anti-mouse IgG (Jackson Immunoresearch, #715-035-151) at 1:10000 dilution for 1 hour at room temperature.

2.2.7. Enzyme linked immunosorbent assays

2.2.7.1. ELISA buffers and sample preparation/handling

All ELISAs were carried out using Maxisorp (Nunc) 96-well immunoplates (Fisher Scientific #442404), coated for 1 hour at 37°C or overnight at 4°C. The buffers used are listed in Table 2.5. Antibodies (either commercial or produced in house) were used at 1 – 10 µg/ml, and pure protein was used to plot a standard curve for accurate quantification. Samples used throughout this study were serum, plasma from blood collected in EDTA tubes, or CSF samples collected by lumbar puncture. Samples were stored at -80°C, transported on dry ice, defrosted immediately prior to use in ELISA, vortexed briefly, diluted in the appropriate sample diluent buffer, and kept on ice until used. Diluted samples were often frozen at -80°C for future use to measure proteins whose integrity would not be compromised by freeze-thaw cycles.

Table 2.5. Buffers used in ELISA.

Buffer	Composition
Coating buffer	0.1 M $NaHCO_3/Na_2CO_3$, pH 9.6
Wash buffer	0.05% Tween-20 in PBS
Blocking buffer	2% BSA
Sample diluent	0.2% BSA in wash buffer
Developing solution	OPD tablets dissolved in ddH_2O (Sigma-Aldrich #P9187) or TMB (ThermoFisher Scientific # BDB555214)
Stop solution	5% H_2SO_4 in H_2O

2.2.7.2. HRP labelling of mAbs

To set up an ELISA for measuring clusterin levels in biological fluids using the mAbs generated, 200 µl of each antibody (1 – 4 mg/ml) were conjugated to HRP in order to be paired with each other in a sandwich ELISA. HRP (EZ link plus activated peroxidase kit, ThermoFisher #31489) was reconstituted with 100 µl distilled H2O, 20 µl added to each antibody and incubated at 4°C for 16 hours. Cyanoborohydride (2 µl) was added to each antibody and incubated for 1 hour at RT. Quench buffer (4 µl) was then added to each antibody and incubated for 30 min in the dark. HRP labelled antibodies were tested in direct ELISA and stored at 4°C.

2.2.7.3. Direct/indirect ELISA

Direct ELISAs were performed using 96-well plates and the buffers described above. Plates were coated with pure protein (clusterin) at 0.5 µg/ml in coating buffer for 1 hour at 37°C, tapped dry on absorbent paper tissue, and blocked with 100 µl blocking buffer for 30 mins at 37°C. Plates were washed once using an automated plate washer, and 50 µl/well detection antibody added at a suitable dilution in sample diluent for 1 hour at 37°C. Plates were washed 3 times and, if the detection antibody was not HRP labelled, a secondary antibody conjugated to HRP (anti-mouse or anti-rabbit IgG as appropriate, Jackson ImmunoResearch, #715-035-151, #711-035-152) was added at 1:1000 to each well (50 µl) for 1 hour at 37°C. Plates were washed 3 times and 50 µl developing solution was added to each well for 3 – 15 mins at RT, until strong colour development was observed. Stop solution was then added to each well (50 µl) and

absorbance measurements were taken immediately at 492 nm using a microplate reader (Labtech International, Infinite F50 Tecan #30190077).

2.2.7.4. Sandwich ELISA

Capture antibodies were immobilised overnight at 4°C on 96-well immunoplates at concentrations between 2–5 µg/ml in 50 µl/well carbonate-bicarbonate buffer. Wells were blocked by incubation with 100 µl blocking buffer for 1h at 37°C, washed once with PBST, and plasma samples or protein standards (50 µl) added at a suitable dilution. Plates were incubated for 2 hours at RT or 90 mins at 37°C, washed three times and detection antibodies added at concentrations between 1–2 µg/ml in 50 µl/well 0.2% BSA in PBST for 1h at 37°C. For assays where the detection antibody was not directly labelled, an HRP-labelled secondary antibody (anti-mouse or anti-rabbit IgG as appropriate, Jackson ImmunoResearch #715-035-151, #711-035-152) was added to washed plates at a suitable dilution for 1h at 37°C. Finally, plates were washed and developed using OPD substrate for 5 minutes, followed by addition of stop solution to quench the reaction. Optical densities were read at 492 nm using a microplate reader (Labtech International, Infinite F50 Tecan #30190077) and interpolated on the standard curve using GraphPad Prism 5. All samples were measured in duplicate, blinded to diagnosis. Intra- and inter-assay coefficients of variation were below 15% for all assays.

2.2.7.5. Development of clusterin ELISA

To identify an optimal pair of antibodies against human clusterin for validating an ELISA with the purpose of measuring clusterin levels in biological fluids, all eight selected mAbs were paired in sandwich ELISA as capture or detection. ELISA plates were coated with each antibody at 2 µg/ml (50 µl per well), blocked with 2% BSA in PBST, incubated with 1 µg/ml purified human clusterin for 2 hours at RT, and HRP-labelled antibodies were used to detect clusterin from 4 µg/ml serially diluted 1:2 in 1% BSA in PBST, with a blank well to determine background absorbance. After washing, plates were developed using 50 µl TMB per well and the reaction stopped by adding 50 µl stop solution per well. Absorbance was read at 450 nm using a spectrophotometer and results plotted as sigmoidal dose-response curves. The pair that showed the highest signal/noise ratio was selected for further optimisation, and

the two optimally paired hybridoma clones producing the mAbs were seeded in Integra flasks for bulk production as described in section 2.4.8.

2.2.7.6. ELISA optimisation with selected antibody pair

To set up a sandwich ELISA using in-house produced mAbs, an optimisation process was performed involving the establishment of optimal concentrations for the capture and detection antibody, the upper and lower limits of detection of the assay, the signal/noise ratio (background), the linearity of the assay, spike recovery, and assay precision (intra- and inter-assay coefficients of variability). ELISA plates were coated with varying concentrations (2-4.5 µg/ml) of 2D5, while 4C7-HRP was used to detect clusterin (1 µg/ml) at varying dilutions (1:200-1:12800) to identify the lowest concentrations giving strong signal. The upper and lower limits of detection were determined by producing a standard curve using pure clusterin at a starting concentration of 10 µg/ml, serially diluting this 1:2 across twelve dilution points, and included eight blank wells. The lower limit of detection was determined by averaging the blank measurements, adding x10 their standard deviations to the average, and interpolating the obtained value on the standard curve. The signal/noise ratio was calculated by dividing the highest optical density value by the lowest, after background absorbance was removed from all readings. The linearity of the assay was determined by measuring clusterin levels in five plasma samples with dilutions starting at 1:200 up to 1:3200 interpolated on the standard curve and quantified. Spike recovery was tested by adding a known amount of pure clusterin to clusterin-depleted plasma and measuring its concentration in the assay. To calculate the intra- and inter-assay coefficients of variability (CVs), 16 plasma samples were measured in duplicate three times across three independent experiments. Each sample's duplicate measurement was averaged, the standard deviation divided by the average, and multiplied by 100 (intra-assay CV); each sample's measurement determined from each plate was averaged, the standard deviation divided by the average, and multiplied by 100 (inter-assay CV).

2.2.7.7. Implementation of newly developed ELISA in plasma and CSF from healthy donors

Following the optimisation steps, the assay was used to measure clusterin in eight matched serum and CSF samples from healthy individuals. Plates were coated overnight at 4°C, tapped dry, blocked with 2% BSA for 1h at RT, washed once, standard protein and serum samples from healthy volunteers diluted 1:2000 or CSF samples diluted 1:50 were added in duplicate (50 µl/well) for 2 hours at RT. Plates were washed three times, detection antibody added for 1 hour at RT (50 µl/well), followed by washing and developing in OPD. The reaction was stopped after 5 minutes and absorbance read at 492 nm using a microplate reader. Samples' optical densities were interpolated on the standard curve and quantified by multiplying raw values by the dilution factor.

Additionally, the in-house assay was compared to a previously set up assay using two commercial monoclonal antibodies (J29 #3173-5-250 and J84 #3713-6-250, Mabtech) in plasma from healthy volunteers (n=23). J29 (capture) was used at 2 µg/ml, in house purified clusterin was used from 1 µg/ml serially diluted 1:2, plasma samples diluted 1:4000 and J84-HRP (detection) was used at 1:100. Plasma clusterin levels from the same samples obtained using the different assays were compared using an unpaired t test to determine whether concentrations were significantly different.

2.3 Results

2.3.1 Clusterin purification by affinity chromatography

To obtain pure clusterin for immunisation of mice and use as standard protein in ELISA, clusterin was purified from normal human serum by affinity chromatography on the AKTA system as described in section 2.1.4. An example chromatogram trace is displayed in Figure 2.1. The UV tracer shows the sample being applied through the column and the elution peak as clusterin is released from binding to MBI40 anti-clusterin mAb. Clusterin was purified from 60 ml normal human serum in two runs over the column, yielding 550 µg/ml and 300 µg/ml respectively for the first and second runs in the pooled elution peaks (tubes containing eluted protein over the highest UV value). Purity of clusterin was assessed by SDS-PAGE using 5 µg of purified clusterin under non-reducing (NR) or reducing (R) conditions. Results showed one band aligned

with the 70 kDa marker corresponding with clusterin under non-reducing conditions, and one band aligned with the 40 kDa marker corresponding to the α and β chains of denatured clusterin. Contaminants at 150-200 kDa (NR) and 20 kDa (R) presumably represent immunoglobulin eluted from the column (Figure 2.2).

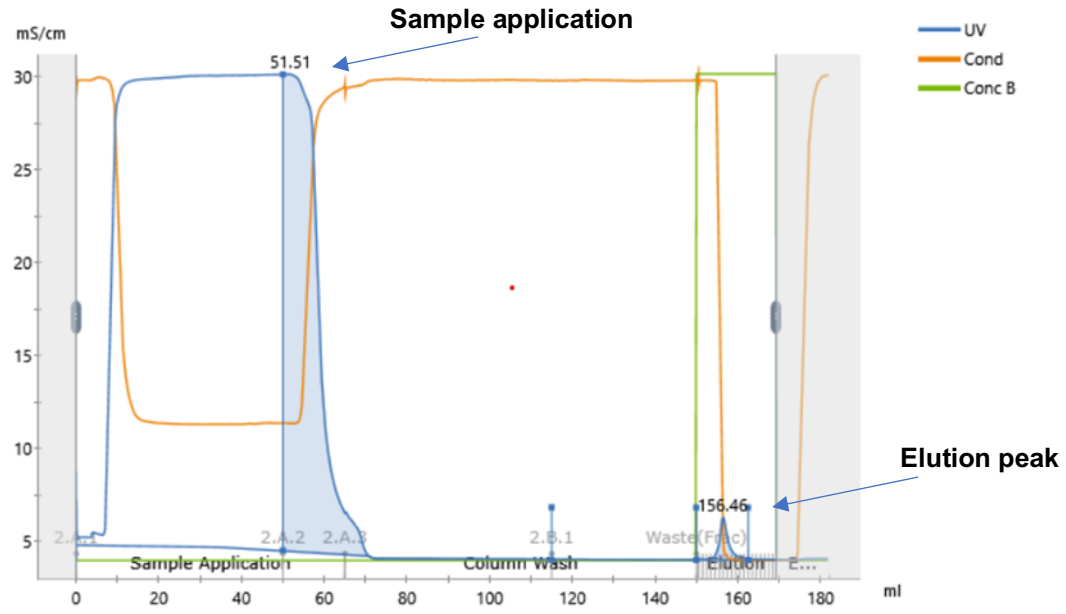

Figure 2.1. Chromatogram displaying clusterin purification from human serum by affinity chromatography using mAb MBI-40 column. Sixty ml of serum were loaded on a HiTrap column (sample application), the column was then washed (column wash), and bound clusterin eluted into 1 ml fractionation tubes (elution). The blue line indicates changes in UV as the sample moves through the column, the orange line represents conductivity, and the green line indicates the concentration of elution buffer.

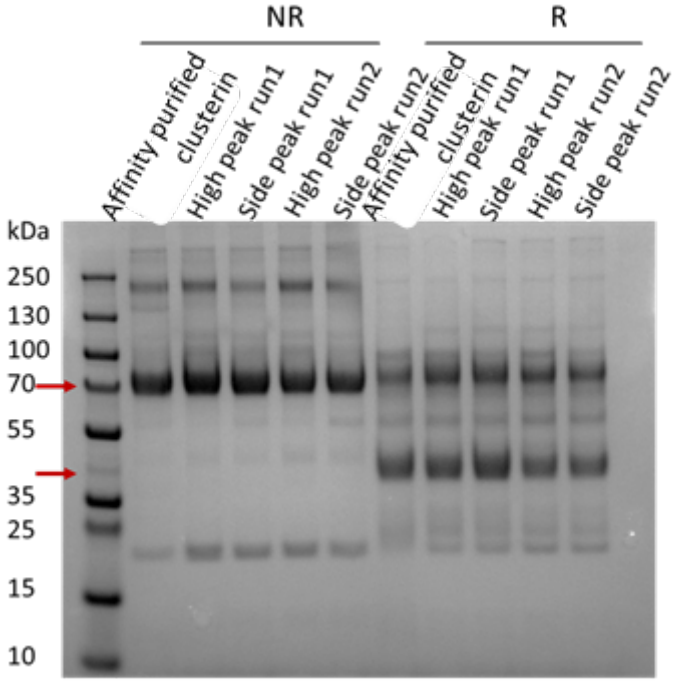

Figure 2.2. SDS-PAGE followed by Coomassie blue staining. Affinity purified clusterin high and side peaks pooled together from the fractionation tubes containing the eluted protein were subjected to SDS-PAGE (5 µg protein/lane). Each sample contained IgG (150 kDa) and other (20 kDa) contaminants. Red arrows indicate full-size clusterin (70 kDa band) and reduced clusterin alpha and beta chanins (40 kDa band). NR=non-reduced conditions, R=reduced conditions. N=1 experimental repeat.

To address the issue of clusterin co-purifying with IgG, a new NHS HiTrap 1 ml column was coupled with a novel mAb (2D5; described below) according to the manufacturer's instructions. Clusterin was purified using the AKTA FPLC system as described above, by applying 25 ml plasma through the column at 1 ml/min flow rate, washing the column and applying a low pH buffer to elute the protein. Purified clusterin was eluted into two fractionation tubes and assessed for purity by SDS PAGE. Both fractions contained contaminants at 55 and 20 kDa, with IgG contaminant in the second fraction (Figure 2.3).

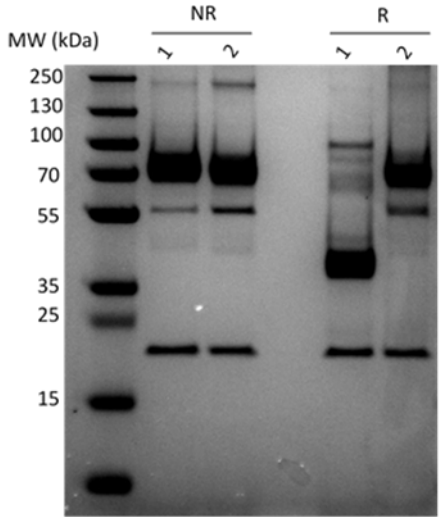

Figure 2.3. SDS-PAGE followed by Coomassie blue staining. Affinity purified clusterin eluted in fractionation tubes (1 and 2) on 2D5 column was subjected to SDS-PAGE (2 µg protein/lane). Both fractions show 55 kDa and 20 kDa contaminants with IgG contaminant in the second fraction. NR = non-reducing conditions, R = reducing conditions. N = 1 experimental repeat.

Clusterin was successfully purified as shown by the chromatogram, however contaminants were also found when purity was assessed by SDS-PAGE, prompting further polishing of the protein of interest.

2.3.2 Clusterin polishing by gel filtration

To further purify clusterin obtained by affinity purification, gel filtration (GF) was used to separate clusterin from contaminants following the steps described in section 2.2.4.1. Affinity-purified clusterin was concentrated to 2.7 mg/ml in 0.5 ml using a 30 kDa protein concentrator tube and loaded onto a gel filtration column (Superdex 200). Eluted protein was collected in 1 ml fractionation tubes (Figure 2.4), then checked for purity by SDS-PAGE as described above. Each fraction showed one band corresponding to clusterin (70 kDa) and one band corresponding to IgG (150 kDa) when run NR, while R fractions showed clusterin α and β chains at 40 kDa and residual NR clusterin at 70 kDa (Figure 2.5). These results indicated that GF was not efficient at removing IgG contaminant provoking use of other purification/separation methods.

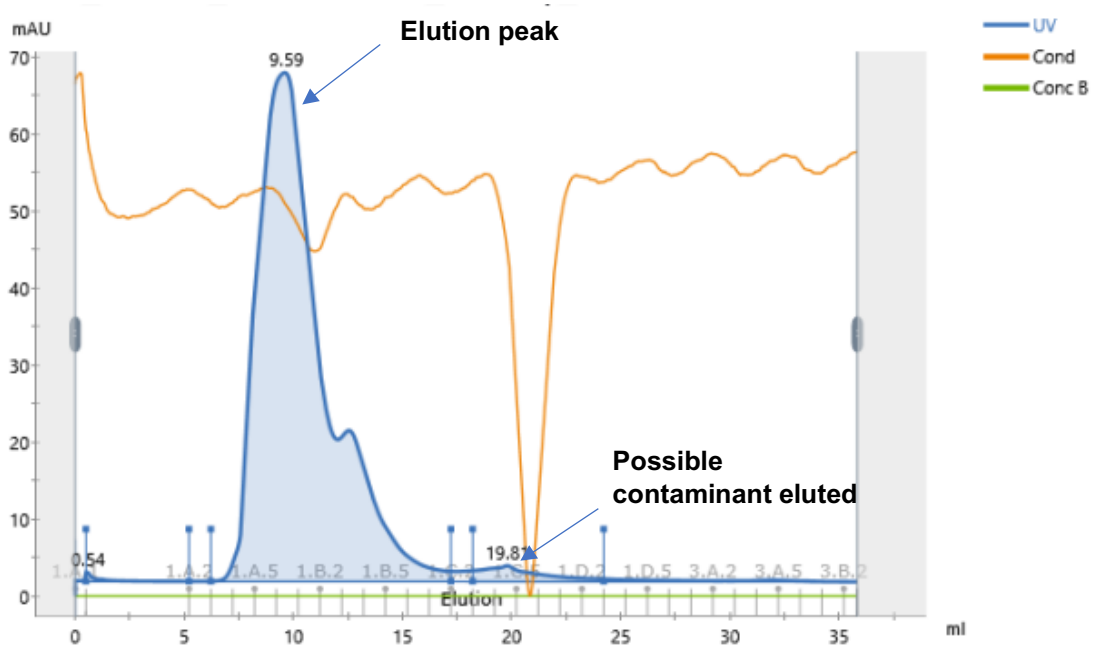

Figure 2.4. Chromatogram displaying gel filtration of clusterin to remove contaminants. The blue line indicates changes in UV as the sample passes through the column during isocratic elution of clusterin. The orange line indicates changes in conductivity, while Conc B refers to the concentration of elution buffer.

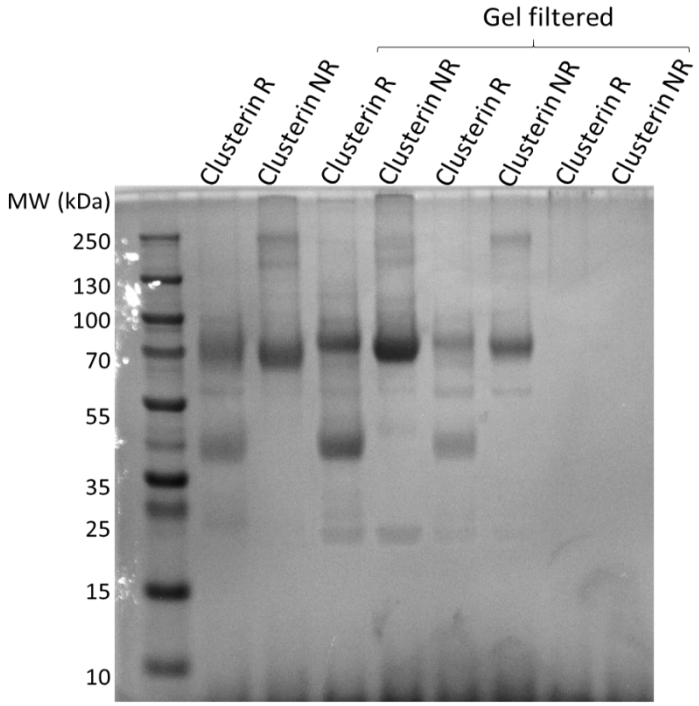

Figure 2.5. SDS-PAGE followed by Coomassie blue staining. Affinity purified clusterin (first two lanes) and gel filtered clusterin eluted into three fractions are shown under reduced (R) or non-reduced (NR) conditions. NR clusterin appears as a 70 kDa protein while reduced clusterin appears as a single 40 kDa band. IgG contaminant (150 kDa) is present in each gel filtered fraction. Fraction 3 - contains an undetectable amount of protein in SDS-PAGE. N=1 experimental repeat.

Gel filtration of purified clusterin led to three elution peaks, indicating that the contaminant might have been separated from clusterin. However, traces of the contaminant were still present when assessed by SDS-PAGE, suggesting that gel filtration might not be the optimal purification method.

2.3.3 Clusterin polishing by ion exchange chromatography

Clusterin, purified as described in section 2.2.2, was dialysed low salt buffer (0.1 M NaCl, 10 mM Tris) and applied to an ion exchange column (Mono Q) equilibrated with the same buffer on the AKTA Pure 01 system (GE Healthcare). Protein was eluted using a linear NaCl gradient from 0.1 M to 1 M NaCl at 5 ml/min flow rate, and 1 ml fractions collected (Figure 2.6). These were assessed for purity by SDS-PAGE and Coomassie blue staining as described above, and revealed contaminants still present in the sample following ion exchange chromatography (Figure 2.7).

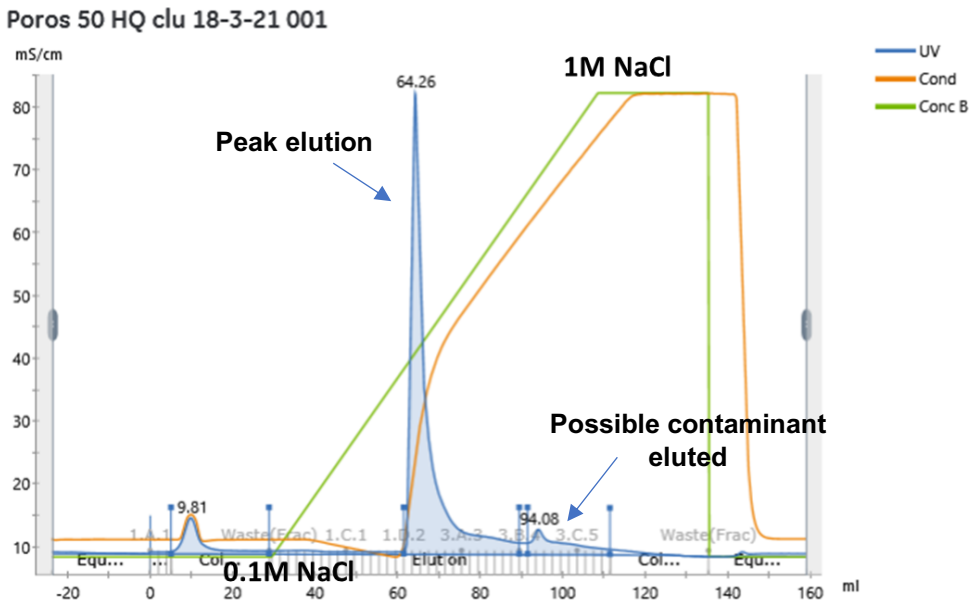

Figure 2.6. Ion exchange chromatography. Affinity purified clusterin containing an IgG contaminant was applied through an ion exchange column and eluted using a salt gradient. The blue line indicates changes in UV as the sample travels through the column, with a sharp spike during elution. The green line indicates an increase in the concentration of elution buffer. The orange line is an indicator of conductivity as the concentration of salt increases during the elution step.

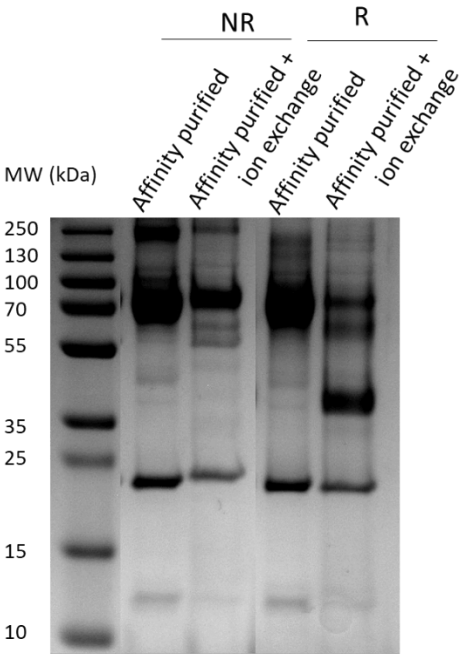

Figure 2.7. SDS-PAGE followed by Coomassie blue staining. Affinity purified clusterin and clusterin polished by ion exchange are shown under R or NR conditions. NR clusterin appears as a 70 kDa protein while R clusterin appears as a single 40 kDa band. IgG contaminant (150 kDa) is present in both samples. N=1 experimental repeat.

Ion exchange chromatography resulted in a large elution peak, containing the protein of interest, and a smaller peak, possibly containing the contaminant. When assessed by SDS-PAGE, in comparison to affinity purified clusterin, ion exchange purified clusterin showed a similar band pattern, indicating contaminants are still present.

2.3.4 Clusterin polishing by removal of contaminants on protein A/G columns

To remove the IgG contaminant from purified clusterin, a protein G column was used to trap the IgG while clusterin would freely flow through the column. Clusterin was purified from 50 ml plasma by affinity chromatography as described, dialysed into HBS buffer overnight and manually applied to a HiTrap NHS activated 5 ml protein G column (GE Healthcare) (section 2.2.2). Fractions were collected and concentrated to 0.6 mg/ml using a 30 kDa protein concentrating tube. The protein was subjected to SDS-PAGE to check purity and stored at -80°C. Results showed the sample was free of IgG, but contained residual contaminants at 55 and 20 kDa (Figure 2.8).

To further polish clusterin purifications and remove residual contaminants, clusterin preparations, either post-affinity (on two different columns) or post-gel filtration, were

incubated with protein A beads (section 2.2.4.3) and run on SDS-PAGE. For each preparation, bands corresponding to NR and R clusterin were dominant with a minor 20 kDa (Figure 2.9) contaminant in all lanes. The band intensity was examined in ImageJ, the clusterin band was >84% of the protein in each sample. The affinity purified samples were concentrated, aliquoted and stored at -80°C for future use as standard protein in ELISA.

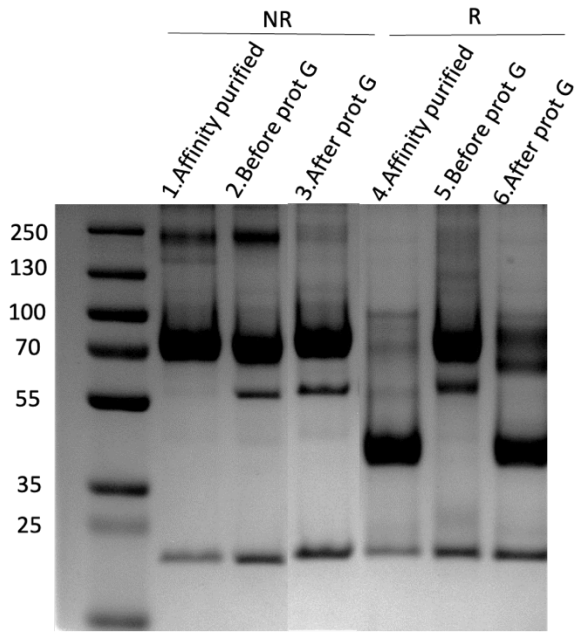

Figure 2.8. SDS-PAGE followed by Coomassie blue staining. Affinity purified clusterin and clusterin before and after IgG removal on protein G column (5 µg per lane) are shown. NR clusterin appears as a 70 kDa protein while R clusterin appears as a single 40 kDa band. IgG contaminant (150 kDa) is present in samples not applied through protein G column. Bands at 55 and 20 kDa can be observed in lanes 2 and 3 as contaminants co-purified with clusterin. Lane 5 has failed reduction, likely a loading error. N=1 experimental repeat.

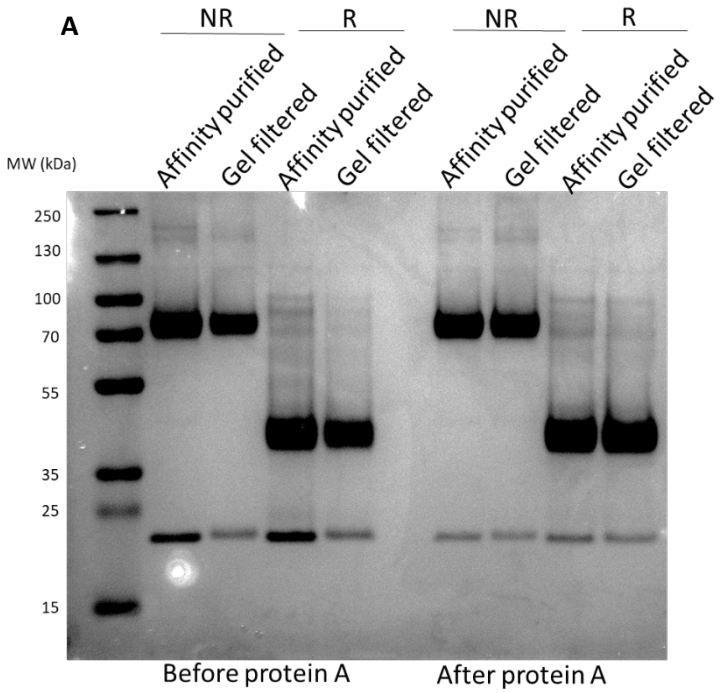

Figure 2.9. SDS-PAGE followed by Coomassie blue staining. Affinity purified and GF clusterin before and after IgG removal with protein A beads (2 µg per lane) are shown under R or NR conditions. NR clusterin appears as a 70 kDa protein while R clusterin appears as a single 40 kDa band. IgG contaminant (150 kDa) is present in samples before protein A beads incubation with lower intensity in the protein A cleaned-up samples. An additional band at 20 kDa can be observed in all samples as a contaminant co-purified with clusterin (**A**). Affinity purified clusterin on 2D5 column after removal of IgG using protein A beads (**B**). No IgG contaminant can be detected, however a 55 kDa contaminant is still present. N=1 experimental repeat.

Following the application of several different purification methods to obtain highly pure clusterin, protein A beads removal of IgG proved to be the most efficient, resulting in >84% pure clusterin. Although protein G beads also appeared to remove the higher molecular weight contaminant, 55 kDa and 20 kDa contaminants were still present (Figure 2.8). Lane 5 shows failed reduction of the protein, a limitation of performing a single round of SDS-PAGE experiments.

2.3.5 Generation of mAb against clusterin

To establish a sensitive assay able to measure clusterin levels in human biofluids, mAbs against clusterin were produced using hybridoma technology (section 2.2.6). Clusterin purified by affinity chromatography was used in the immunisation of three mice, which were screened for antibody production after a second boost. Serum from all three mice, and negative control WT serum from a non-immunised mouse, was screened in direct ELISA to determine which animal produced the highest antibody titre. A commercial mAb J84 anti-clusterin was used as a positive control (dilution range 1 - 0.0156 µg/ml). Data showed all animals produced mAbs against human clusterin in similar titres (Figure 2.10), and 2 of the mice (0, 1) were selected for progression.

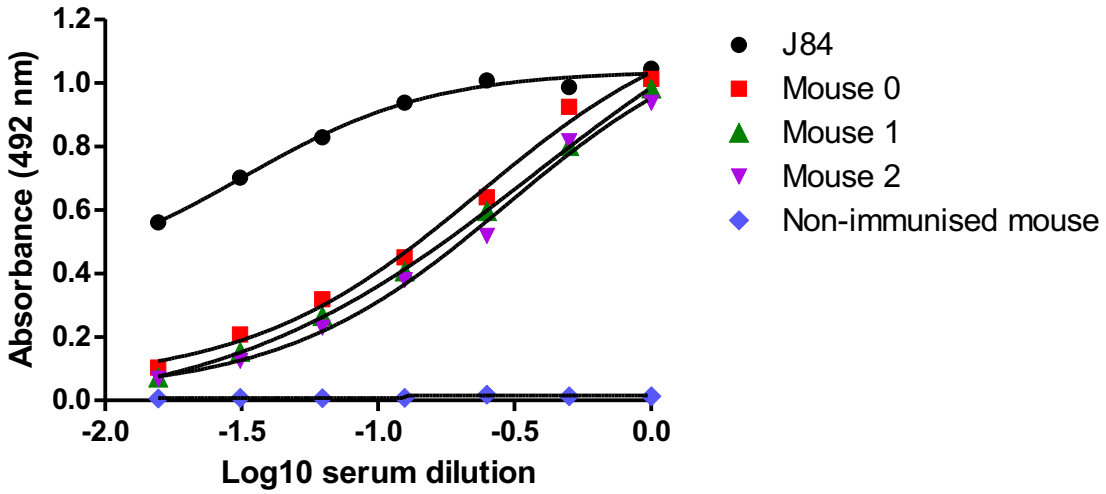

Figure 2.10. Direct ELISA screening for anti-clusterin mAb in serum of mice immunised against human clusterin. All three animals produced antibodies binding clusterin in a dose-dependent manner, while non-immunised (WT) mouse did not show mAb binding clusterin in ELISA. Samples were assayed in duplicate. N=1 experimental repeat.

The selected mice received a third injection of purified clusterin in PBS intraperitoneally two days before being sacrificed and their spleens harvested. The generation and re-cloning of hybridomas are described in detail in section 2.2.6.6. Clones were screened for antibody production before each re-cloning by direct ELISA as described above and 20 clones from each fusion (usually the lowest row with strong ELISA signal) were selected for a further re-cloning (Figure 2.11).

1	2	3	4	5	6	7	8	9	10	11	12
1.103	1.170	1.178	0.261	1.180	1.148	0.092	0.082	0.082	0.083	0.084	0.082
1.171	0.638	1.180	0.112	0.615	1.103	0.090	0.090	0.084	0.081	0.086	0.082
1.101	0.182	0.405	0.086	0.169	0.147	0.085	0.081	0.084	0.080	0.079	0.077
1.332	1.396	0.140	1.430	0.104	0.095	0.936	0.875	0.815	0.081	0.078	0.637
0.253	1.482	1.509	1.473	1.474	1.486	0.725	0.084	0.548	0.080	0.082	0.074
0.125	1.460	0.301	1.410	0.100	0.087	0.089	0.080	0.290	0.080	0.077	0.074
0.334	0.278	0.315	0.295	0.276	0.144	0.381	0.264	0.246	0.176	0.130	0.092
0.283	0.194	0.129	0.084	0.126	0.080	0.106	0.093	0.086	0.086	0.080	0.080

Figure 2.11. Absorbance values at 492 nm after a direct ELISA screening. TC supernatant from each well containing hybridoma cells producing antibodies against clusterin was added to an ELISA plate pre-coated with clusterin to identify the clones with highest antibody titres as highlighted in the table.

2.3.5.1 Antibody isotyping using sandwich ELISA

To determine the class and subclass of each mAb produced, isotyping was performed on TC supernatant from each clone during the fifth re-cloning. This method is described in section 2.2.6.7 and results are displayed in Figure 2.12. The mAbs were identified as IgG2b (clones 1A4, 1D5, 2D5, 6C12, 3C9, 5D11, 6D1), IgG2a (4C7), or IgG1. The mAbs and their isotypes are listed in Table 2.6.

	IgG1						
						controls	
Fusion 1	0.046	0.042	0.058	0.061	0.056	0.362	IgG1
	0.045	0.091	0.062	0.564	0.044	0.065	IgG2a
	0.070	0.044	0.041	0.067	0.052	0.045	IgG2b
	0.073	0.494	0.063	0.048	0.052	0.039	IgM
Fusion 2	0.053	0.054	0.064	0.045	0.041	0.038	
	0.053	0.079	0.050	0.060	0.061	0.039	
	0.080	0.096	0.087	0.390	0.276	0.038	
	0.051	0.472	0.559	0.480	0.072	0.040	

	IgG2a						
						controls	
	0.052	0.046	0.075	0.077	0.067	0.051	IgG1
	0.049	0.120	0.080	0.046	0.051	0.416	IgG2a
	0.614	0.051	0.046	0.534	0.517	0.062	IgG2b
	0.538	0.049	0.075	0.049	0.057	0.049	IgM
	0.065	0.070	0.101	0.048	0.046	0.046	
	0.058	0.596	0.593	0.584	0.072	0.044	
	0.092	0.122	0.100	0.519	0.467	0.047	
	0.061	0.060	0.054	0.054	0.173	0.049	

	IgG2b						
						controls	
Fusion 1	0.69	0.53	0.65	0.64	0.58	0.10	IgG1
	0.62	0.70	0.66	0.13	0.09	0.05	IgG2a
	0.20	0.63	0.60	0.39	0.18	0.49	IgG2b
	0.30	0.24	0.62	0.65	0.62	0.05	IgM
Fusion 2	0.59	0.63	0.54	0.62	0.61	0.05	
	0.58	0.37	0.62	0.63	0.66	0.04	
	0.60	0.66	0.64	0.64	0.71	0.05	
	0.65	0.52	0.14	0.57	0.65	0.05	

	IgM						
						controls	
	0.58	0.42	0.52	0.44	0.50	0.50	IgG1
	0.55	0.53	0.51	0.48	0.53	0.54	IgG2a
	0.51	0.52	0.51	0.47	0.53	0.52	IgG2b
	0.54	0.48	0.52	0.44	0.53	0.53	IgM
	0.51	0.53	0.55	0.51	0.40	0.28	
	0.56	0.56	0.62	0.55	0.43	0.45	
	0.55	0.56	0.61	0.53	0.54	0.39	
	0.57	0.54	0.57	0.53	0.52	0.34	

Figure 2.12. Isotyping of mAbs by ELISA. Supernatant containing antibodies against clusterin was added to plates coated with antibodies against IgG1, IgG2a, IgG2b, IgM to identify the class/subclass of each mAb generated. IgM isotyping could not be determined due to the secondary antibody binding to other IgG, giving positive signal for all control wells.

2.3.5.2 Antibody characterisation by ELISA and WB

mAbs produced (20 from each fusion) were tested in ELISA for their ability to recognise and bind human clusterin. Supernatant from each clone was used to detect clusterin in direct ELISA after the 5th recloning (Figure 2.13A). Out of forty clones, thirty eight displayed strong optical densities, and eight of them displaying the highest optical densities in direct ELISA (1A4, 1D5, 2D5, 3C9, 4C7, 6D1, 6C12 - highlighted in green) were selected to be expanded to T75 and T125 flasks for bulk purification. When used as capture in sandwich ELISA (Figure 2.13B), all antibodies displayed very similar optical densities. The eight mAbs selected were all of IgG subclasses (2a or 2b), preferred due to ease of affinity purification on protein G columns. All eight mAbs were tested in WB for their ability to specifically recognise clusterin in purified form and in human serum or plasma. Purified clusterin at 1 µg protein/lane and plasma diluted 1:300 in PBS were used in WB as described in section 2.4.2. Results showed all antibodies generated detected both NR and R clusterin, both purified and in plasma (Figure 2.14). A summary of antibody binding strength is included in Table 2.6.

A. Direct ELISA screening

0.69 1A4	0.49	0.67	**0.68 2D5**	0.57	**0.23 1A4**	0.22	0.25	**0.21 2D5**	0.23	0.43	+ control
0.42	**0.55 6C12**	0.55	0.53	0.17	0.25	0.24	0.25	0.25	**0.23 6C12**	0.15	PBS only
0.53	0.66	0.58	0.55	0.49	0.25	0.27	0.26	0.21	0.23		
0.48	0.54	0.49	0.49	0.49	0.28	0.23	0.27				
0.62	**0.62 1D5**	0.60	0.47	0.54	0.25	0.23	0.23	0.25	0.24		
0.60 3C9	**0.63 4C7**	0.61	0.61	**0.59 5D11**	**0.23 3C9**	0.26 4C7	0.24	0.25	**0.26 5D11**		
0.71 6D1	0.68	0.66	0.45	0.41	**0.24 6D1**	0.21	0.25	0.22	0.24		
0.50	0.18	0.52	0.58	0.51	0.24	0.23					

B. Sandwich ELISA using mAbs as capture

Figure 2.13. Testing of mAbs in direct ELISA following the 5th recloning (**A**), and in sandwich ELISA as capture (**B**) for their ability to recognise human clusterin. Clones highlighted in green were selected for antibody purification.

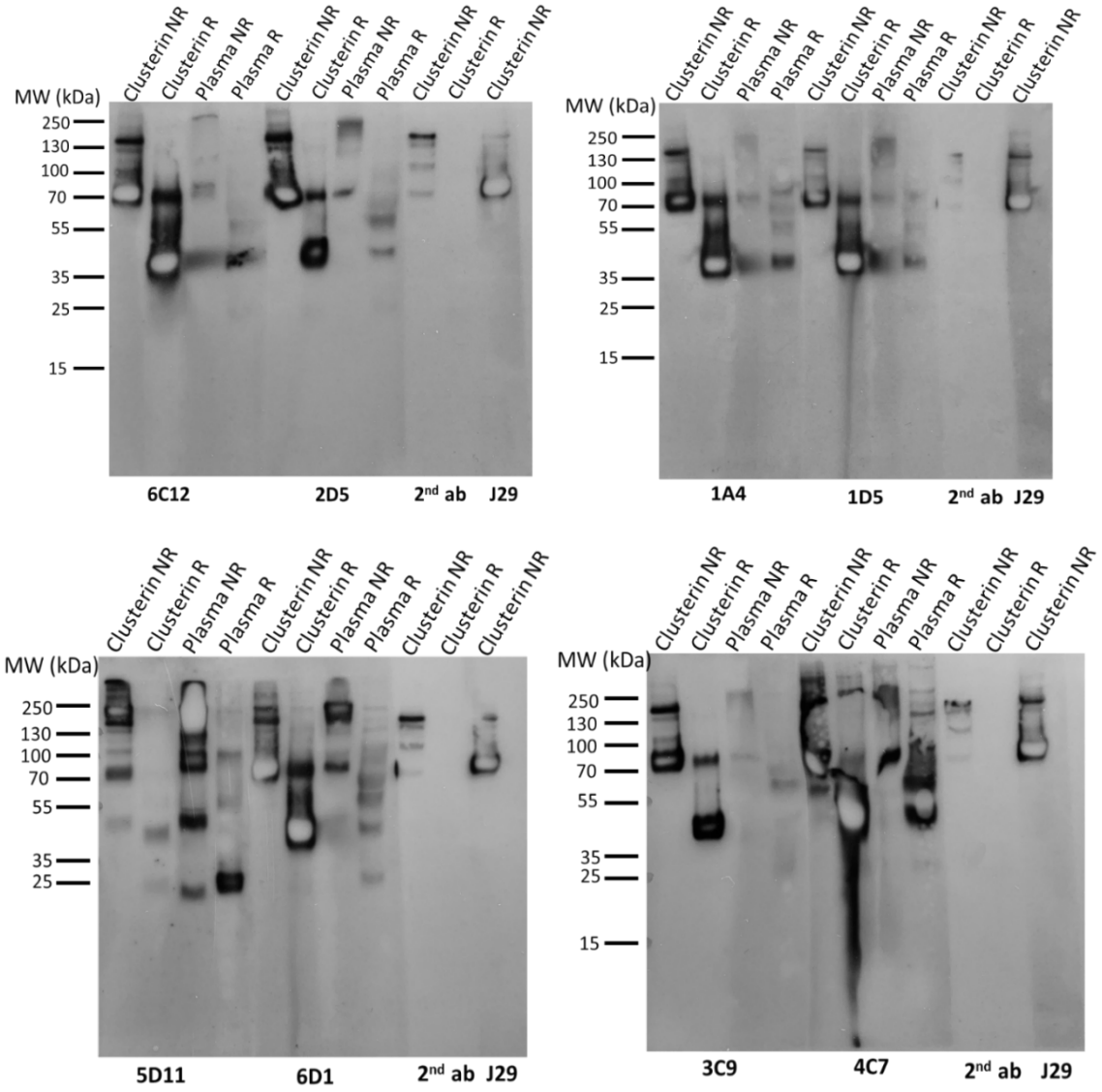

Figure 2.14. WB images of mAbs generated probed onto human clusterin. Antibodies in supernatant were used at 1:4 dilution in blocking buffer. A 70 kDa band corresponding to clusterin was identified in all blots on NR purified clusterin and plasma lanes. A ~40 kDa band corresponding to the α and β chains of denatured clusterin was identified in all blots on reduced purified clusterin and plasma lanes. Commercial antibody J29 was used as a positive control and showed a 70 kDa band in all blots, corresponding to full length clusterin. Bands of 150 kDa were also identified in NR plasma samples as IgG recognised by the donkey-anti-mouse IgG secondary antibody. N=1 experimental repeat for each antibody tested.

The antibodies generated in this chapter were thoroughly assessed before purification and assay set up to identify the ones most likely to perform well in sandwich ELISA. Direct ELISA screening was used to narrow down the candidate antibodies, isotyping was performed to determine their class, and Western blotting was carried out to determine their specificity. Band patterns were similar among antibodies as well as

compared to J29, a commercial antibody against clusterin used as a positive control. As antibodies were used in non-purified form (supernatant), this might have contributed to the differences in number and size of bands.

2.3.5.3 Antibody purification

All eight antibodies tested in ELISA and WB were purified on protein G affinity columns (Section 2.2.6.9). Purified mAbs were dialysed in PBS overnight at 4°C using 30 kDa cut-off cellulose dialysis membranes. mAb concentrations were determined by their absorbance at 280 nm (NanoDrop) and antibodies with concentrations below 1 mg/ml were concentrated using 10 kDa concentrator tubes. An example chromatogram trace is shown in Figure 2.15. Their purity was assessed by SDS-PAGE followed by Coomassie staining of the gels as previously described. Results showed one 150 kDa band corresponding to whole IgG in NR samples, and 55 kDa (IgG heavy chain) and 25 kDa (IgG light chain) bands for each R sample (Figure 2.16A). Boiling samples to 100°C before loading on the gel led to aggregation of IgG appearing as a >250 kDa band, as well as denaturing of the IgG molecule, with heavy and light chain bands appearing under NR conditions (Figure 2.16B).

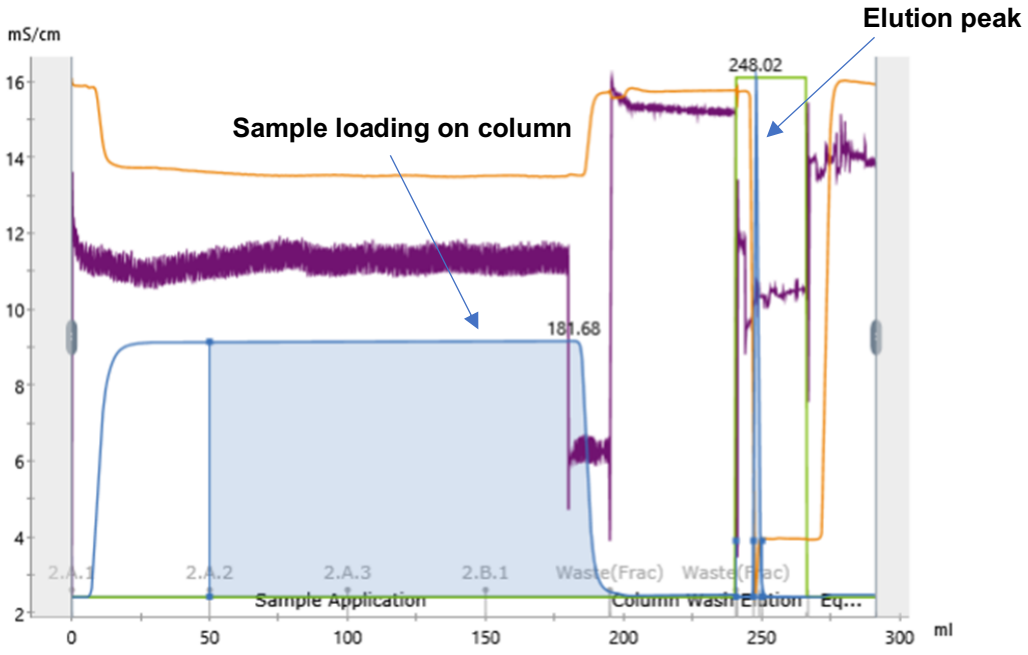

Figure 2.15. Example chromatogram for IgG purification of anti-clusterin mAbs by affinity chromatography on a protein G column. The blue trace indicates changes in UV as the sample passes through the column. The green trace indicates the concentration of elution buffer. The orange trace is a conductivity indicator showing changes in salt concentrations. The purple trace shows changes in the column pressure. All antibodies were purified following the same method, with column washes between each antibody.

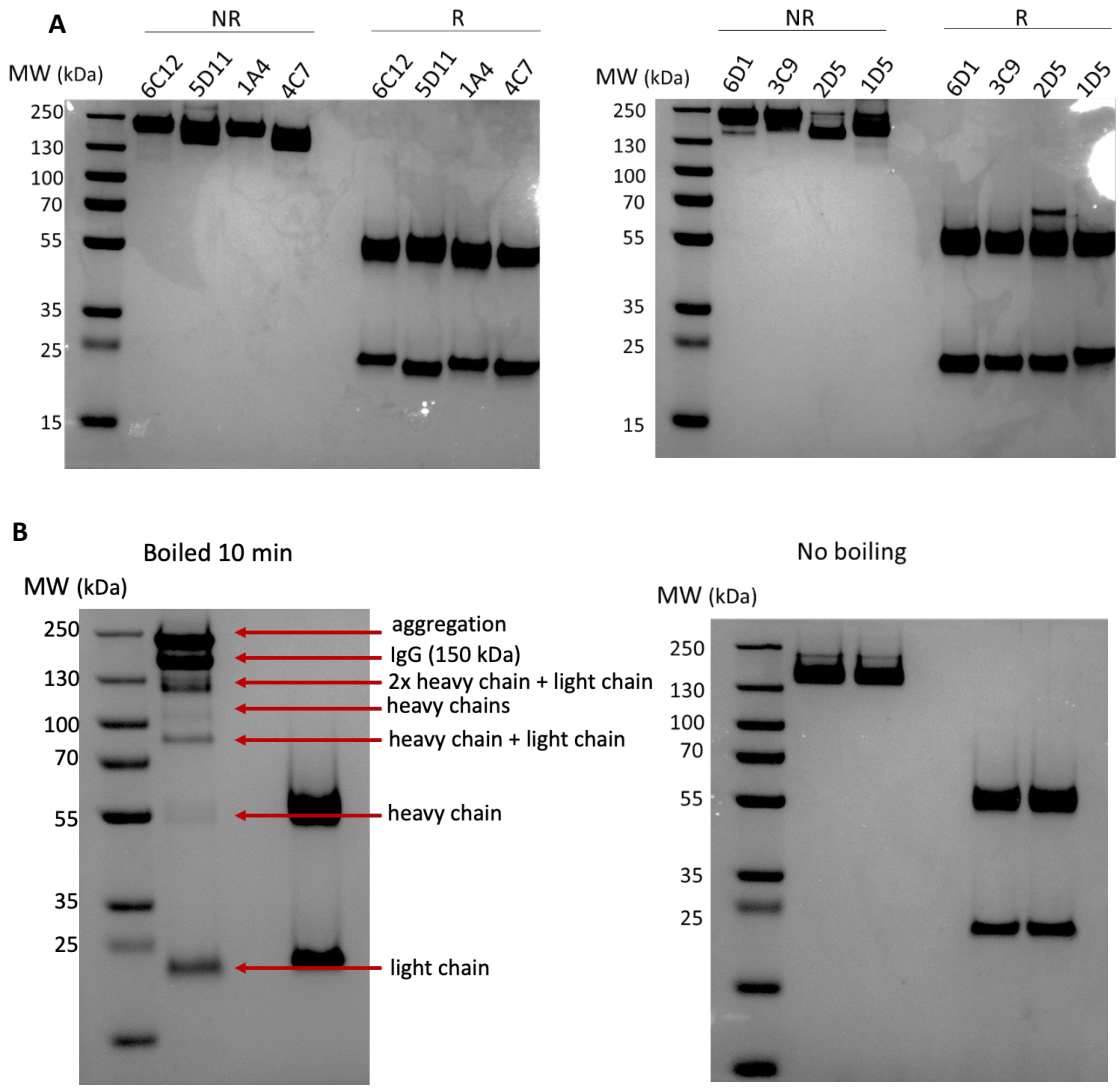

Figure 2.16. SDS-PAGE with Coomassie staining to verify the purity of mAbs. Non-reduced (NR) samples appear as one 150 kDa band corresponding to IgG, while reduced (R) samples appear as one 55 kDa band (IgG heavy chain) and one 25 kDa band (IgG light chain) (**A**). Heating IgG samples (clone 4C7 as example) to 100°C led to aggregation and denaturation of the IgG (**B**). n=1 experimental repeat.

2.3.6 Establishment of a sandwich ELISA capable of measuring clusterin in plasma

2.3.6.1 HRP labelling of mAbs

To set up an ELISA for measuring clusterin levels in biological fluids using the mAbs generated, 200 µl of each antibody (1 – 4 mg/ml) was conjugated to HRP in order to be paired with each other in a sandwich ELISA. This was performed according to the manufacturer's instructions, described in section 2.5.3.1. The labelled mAbs were tested in direct ELISA. Results showed all HRP-labelled mAbs except for clone 5D11

detected clusterin at concentrations ranging from 40 µg/ml to 9.8 ng/ml (Figure 2.17). The weak binding of clone 5D11 might suggest that the mAb affinity is impacted by the HRP labelling, and other tags such as biotin might be more suitable here.

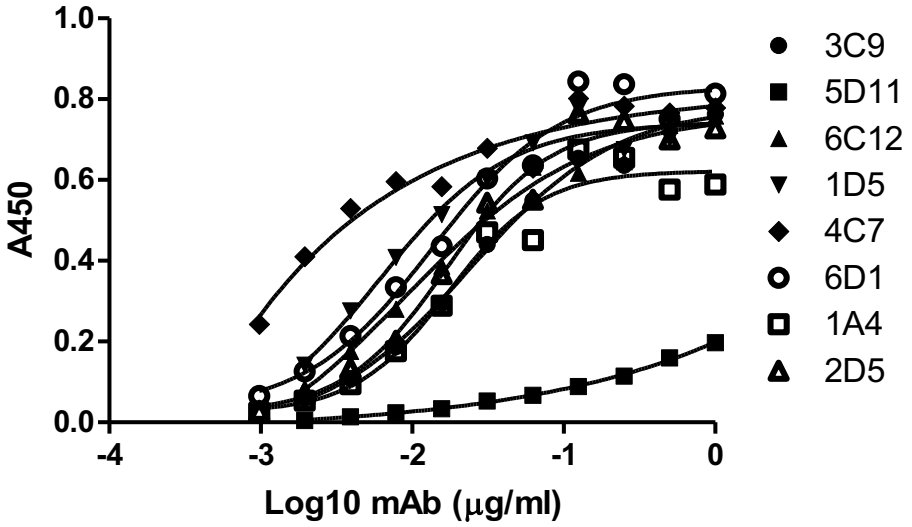

Figure 2.17. Standard curves of antibody binding following a direct ELISA test of HRP-labelled monoclonal antibodies against clusterin.

A summary of all the antibodies generated and tested in Western Blot and ELISA in this chapter is shown in Table 2.6.

Table 2.6. Clone name, isotype, binding in Western blot and ELISA, and concentration for each antibody generated in this chapter.

Clone	Isotype	Western Blot	ELISA capture	ELISA detection	Binding strength	Concentration (mg/ml)
1A4	IgG2b	Yes	Yes	Yes	Moderate	0.42
1D5	IgG2b	Yes	Yes	Yes	Weak	1.5
2D5	IgG2b	Yes	Yes	Yes	Strong	0.75
6C12	IgG2b	Yes	Yes	Yes	Moderate	0.6
3C9	IgG2b	Yes	Yes	Yes	Strong	1
4C7	IgG2a	Yes	Yes	Yes	Strong	0.42
5D11	IgG2b	Yes	Yes	No	Weak	1.2
6D1	IgG2b	Yes	Yes	Yes	Moderate	0.7

2.3.6.2 Development of the clusterin sandwich ELISA

To identify an optimal pair of mAbs against human clusterin for validating an ELISA with the purpose of measuring clusterin levels in biological fluids, all eight selected mAbs were paired in sandwich ELISA as capture or detection as detailed in section 2.2.7.6. Absorbance was read at 450 nm using a spectrophotometer and results plotted as sigmoidal dose-response curves (Figure 2.18). Results showed the combination of mAbs 2D5 and 4C7 gave the highest optical densities, followed by pair 3C9 and 6D1. No signal was detected when the same mAb was used as both capture and detection, showing all antibodies were monoclonal and recognised a single epitope on clusterin. Certain pairs (e.g. 2D5 with 6D1; 1D5 with 6C12, 1A4, 3C9) showed very weak signals, suggesting that they recognised the same or overlapping epitopes on human clusterin. mAb 4C7 detected clusterin regardless of the antibody used as capture indicating that it was against a unique epitope, but showed strongest signal when paired with mAb 2D5. Therefore, this pair was used to set up and optimise a sandwich ELISA (Figure 2.18).

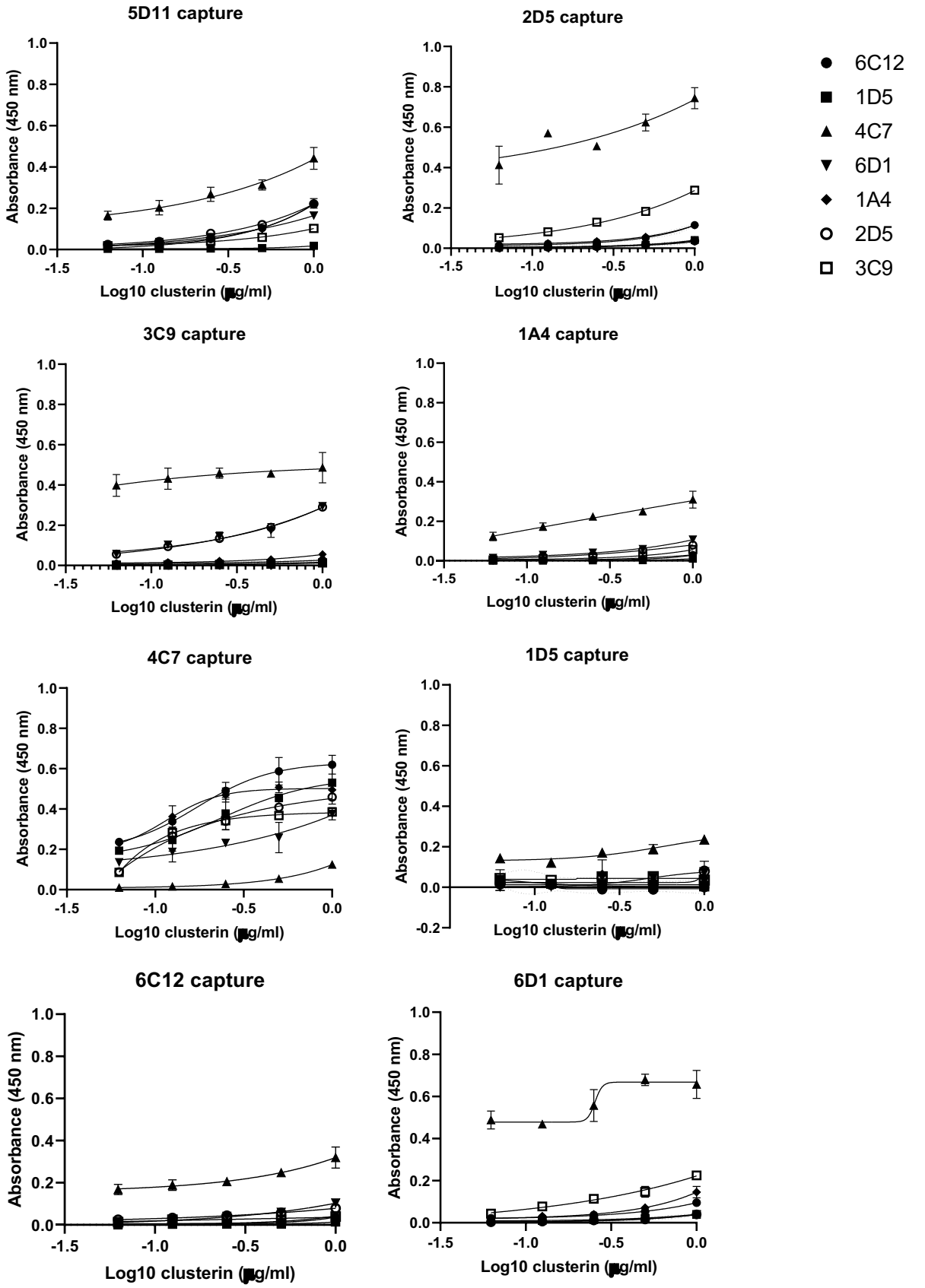

Figure 2.18. mAb pairing in sandwich ELISA. Each antibody was used as capture at 2 µg/ml, pure clusterin was used as standard from 1 µg/ml, and HRP-labelled detection antibodies were used at 1:200. N=1 experimental repeat.

The antibodies generated in this chapter showed strong and specific binding to human clusterin, and were demonstrated to be monoclonal. The optimal pair was selected based on sandwich ELISA screening to obtain a standard curve with a high signal to noise ratio.

2.3.6.3 Clusterin sandwich ELISA optimisation

mAb 2D5 and 4C7-HRP were selected as capture and detection, respectively from the above characterisation and the impact of different concentrations on the mAbs on signal was tested (Figure 2.19). The optimised assay used 5 µg/ml capture antibody, 2 µg/ml HRP-labelled detection antibody, standard curve starting at 2 µg/ml clusterin serially diluted 1:2 (Figure 2.20A). The lower limit of detection was 8 ng/ml while the upper limit of detection was 5 µg/ml (Figure 2.20B). The spike recovery of the assay was assessed by depleting plasma of clusterin by affinity chromatography, adding pure clusterin back to plasma at a concentration of 150 µg/ml and measuring it to test how much of the added protein was recovered (Figure 2.20C). The reproducibility of the assay was challenged by measuring the same 16 samples three times in separate experiments to determine the assay CVs (3.93% intra-assay CV, 8.5% inter-assay CV, Figure 2.20D). Five plasma samples were used to test the linearity of the assay, by interpolating serial 1:2 dilutions from 1:200 – 1:3200 on the standard curve (Figure 2.20E, F). The assay was able to measure clusterin levels in matched serum (mean=267.2 µg/ml, range 144.5 – 485.9 µg/ml) and CSF (mean=3.55 µg/ml, range 2.51 – 3.21 µg/ml) samples at 1:2000 or 1:50 dilutions, respectively (Figure 2.20G). The samples were a subset of heathy controls recruited as part of a multiple sclerosis observational study in South East Wales (Ethics REC ref: 05/WSE03/111, 19/WA/0289).

Detection / Capture (µg/ml)	1:200	1:400	1:800	1:1600	1:3200	1:6400	1:12800
4.5	1.5199	1.4617	1.40525	1.3292	1.2954	1.17365	0.83005
3.125	1.48755	1.42295	1.3429	1.22945	1.1515	1.11205	0.824
2	1.3377	1.37145	1.3162	1.1267	1.17245	1.0201	0.76985

Figure 2.19. Optimising concentrations of capture and detection mAbs in the sandwich ELISA. Different concentrations of capture and detection (dilutions from 1mg/ml stock) mAbs were tested to determine the optimal signal with a saturating amount of clusterin (1 µg/ml).

A

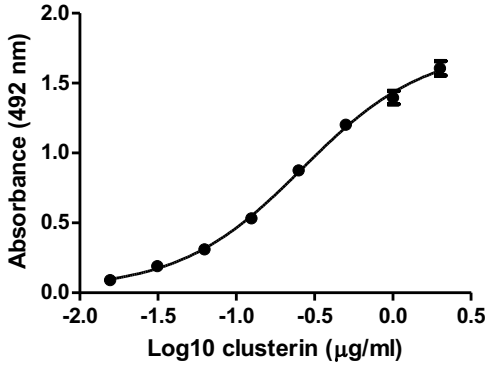

B

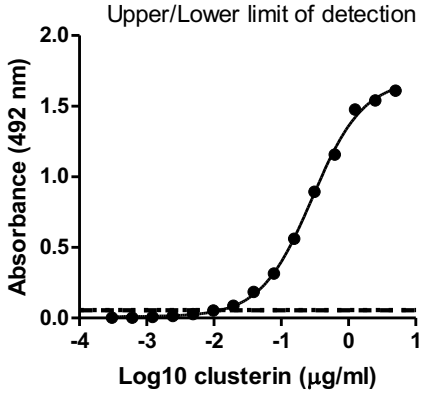

C

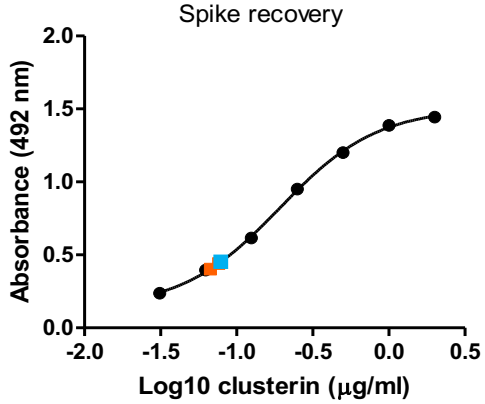

D

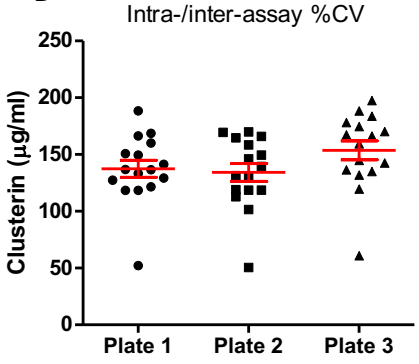

E

Dilution factor	1	2	3	4	5
200	158.55	142.90	141.79	136.82	128.73
400	152.66	124.42	121.82	117.44	114.77
800	142.83	115.85	134.13	124.98	132.14
1600	141.27	114.29	129.76	131.34	127.74
3200	157.84	136.85	149.23	127.89	144.63
Average (µg/ml)	150.63	126.86	135.35	127.70	129.60
%CV	5.43	9.99	7.84	5.66	8.24

F

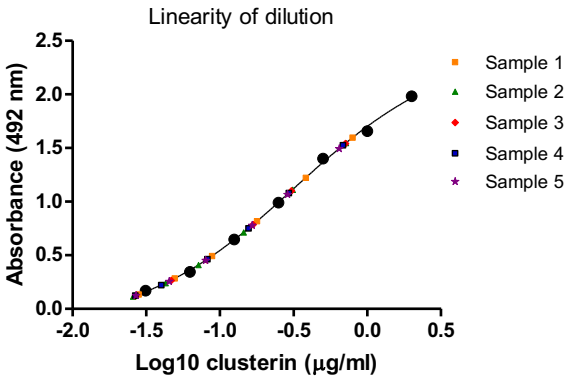

G

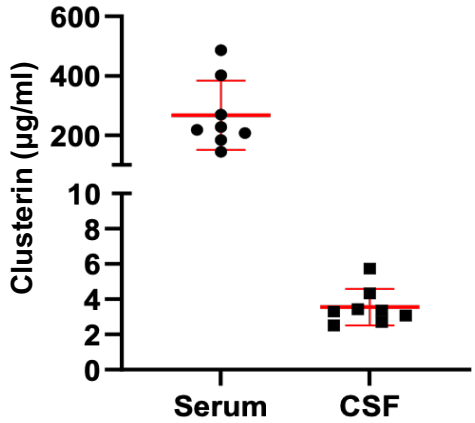

Figure 2.20. Set up and characterisation of sandwich ELISA using in-house mAbs against human clusterin. A standard curve was prepared by serially diluting purified clusterin starting at 2 µg/ml, with 2D5 as capture and 4C7 as detection (**A**). The upper and lower limits of detection were determined as 5 µg/ml and 8 ng/ml, respectively. The dashed line indicates the detection limit of the assay (**B**). Spike-recovery was determined by adding known amounts of pure clusterin (150 µg/ml) to clusterin-depleted plasma and quantifying them in ELISA. The orange dot represents human plasma (diluted 1:2000) and the blue dot represents the same plasma sample (diluted 1:2000) with 150 µg/ml clusterin added back following clusterin depletion interpolated on the standard curve (**C**). The intra- and inter-assay CVs were calculated by measuring plasma clusterin levels three times in 16 plasma samples (**D**). The linearity of the assay was assessed by interpolating a wide range of plasma dilutions on the standard curve (**E, F**). Matched serum and CSF samples were obtained from a multiple sclerosis observational study in South East Wales and used to test the assay's ability to measure clusterin in complex biological matrices (**G**).

The ELISA established in this chapter was characterised following a set of well-established experiments to determine its lower and upper limits of detection, test its spike recovery, linearity of dilution, and ensure it is suitable for measuring clusterin in plasma and CSF samples. Mean clusterin levels in serum were 267.2 µg/ml, similar to previously published results using a different assay (Hakobyan et al, 2016), while CSF levels (3.55 µg/ml) were also similar to literature reported values (3.5 µg/ml, Jongbloed et al, 2015).

2.3.6.4 Measuring plasma clusterin levels using commercial antibodies in ELISA

The new assay was compared with a previously reported sandwich ELISA using commercially available antibodies (described in section 2.2.7.7) by measuring clusterin levels in plasma samples from 23 healthy volunteers; the average plasma value using the commercial assay was 81.59 µg/ml, significantly lower than that obtained using the in-house assay (137.4 µg/ml) confirming greater sensitivity (Figure 2.21).

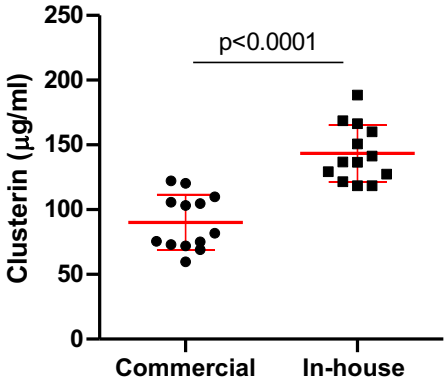

Figure 2.21. Clusterin plasma values determined in an ELISA using commercial mAbs compared to the novel in-house assay. Samples were quantified in duplicate. N=23 healthy subjects. *** p<0.001, two-tailed unpaired t-test.

Several human clusterin ELISA kits are commercially available from independent vendors and have been used in previous publications to measure clusterin in human plasma. Table 2.7 shows technical data for three commercial ELISAs (Biovendor RD194034200R, R&D Quantikine DCLU00, Invitrogen 15414953) compared to the assay generated in this chapter. All commercial assays appear to have greater sensitivities, while intra- and inter-assay CVs are similar.

Table 2.7. Range, lower limit of detection, plasma dilution, intra- and inter-assay CVs for commercial assays compared to the in-house assay.

ELISA kit source	Range	LLOD	Plasma dilution	Intra-assay %CV	Inter-assay %CV
BioVendor (RD194034200R)	5-160 ng/ml	0.5 ng/ml	1:3000	6.2	7.8
Quantikine R&D (DCLU00)	0.064-1.05 ng/ml	0.189 ng/ml	1:2000	3.6	7.5
Invitrogen (15414953)	15.53-20,000 pg/ml	15 pg/ml	1:100,000	<10%	<12%
In-house	8-5000 ng/ml	8 ng/ml	1:2000	3.93	8.5

2.4 Discussion

This chapter describes the production of mAbs against human clusterin using hybridoma technology and purification of native human clusterin protein through affinity chromatography, two well-established molecular biology techniques for immunoassays. Hybridoma technology, the most common method for mAbs generation, dates back to 1975 (Kohler & Milstein, 1975), and was used successfully in this chapter to obtain mAbs against human clusterin. Affinity chromatography, a purification method involving an antibody against the target protein coupled to a chromatography column through which the samples pass, was used to purify clusterin and IgG using columns packed with in-house anti-clusterin antibodies or protein G columns. Although this technique is reliable and relatively straightforward when purifying IgG, other proteins can be more difficult to purify and may require additional polishing steps to obtain samples of high purity. Following clusterin purification, SDS-PAGE analysis revealed contaminants of ~150, ~55 and ~20 kDa, in addition to clusterin (80 kDa). Size exclusion chromatography was then used to separate these

molecules based on their size, but it did not completely remove the contaminants and resulted in lower yields of clusterin. Because the ~150 kDa contaminant was believed to be IgG due to the very high IgG content of plasma, and due to previous findings that clusterin and IgG may interact to form immune complexes (Wilson et al, 1992), purified clusterin was incubated with protein A beads in order to remove the contaminant if it was indeed IgG. This proved to be the best strategy for obtaining human clusterin of high purity.

At the start of this project, very few antibodies against clusterin and ELISA kits for quantification of clusterin in human samples were commercially available, and their high cost and compromised sensitivity makes it difficult to measure clusterin in large sample sets. Since clusterin has been shown to be implicated in AD pathology and may be a plasma biomarker for AD, specific antibodies against clusterin that could be used in various immuno-assays were needed to study this enigmatic protein. As described in Chapter 1, numerous studies have already investigated clusterin levels in human plasma from various cohorts, and results varied depending on the type of assay used. Due to the high affinity and specificity for human clusterin of the two antibodies (2D5 and 4C7) selected for the sandwich ELISA in this thesis, they have been licensed to Hycult Biotech (#HM2435, #HM2436) to be commercialised and used by the scientific community in ELISA and WB.

A sandwich ELISA to accurately quantify clusterin in human biological fluids was set up using two of the antibodies and purified clusterin as standard protein, and was used to measure clusterin in human plasma, CSF, cell lysate and supernatant throughout this project. Additionally, all antibodies bound secreted clusterin in human serum in WB, and some of them also bound intracellular clusterin isoforms in brain immunohistochemistry (Chapter 3) and iPSC-derived astrocyte lysate (Chapter 5). These antibodies therefore have the potential to improve our understanding of roles of clusterin in disease and aid research by facilitating quantification and localisation of a ubiquitous and important protein.

In the following Chapters I will utilise these reagents and assays to further explore the role of clusterin as a biomarker in plasma and CSF from AD patients and healthy controls, quantify clusterin in supernatant and cell lysate from iPSC-derived astrocytes, and visualise clusterin protein in AD brain tissue by immunohistochemistry.

CHAPTER 3: Quantification of clusterin in plasma and CSF from Alzheimer's disease patients and cognitively normal individuals

3.1. Introduction

Alzheimer's disease, a slowly progressing neurodegenerative disease with brain pathology beginning as early as 20 years before the onset of symptoms, requires specialist assessment in order for a correct diagnosis to be determined. This often involves a clinical assessment based on cognitive tests, such as MMSE, and may be accompanied by PET imaging of plaques and tangles in the brain or measurements of Aβ and pTau in CSF. CSF levels of neurofilament light (NfL), a nonspecific marker of neuronal damage, and GFAP, a marker of astrocytic reactivity, are useful aids in diagnosing AD that, together with the Aβ peptides and pTau, establish the AT(N) (amyloid/tau/neurodegeneration) diagnostic framework (Alcolea et al, 2021; Jack et al, 2018). While PET imaging and CSF analyses can be extremely informative of disease stage and progression, they are expensive and invasive, which prompted the search for reliable blood-based biomarkers that facilitate early diagnosis. Since blood is an easily accessible biofluid which can be collected with minimal discomfort to the patient, blood biomarkers enable longitudinal studies to be carried out; however, many proteins are synthesised in the liver and circulate in blood, which can interfere with plasma measurements of CNS-specific biomarkers. AT(N) markers measured in plasma can perform very well in distinguishing AD from controls with receiver operating characteristic (ROC) curve analyses delivering an area under the curve (AUC) >0.75 for the combined analytes (Palmqvist et al, 2021). CSF may reflect brain pathology more closely, however CSF collection is invasive and costly, and needs to be performed in a clinical setting. Nevertheless, CSF remains a valuable tissue that can inform of disease presence, severity, and progression, unlike brain tissue which can only be obtained following autopsy.

Clusterin was first linked to AD pathology in 1992, when two studies showed clusterin colocalization with Aβ plaques in brain tissue from AD patients, as well as increased clusterin concentrations in CSF from AD patients compared to healthy controls (McGeer et al, 1992; Choimiura et al, 1992). Further studies confirmed the presence of clusterin in Aβ plaques (Verbeek et al, 1998; Lidstrom et al, 1998); however, investigations of clusterin levels in CSF and blood from AD patients compared to

controls led to inconsistent results (Liao et al, 2007; Sihlbom et al, 2008). While several studies have shown increased clusterin levels in plasma or CSF from AD patients compared to healthy controls, other studies have found no significant differences, and a meta-analysis conducted by Shi et al in 2019 concluded that neither plasma nor CSF levels of clusterin were significantly altered in AD vs control. In the brain, clusterin levels measured by ELISA were found to be highest in regions affected by Aβ pathology, especially in *APOEε4* homozygotes (Miners et al, 2016). In inferior temporal lobe brain tissue, using Western blot quantification, both intracellular and secreted clusterin were shown to be elevated in AD vs control, and increased together with Aβ deposition and insoluble total tau (Shepherd et al, 2020). In contrast, using multiple reaction monitoring mass spectrometry, Chen et al (2012) found a significant increase in clusterin levels in severe AD compared to control in frontal cortex, and not temporal cortex. In this chapter, temporal cortex tissue from AD and control subjects will be used for immunostaining.

While most AD cases arise spontaneously, without a clear genetic determinant, rare mutations in the amyloid precursor protein (*APP*) and presenilin (*PSEN1*, *PSEN2*) genes have been confirmed to cause familial AD (Ertekin Taner, 2007). In people with Down Syndrome (DS), a consequence of triplication of chromosome 21 harbouring the *APP* gene is an increase in *APP* expression and rapid and sustained deposition of Aβ in the brain, causing AD in these individuals. By the age of 40, almost all people affected by DS display typical AD neuropathology, notably the presence of Aβ plaques, a pathological hallmark of AD which is associated with early onset dementia. Stoltzner et al (2000) showed clusterin colocalization with Aβ plaques in brain tissue from individuals with DS, however clusterin has not been measured in plasma or CSF from people with DS. As clusterin plays an essential role in Aβ pathology, its plasma levels in people with DS could be informative in a population with a genetically determined form of AD, in addition to cohorts involving sporadic AD cases.

To investigate the role of clusterin in AD as a blood or CSF biomarker, and explore its role in the brain, this chapter has four aims: 1) utilise the assay developed in chapter 3 to accurately quantify levels of clusterin in plasma from a very large cohort (1907 samples) of non-familial early onset or late onset AD patients and healthy elderly controls, two small CSF sample sets from individuals diagnosed with AD following

amyloid and tau CSF measurements, and a cohort of individuals with DS with and without AD; 2) determine whether clusterin is a reliable biomarker in distinguishing AD from control using ROC curve analyses; 3) correlate the results with measurements of AT(N) biomarkers and demographic data.

3.2 Methods

3.2.1 Biological sample processing and demographic data

Plasma samples forming the AD cohort (n=504 control, 912 early onset AD, 492 late onset AD) were part of the AD Cardiff Cohort (ADCC). These were collected between 2004 and 2020 using MRC, Moondance Foundation, and Health and Care Research Wales funding. Information on age at assessment, sex, MMSE, and genome-wide array genotyping was available for almost all samples. Information on age at onset was also available for 1396 cases, and disease duration was calculated for these samples. All participants were of Caucasian descent. Demographic data are shown in Table 3.1. Additionally, levels of AT(N) biomarkers (Aβ40, Aβ42, ptau-181, NfL, GFAP) were determined using the Simoa P-tau181 Advantage Kit and the Simoa Human Neurology 4-Plex E (N4PE) assay (Quanterix, Billerica, MA) at University College London. These data were used for correlations with measurements obtained in this study.

CSF samples from probable AD patients and age-matched controls were obtained from collaborators at the University of Gothenburg (n=30 control, 30 AD) or University College London (n=8 control, 31 AD) and were not matched to plasma samples. CSF was collected by lumbar puncture from individuals referred to the clinic for neurological assessment, and diagnosis established based on measurements of Aβ and pTau CSF levels. No clinical assessment was carried out for the patients and therefore diagnosis was not confirmed by clinicians. Demographic data are shown in Table 3.2.

Plasma samples from individuals with DS (n=71) were obtained from the London Down Syndrome Consortium (LonDownS), a prospective longitudinal study following adults with DS. Presence of DS was confirmed genetically using OmniExpressExome arrays (Illumina, San Diego, CA, USA) on blood or saliva samples, with trisomy status being visually confirmed in GenomeStudio software (Illumina). *APOE* status was determined using TaqMan assays for rs7412 and rs429358 (Thermo Fisher Scientific, Waltham,

MA, USA). Level of intellectual disability was based on ICD-10 diagnostic criteria and dementia diagnosis was taken from clinical records and medical history. Plasma samples were collected in EDTA tubes, centrifuged at 2000 x g at 4°C for 10 minutes, and stored at the Social, Genetic and Developmental Psychiatry Centre, King's College London in -80°C until analysis. Age-matched control plasma samples (n=46) were from healthy volunteer donors at Newcastle University and Cardiff University. Informed consent was obtained from each participant. Blood was collected in EDTA tubes, centrifuged at 4°C for 10 minutes, and plasma collected and stored at -80°C. Demographic data are shown in Table 3.3.

Table 3.1 Demographic data and genotypes at *CLU* SNPs for AD and control subjects in the ADCC cohort.

	EOAD	LOAD	Control
Number	912	492	504
Sex, n (%)			
Female	425 (46.6)	243 (49.39)	282 (56)
Male	487	249	222
Age at onset			
Mean (SD)	58 (5.16)	71 (5.34)	n/a
Range	28 – 65	66 – 90	n/a
Age at inclusion			
Mean (SD)	64 (5.7)	76 (5.46)	82.5 (6.8)
Range	30 – 90	66 – 97	59 – 100
Disease duration			n/a
MMSE score (SD)	16.34 (10)	18 (9.23)	27.4 (5.5)
***APOE* status, n (%)**			
ε4 (-)	402	184	400
ε4 (+)	491 (55)	289 (61)	93 (18.9)
rs11136000, n			
CC	370	204	172
TC	412	227	242
TT	130	61	82
rs9331888, n			
CC	462	236	254
GC	374	177	201
GG	74	46	35

Table 3.2 Demographic data and AT(N) status of AD and control participants in the CSF cohorts.

	Gothenburg Samples		UCL samples	
	AD	Control	AD	Control
Number	30	30	31	8
Sex, n (%)				
Female	17 (56.6)	15 (50)	21 (68)	2 (25)
Male	13	15	10	6
Age				
Mean (SD)	48.53 (8.17)	52.27 (11.51)	63 (7)	70 (8)
Range	31 – 66	30 – 79	52 – 80	62 – 82
AT(N) status				
Aβ (pg/ml)	465	908.6	395	N/A
Tau (pg/ml)	783	228.3	805	N/A
p-tau (pg/ml)	106	27.6	N/A	N/A
CSF albumin (µg/ml)	623	557	775	823

Table 3.3 Demographic data and genotypes at *CLU* rs11136000 for subjects with DS part of the LonDownS study, and healthy controls.

	Down Syndrome	Control
Number	71	46
Sex, n (%)		
Female	25 (35.2)	29 (63)
Male	46	17
Race, n		
White	62	
Other	6	
Unknown	3	46
Age		
Mean (SD)	40.69 (13.22)	37 (11.7)
Range	21 – 69	22 – 65
Learning disability, n		
Mild	30	n/a
Moderate	34	n/a
Severe/profound	6	n/a
Dementia, n	13	n/a
Age at dementia onset (SD)	52.5 (13.3)	n/a
***APOE* status, n**		
ε4 (-)	47	
ε4 (+)	16	
Unknown	9	46
rs11136000 genotype, n		
CC	21	n/a
TC	25	n/a
TT	12	n/a

3.2.2. Quantification of clusterin using sandwich ELISA

Sandwich ELISA to quantify clusterin in plasma and CSF samples was performed as detailed in section 2.4.3. Antibodies used were 2D5 α-Clusterin at 5 µg/ml (capture) and 4C7-HRP α-Clusterin at 2 µg/ml (detection). Pure clusterin was used to construct a 9-point standard curve starting at 2 µg/ml, serially diluted 1:2. Plasma samples were diluted 1:2000, and CSF samples 1:50. Clusterin concentrations in samples were obtained by interpolating the averaged optical density values for each sample on the curve and multiplying the obtained values by the dilution factor. Experiments were performed blinded to diagnosis. Samples were measured in batches of 288 – 360/day, and the same two plasma samples were included on each plate to control for variation between plates and batches. All plates were incubated with developing solution for 5 minutes. All measurements were performed in duplicate. Where a sample qualified as an outlier (1.5 times higher than the third quartile or 1.5 times lower than the first quartile in the interquartile range of the whole cohort), this was remeasured at a suitable dilution that allowed interpolation on the standard curve.

3.2.3. Statistical analyses

Data were plotted using GraphPad Prism 5, tested for normality of distribution using the Kolmogorov-Smirnov test and analysed statistically using IBM SPSS Statistics 26 by t-tests, ANOVA, general linear models adjusting for sex and age, or Pearson correlations as appropriate. To determine if the duration of storage at -80ºC of plasma samples had an effect on clusterin levels, storage time and clusterin levels were tested for correlation. There was no significant effect of storage time on clusterin levels ($r=0.006626$, $p=0.7768$), therefore this was not included as a confounder in statistical analyses. Receiver operating characteristic (ROC) curves were used to assess the predictive power of clusterin as a biomarker to distinguish between cases and controls. ROC curves were performed using GraphPad Prism 9.5.1, with area under the curve (AUC) reported as a percentage, and confidence intervals calculated using the Wilson/Brown method.

3.2.4. Immunohistochemistry

Immunohistochemistry was performed on 10 µm thick human temporal cortex tissue sectioned using a cryostat by Dr Lewis Watkins, in accordance with the Human Tissue

Act 2004 regulations. Tissue sections on microscope slides were frozen at -80°C and allowed to dry for 20 mins at 37°C before staining. Each section was circled using a water repellent pen to create a hydrophobic barrier around the tissue. Two sections for each condition were fixed using 200 µl 4% PFA for 10 mins, washed twice with PBS, then blocked with 200 µl 3% BSA and 5% normal goat serum in PBS with 0.5% triton-X (blocking buffer) for 1 hour at RT. Primary antibodies were diluted in blocking buffer and 200 µl were added over each tissue section, except for the negative control for which PBS was used. Primary antibodies were used at the following concentrations: 6e10 anti-Aβ mAb (Enzo Life Sciences #ENZ-ABS612-0200) at 1:500, 2D5 and 4C7 anti-clusterin mAbs (in-house) at 1:300, polyclonal rabbit anti-GFAP (Agilent Dako #GA524) at 1:5000. AlexaFluor-conjugated secondary detection antibodies (goat anti-mouse 594 Invitrogen #A32742; goat anti-rabbit 488 Invitrogen #A11008) were used at 1:1000. Negative control staining was performed by omitting the primary antibody step, or using an isotype control at the same concentration as the corresponding primary antibody: mouse IgG2a (Biolegend #401501), mouse IgG2b (Biolegend #400301), rabbit IgG (Invitrogen #02-6102). Slides were incubated at 4°C overnight, washed three times with PBS, and incubated with 200 µl/slice AlexaFluor-conjugated secondary antibodies diluted 1:1000 and Hoechst diluted 1:500 in 0.5% triton-X in PBS for 1 hour at RT. Slides were washed three times with PBS, incubated with 0.5 ml Sudan Black for 5 mins, dipped in 50% EtOH 10 times, rehydrated with H_2O, and mounted using FluorSave reagent (Millipore #345789). Images were captured using a Leica SP8 confocal microscope and Z stacks were analysed using the LASX software.

3.3. Results

3.3.1. Clusterin plasma levels are elevated in AD patients compared to controls

In the AD cohort, plasma levels of clusterin quantified by ELISA were significantly higher in AD patients compared to controls (mean = 217.9 vs 195.8 µg/ml, $p<0.0001$; Figure 3.1A). When the AD group was split into early onset and late onset groups, clusterin levels were significantly higher in early onset compared to late onset (mean = 224.6 vs 205.8 µg/ml; $p<0.001$) and control subjects (mean = 224.6 vs 195.8 µg/ml; $p<0.001$) (Figure 3.1A). There was no significant difference between males and females in clusterin levels in the AD groups; however, in controls clusterin levels were

significantly higher in females compared to males (mean = 206.8 vs 182.8 µg/ml, p<0.001; Figure 3.1A). *APOEε4* carriers showed a trend for increased clusterin levels compared to non-carriers, particularly in the control group (Figure 3.1B). A significant correlation was identified between plasma clusterin levels and Aβ40 in cases (Figure 3.1C). No significant correlations were found between clusterin levels and MMSE scores, age at onset/inclusion in the study, or disease duration.

3.3.2 Plasma clusterin is not a good predictor of AD

To determine whether plasma clusterin can discriminate AD from control, ROC curves were performed on the EOAD and LOAD groups against control. Clusterin was a poor predictor for AD, with AUCs of 52.44% for LOAD (95% CI 0.4884 – 0.5603, p=0.184) and 60.14% for EOAD (95% CI 0.5704 – 0.6323, p<0.0001) (Figure 3.2). While a significant difference between means in the AD and control group was identified likely due to the large number of samples, ROC curves do not replicate these findings as the difference in clusterin concentration between the two groups was only 10%.

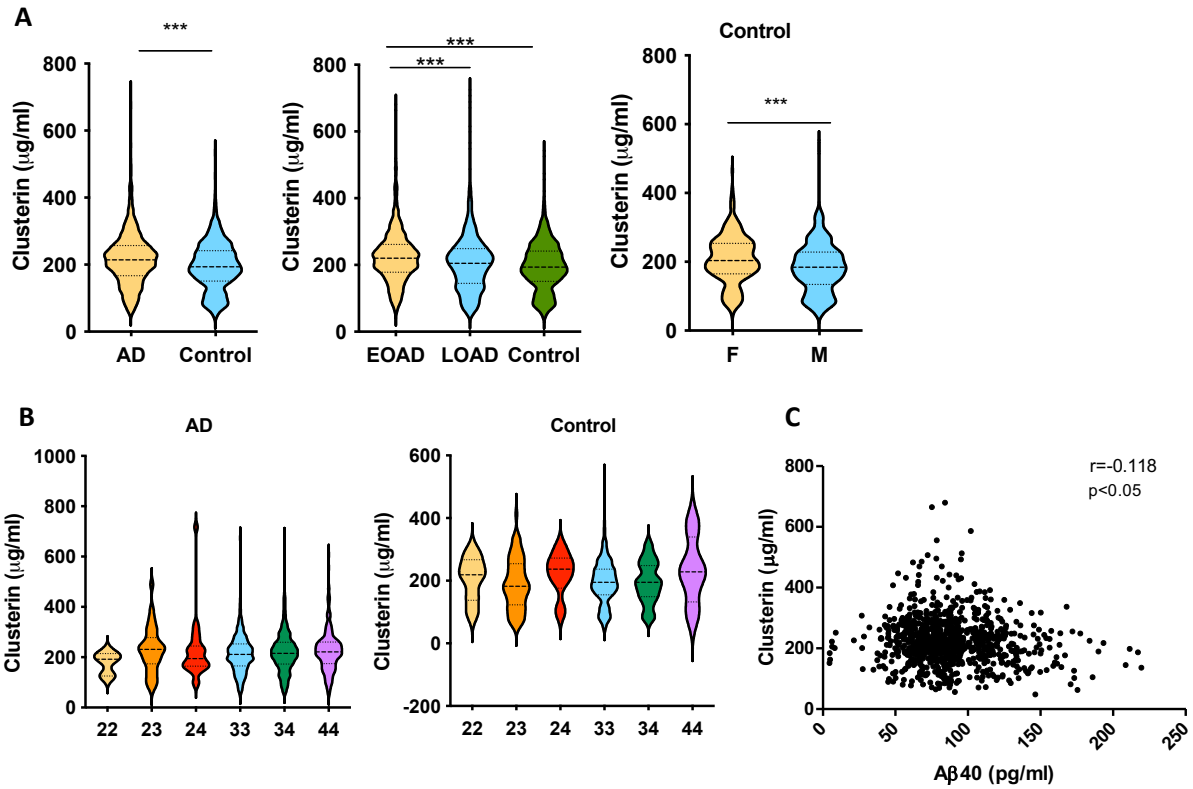

Figure 3.1. Plasma clusterin levels in AD and control samples. Clusterin is significantly elevated in AD plasma versus controls with the largest increase in the early onset AD group (*** p<0.001) (**A**). Clusterin levels were not significantly different between the different *APOE* genotypes (**B**). Plasma clusterin and Aβ40 levels were significantly correlated in AD cases only (r=-0.118, p<0.05) (**C**). Data in panel A were normally distributed while data in panels B and C were normally distributed when tested with the Kolmogorov-Smirnov test. Data were analysed statistically by two-tailed unpaired t tests or general linear models adjusting for age and sex (A), ANOVA with Tukey's post-hoc test (B) or Pearson correlation (C). N numbers for all data sets analysed are found in Table 3.1.

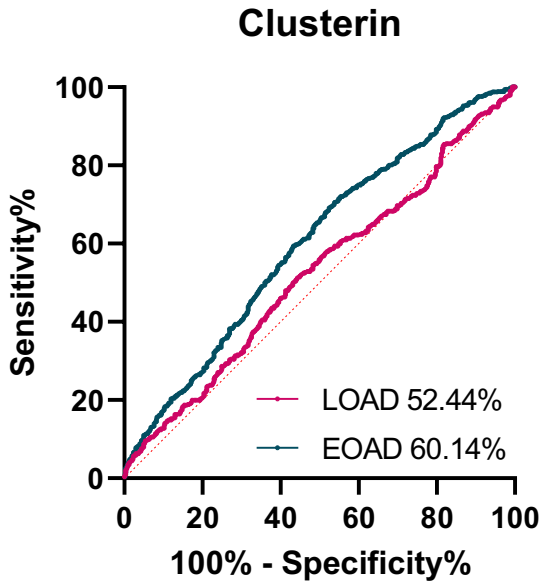

Figure 3.2. ROC curves displaying AUC values for clusterin in distinguishing LOAD (pink; AUC=52.44%) and EOAD (blue; AUC=60.14%) from control.

3.3.3. Clusterin CSF levels do not differ between AD patients and controls

Clusterin levels were measured in two sets of CSF samples from individuals with AD diagnosed following CSF measurements of Aβ, total tau, and pTau181. Measurements of these proteins were also available for control subjects in the Gothenburg cohort only (Figure 3.3A). Total protein concentrations in CSF were determined by BCA assay and were not found to significantly differ between patients and controls (Figure 3.3B, Figure 3.4A). Clusterin levels did not differ significantly between cases and controls in either cohort (Figure 3.3C, Figure 3.4B), however significant positive correlations were identified between clusterin levels and pTau in both cohorts (Figure 3.3D, Figure 3.4C), as well as Aβ levels in control subjects in the Gothenburg cohort (Figure 3.3D).

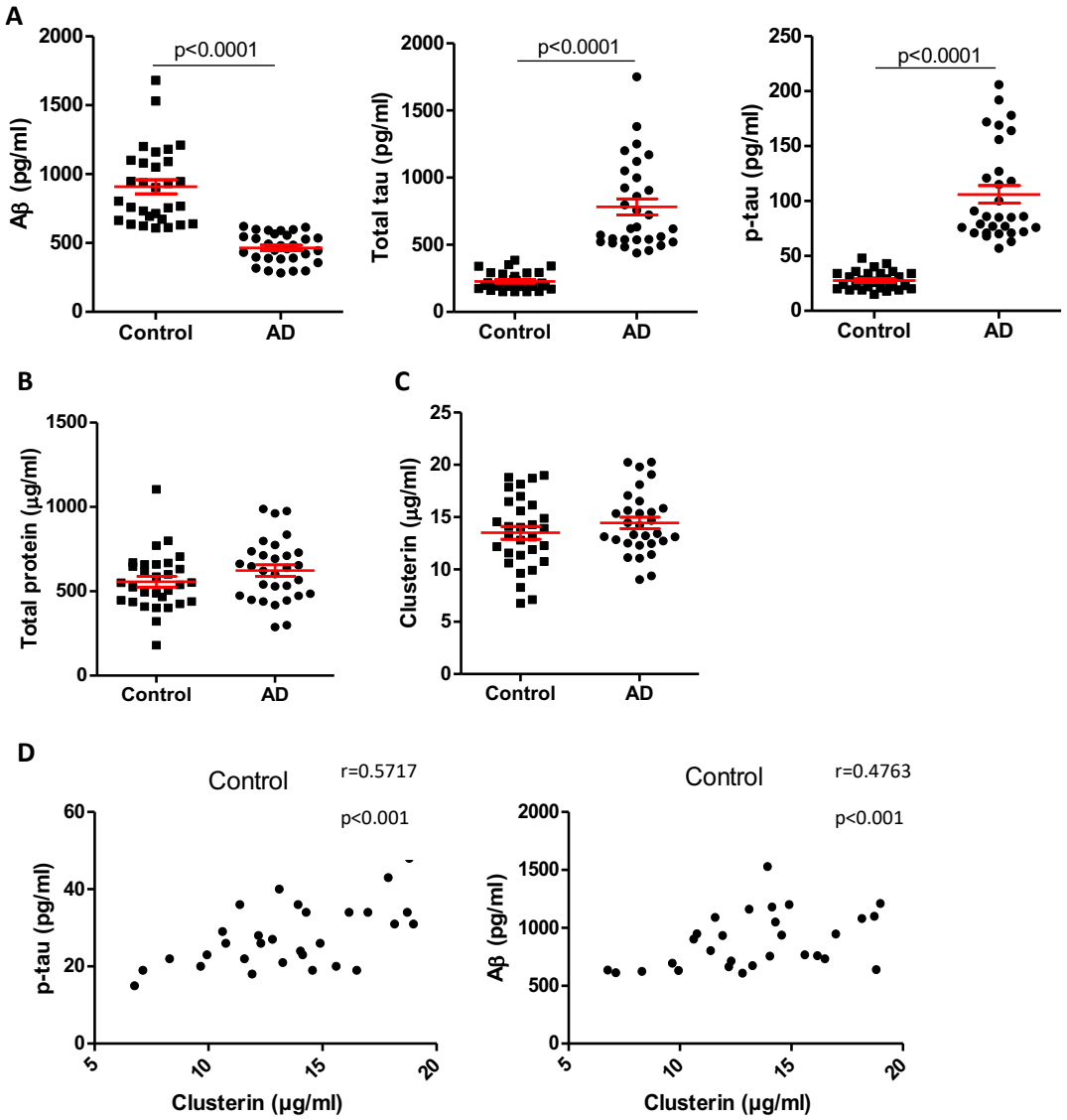

Figure 3.3. AT(N) biomarkers and clusterin in CSF samples from AD and control subjects (Gothenburg cohort). Total tau, pTau, and Aβ levels were significantly different between AD and control (p<0.0001) (**A**). Total protein concentration did not differ between AD and control (**B**), and no difference was seen in clusterin levels either (**C**). Clusterin levels correlated positively and significantly with pTau (r=0.5717, p<0.001) and Aβ levels (r=0.4763, p<0.001) in control subjects (**D**). Data were normally distributed and were analysed statistically by two-tailed unpaired t tests (A, B), general linear models adjusting for age and sex (C), or Pearson correlations (D). n=30 control, 30 AD.

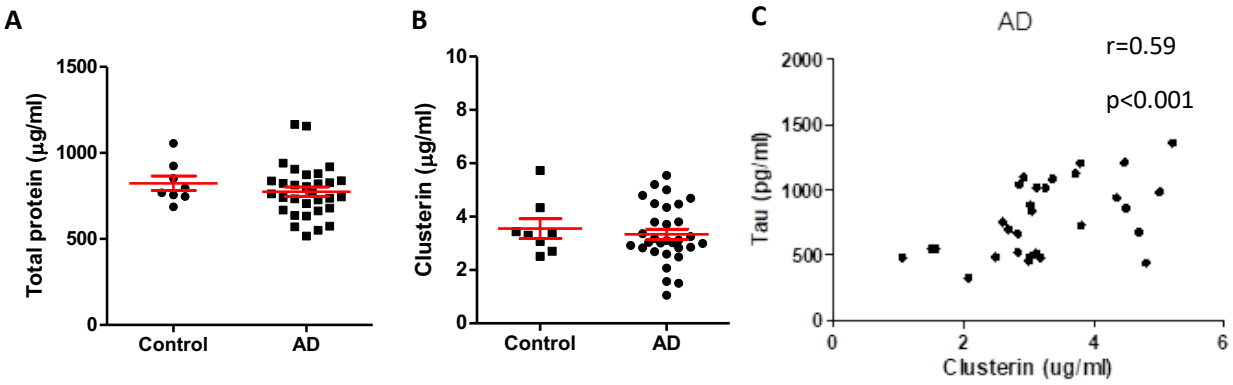

Figure 3.4. ATN biomarkers and clusterin in CSF samples from AD and control subjects (Gothenburg cohort). Total protein concentration did not differ between AD and control (**A**), and no difference was seen in clusterin levels either (**B**). Clusterin levels correlated positively (r=0.59) and significantly (p<0.001) with pTau levels in AD subjects (**C**). Data were normally distributed and were analysed statistically by two-tailed unpaired t tests (A), general linear models adjusting for age and sex (B), or Pearson correlations (C).

3.3.4 Clusterin colocalises with Aβ plaques and astrocytes in temporal cortex tissue from AD patients

Immunohistochemistry of brain tissue using antibodies against Aβ showed large Aβ plaques in tissue from an AD patient (Figure 3.5A), and small, diffuse plaques in aged control tissue (Figure 3.5B). Clusterin colocalised with large plaques in AD tissue, and to a lesser extent with diffuse plaques in tissue from non-demented subjects (2D5 in Figure 3.5, 4C7 in Figure 3.6). Antibody 4C7 displayed astrocytic staining (Figure 3.6A), confirmed by demonstrating that the staining colocalised with GFAP staining in an AD case, but not control (Figure 3.7). Negative control staining showed no background or non-specific staining, demonstrated specific labelling of Aβ, clusterin and GFAP (Figure 3.8). All images are taken on a confocal microscope and displayed as maximum projections of Z-stacks.

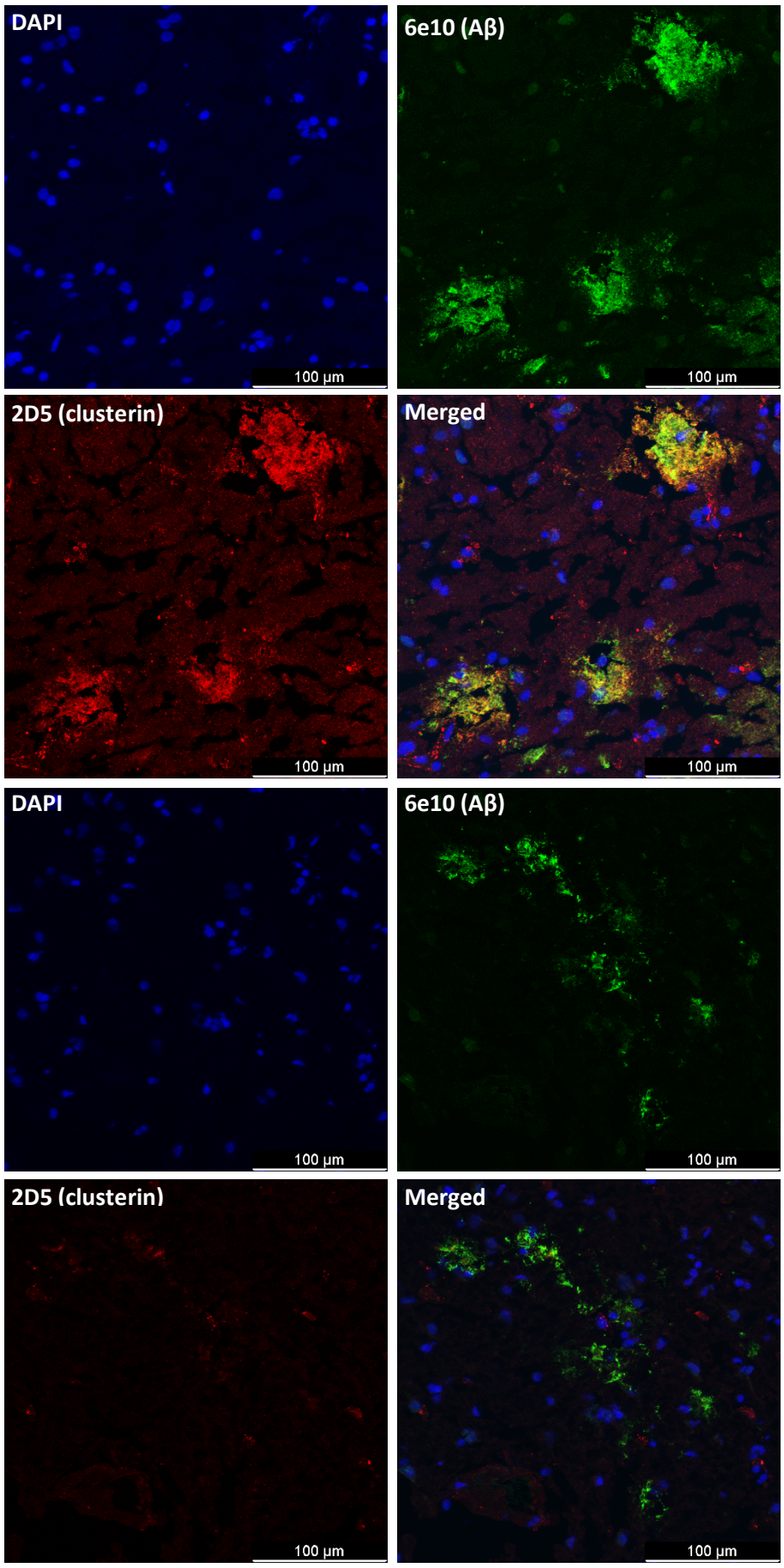

Figure 3.5. Immunohistochemistry of human brain tissue with DAPI nuclear staining (blue) and antibodies against Aβ (green) and clusterin (red) in an AD case (**A**) and an aged control (**B**). Large dense plaques are seen in AD tissue (A), while smaller, diffuse plaques are found in control tissue (B). Clusterin stained by 2D5 colocalised with plaques in AD but not control tissue. Images were acquired from two brain tissue samples from healthy controls and two brain tissue samples from AD subjects, and two sections were stained per brain. Three images were obtained from each section from areas rich in Aß plaques.

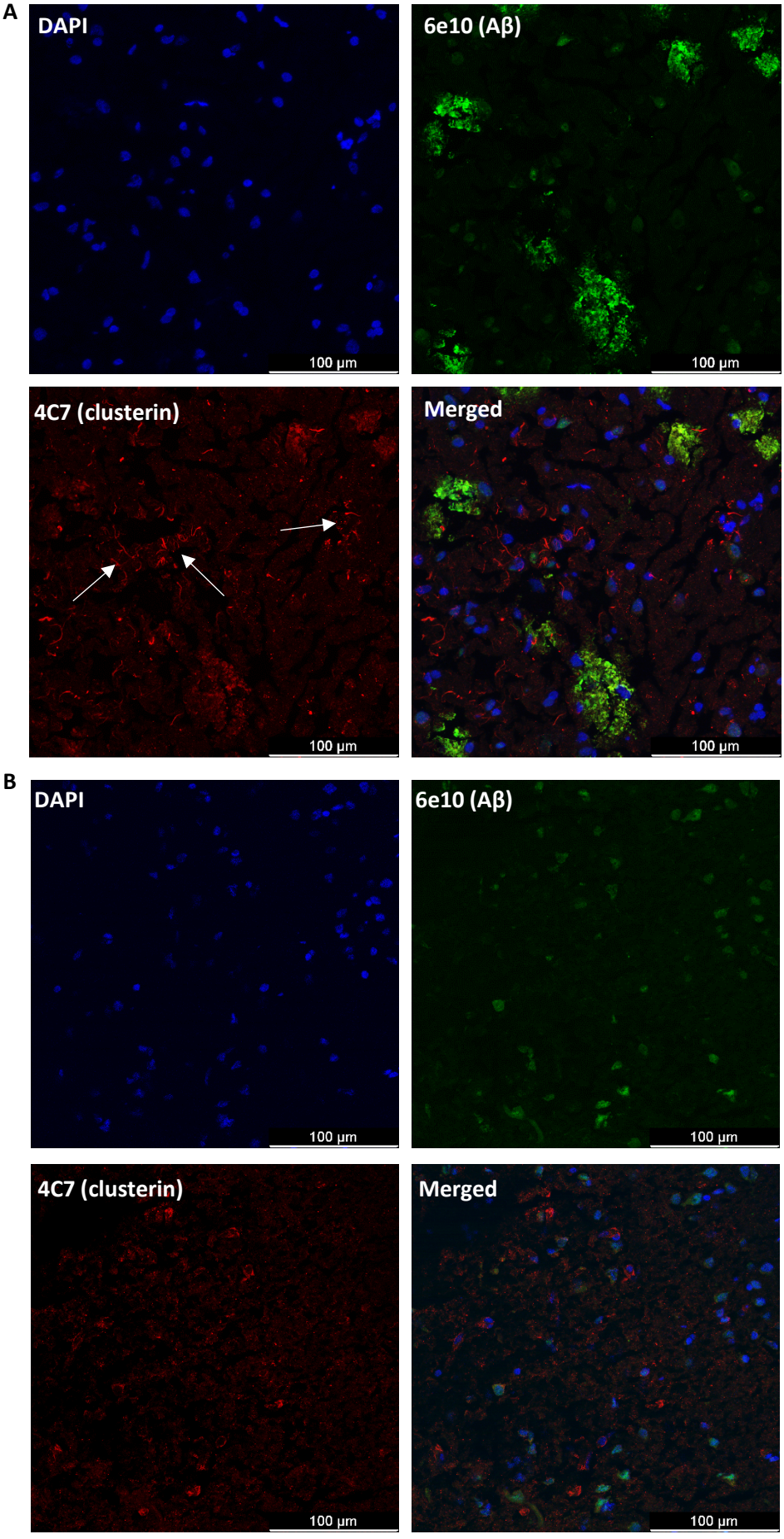

Figure 3.6. Immunohistochemistry of human brain tissue with DAPI nuclear staining (blue) and antibodies against Aβ (green) and clusterin (red) in an AD case (**A**) and a control case (**B**). Large dense plaques can be seen in AD tissue (A), while no plaques were found in control tissue (B). Clusterin stained by 4C7 was found to colocalise with plaques in AD tissue and showed astrocyte-like fluorescence signal. White arrows indicate astrocytes. Images were acquired from two brain tissue samples from healthy controls and two brain tissue samples from AD subjects, and two sections were stained per brain. Three images were obtained from each section from areas rich in Aß plaques.

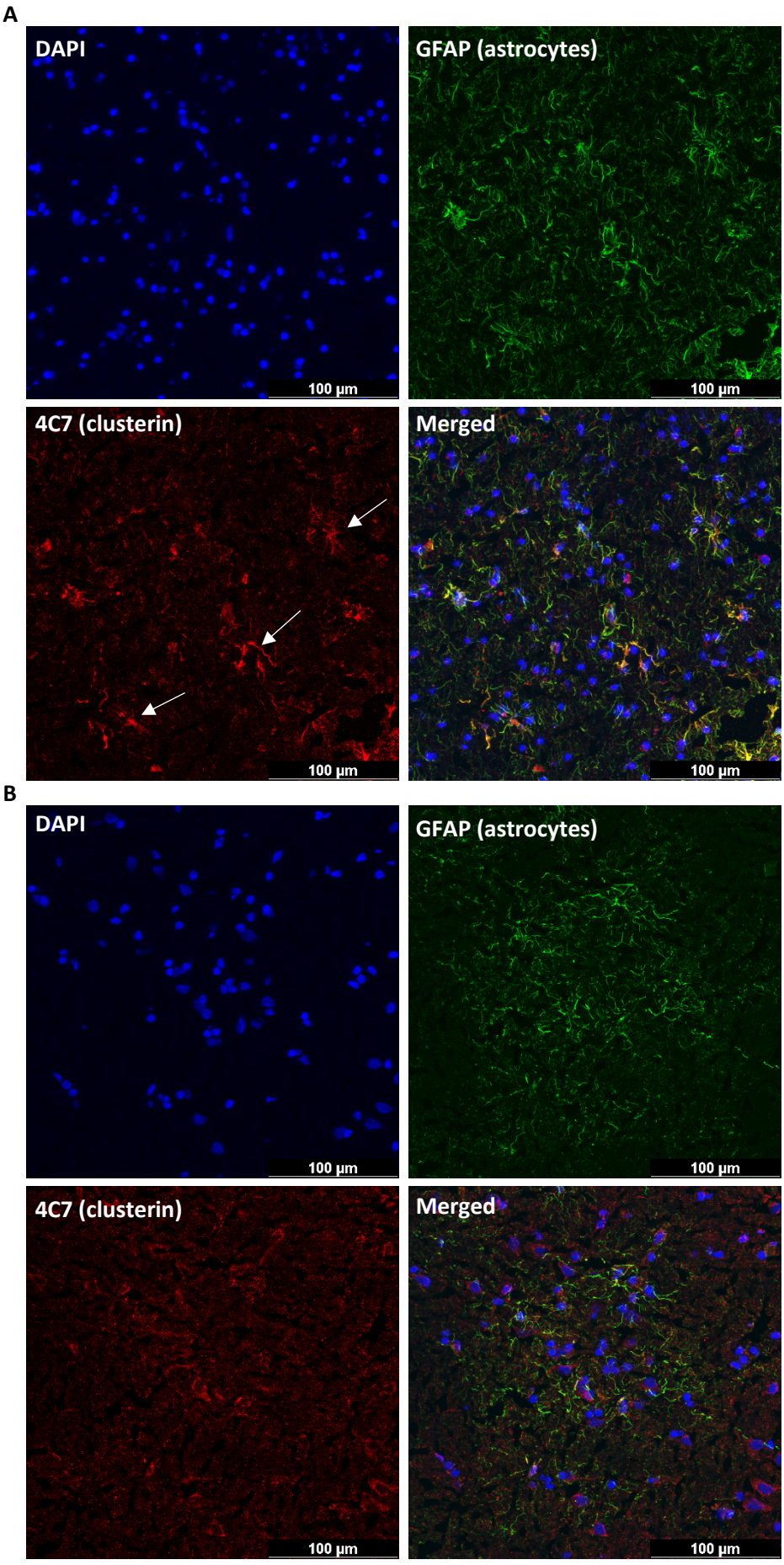

Figure 3.7. Immunohistochemistry of human brain tissue with DAPI nuclear staining (blue) and antibodies against GFAP (green) and clusterin (red) in an AD case (**A**) and a control case (**B**). Astrocytes stained by GFAP were also labelled by 4C7 anti-clusterin. White arrows indicate astrocytes labelled by clusterin. Images were acquired from two brain tissue samples from healthy controls and two brain tissue samples from AD subjects, and two sections were stained per brain. Three images were obtained from each section from areas with obvious astrocytic reactivity.

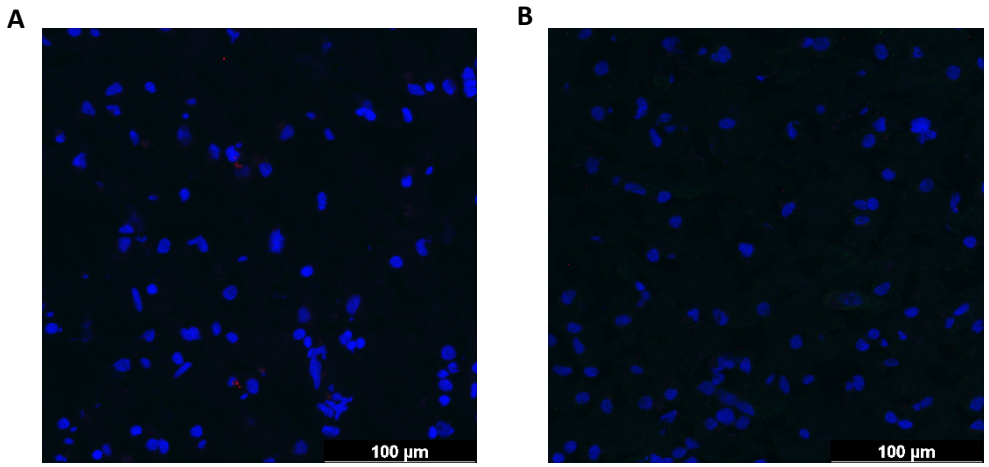

Figure 3.8. Negative control staining in human AD brain tissue. (**A**) Primary antibodies were omitted and secondary antibodies only (ms594, rab488) were used. (**B**) Isotype control antibodies were used as primary antibodies (rabbit IgG, mouse IgG2a, IgG2b). Both images show merged channels (blue, red, green) with lack of background fluorescence staining or non-specific labelling. Images were acquired from two brain tissue samples from healthy controls and two brain tissue samples from AD subjects, and two sections were stained per brain. Three images were obtained from each section.

Immunohistochemistry of clusterin, Aβ and astrocytes showed that clusterin was found within Aβ plaques, which were primarily identified in AD cases, with very little plaque found in control samples. Clusterin was also shown to colocalise with astrocytes, the brain cells secreting clusterin most abundantly. Larger, possibly reactive astrocytes in AD tissue (Figure 3.7A) had clusterin-labelled processes. The staining was shown to be specific as secondary antibody only and isotype controls showed no background staining.

3.3.5. Clusterin is significantly elevated in plasma from individuals with DS compared to healthy controls

Before the start of this project, clusterin had not been measured in plasma from individuals with Down Syndrome. Familial AD is primarily caused by mutations in *APP*, *PSEN1* and *PSEN2*; however, another genetic form of AD also manifests in people with DS, who carry a third copy of the *APP* gene, leading to increased production of Aβ. Accumulation of Aβ in the brain causes Aβ plaques and ultimately AD symptoms by the age of 40. The AD cohort used in this project comprised only subjects with non-familial AD; to investigate clusterin levels in a form of early-onset familial AD, a small cohort of subjects with DS and age-matched controls was used to determine if plasma clusterin levels differed in DS. Clusterin levels were quantified in plasma from adults

with DS and age-matched healthy euploid controls and were found to be significantly increased in DS compared to controls (mean = 291.5 vs 172.2 µg/ml, p<0.0001, Figure 3.9A). When comparing DS subjects with dementia to those without dementia, a small but not significant decrease in clusterin was seen in demented individuals (Figure 3.9B). Carriers of the *APOEε4* allele showed a small but not significant increase in clusterin plasma levels (Figure 3.9C).

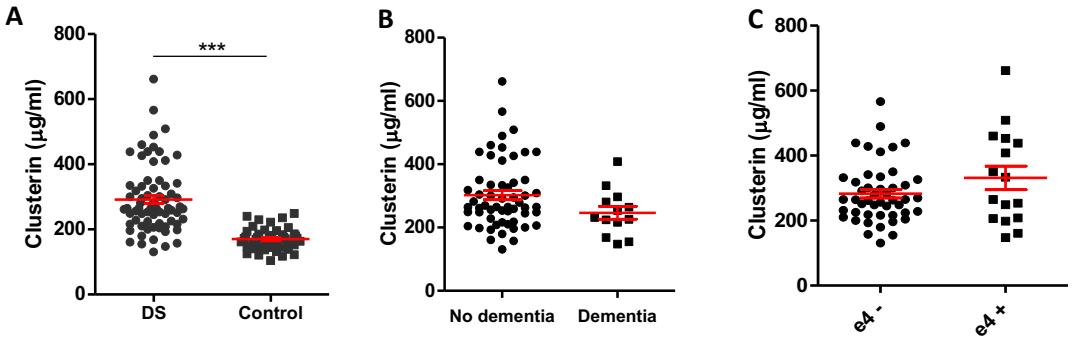

Figure 3.9. Clusterin plasma levels in adults with DS are significantly elevated compared to controls (**A**). In a subgroup of DS subjects with dementia, clusterin levels were slightly decreased compared to non-dementia DS (**B**). *APOEε4* genotype was associated with a small but not significant increase in plasma clusterin levels (**C**). Data are displayed as mean ± SD, were normally distributed and were analysed statistically by two-tailed unpaired t test (A, n=71 DS, 46 control; B, n=58 no dementia, 13 dementia; C, n=47 e4-, 16 e4+); *** p<0.001.

Quantification of clusterin in plasma from subjects with AD or DS compared to healthy controls using a newly established ELISA highlighted important results: clusterin was significantly elevated in AD, but the highest levels were found in DS. As clusterin had not been previously measured in DS, these results provide novel insights into the role of clusterin not only as a lipoprotein, but also as a complement regulator in DS, as discussed in section 3.4.

3.4. Discussion

Clusterin, a multifaceted protein with numerous roles reported since the 1980s, including lipid transporter, extracellular chaperone, and regulator of the complement pathway, plays an important role in AD pathology, as it inhibits Aβ nucleation and enhances its clearance from the brain (Beeg et al, 2016). Clusterin was previously investigated as a blood or CSF biomarker for AD, although results were inconsistent

among studies. Discrepancies between the reagents and types of assay used, AD diagnosis criteria, and stage of disease at assessment, might all contribute to these inconsistencies; for example, Desikan et al (2014) found that clusterin was increased in amyloid-positive individuals only.

A major finding reported in this chapter is the significant increase in clusterin plasma levels in AD patients compared to controls, with highest levels in EOAD patients. Importantly, results are based on measurement of clusterin levels in a very large cohort (n=1907), while most published studies involved fewer than 200 participants (Dukic et al, 2016; Schurmann et al, 2011; Jongbloed et al, 2015). Despite the significant increase in AD compared to control subjects, clusterin did not prove to be a good biomarker in predicting AD using ROC curve analyses. While the significant difference might arise due to the large sample size, clusterin levels in AD plasma were only 10% higher than in control plasma, which could explain the poor predictive power of clusterin in ROC curves. Although the ELISA developed in this chapter has good sensitivity and specificity, with low plate-to-plate variation, a good biomarker should also be able to predict disease progression and correlate with disease severity.

In the control group, subjects carrying the *APOEε4* genotype had the highest levels of plasma clusterin, consistent with previous studies (Hsu et al, 2017; Jackson et al, 2019), although this did not reach significance in a one-way ANOVA comparing levels between genotypes. Moreover, women showed significantly higher clusterin levels compared to men, also reported by Weinstein et al (2016). No significant correlations were found between clusterin plasma levels and demographic data (age at onset or inclusion in study, disease duration, or MMSE score) although previous studies reported significant correlations between clusterin plasma levels and cognitive scores (Jongbloed et al, 2015; Hsu et al, 2017) or age at onset (Weinstein et al, 2016). A significant inverse correlation was found between plasma clusterin and Aβ40 levels in AD cases. As AD progresses, Aβ levels decrease in plasma and CSF as a result of brain deposition and plaque formation, while pTau and NFL levels increase as a consequence of neuronal damage. Clusterin has been shown to sequester Aβ40 (Narayan et al, 2012) and prevent amyloid aggregation from Aβ42 at a 10:1 molar ratio Aβ:clusterin (Geraghty et al, 2021; Yerbury et al, 2007), suggesting plasma correlations may reflect ongoing changes in the brain.

Clusterin levels in CSF did not differ between subjects diagnosed with AD based on elevated CSF tau levels and decreased Aβ levels, compared to controls unlikely to suffer from AD as determined by these neurodegeneration markers. Although albumin quotient was not available for these cohorts to account for blood brain barrier disruption, which may allow proteins from the periphery to penetrate the brain parenchyma, clusterin levels were normalised to total protein levels. Total protein content in CSF was slightly higher in the AD group, and was reflected in clusterin levels. Nevertheless, total protein content fell within the normal range in both groups (200 – 1000 µg/ml), and previous studies reported uncorrected values for clusterin levels in CSF from AD patients, which were either found to be elevated (Deming et al, 2016) or not differ from control subjects (Lidstrom et al, 2001; Nilselid et al, 2006). Additionally, in the control group only, clusterin levels correlated positively with pTau and Aβ levels, suggesting interactions with both proteins. Indeed, in brain tissue immunostaining, clusterin was shown to colocalise with Aβ plaques, a finding replicating numerous reports (DeMattos et al, 2002; Jackson et al, 2019). As an important chaperone for Aβ, clusterin directly interacts with misfolded fibrils to aid their clearance (Beeg et al, 2016), but can also become sequestered in deposited plaques if Aβ concentration exceeds that of clusterin at a 500:1 ratio or higher (Yerbury et al, 2007). Clusterin was also found in astrocytes, the major producers of clusterin in the brain, in both control and AD cases, however this isoform might be implicated in homeostatic functions rather than interacting with Aβ.

While clusterin has been quantified in numerous studies involving patients with sporadic AD, no studies have investigated changes in clusterin plasma levels in Down Syndrome, a genetically determined form of dementia. Previous studies found that plasma levels of Aβ40 and Aβ42 were higher in DS compared to non-familial AD, which may be expected given the extra copy of APP leading to increased production of the two peptides (Wiseman et al, 2018). I found significantly elevated clusterin levels in DS compared to controls, with higher levels in *APOEε4* carriers, a finding which replicates results seen in AD. However, there was no significant difference between individuals with DS who showed signs of dementia and those who did not. As the plasma samples for the AD and DS cohorts were collected and processes independently, the mean age was lower in the DS cohort, and control subjects were recruited separately, it is not possible to compare clusterin levels in the two cohorts;

therefore, the striking increase in clusterin in DS may be due to factors unaccounted for in the AD cohort.

Since DS is associated with immune dysregulation (Mahmoud et al, 2005), the striking increase in plasma clusterin may reflect underlying inflammatory conditions as well as AD-related changes. Other complement proteins were measured in this DS cohort and several inflammatory markers, such as C3, were found to be significantly dysregulated in DS (Veteleanu et al, 2023), suggesting that the increase in clusterin may be related to the complement cascade rather than the lipoprotein effects seen in AD.

In summary, I describe the use of the novel anti-clusterin mAbs and clusterin assays developed during my PhD to demonstrate: 1) increased clusterin plasma levels in AD compared to control, consistent with previous findings; 2) no differences in CSF clusterin levels between AD and controls; 3) confirmation that clusterin is found in Aβ plaques in AD brain tissue. Some limitations of this work include the age difference between AD cases and controls in the AD Cardiff cohort, for which controls were deliberately selected for advanced age to minimise risk of conversion to AD in genetic studies, and the lack of clinical diagnosis of AD subjects in the CSF cohorts, together with their small sample size. It is important that future studies use a longitudinal approach to follow up healthy subjects at risk of developing AD, monitoring plasma levels of clusterin and other biomarkers of interest at different timepoints.

CHAPTER 4: Investigating the effects of SNPs in *CLU* on clusterin plasma levels using genetic analyses

4.1. Introduction

Since its discovery as a GWAS hit in AD in 2009 (Lambert et al, 2009; Harold et al, 2009), clusterin (*CLU*) has received more attention as a biomarker (Mullan et al, 2013; Dukic et al, 2016) as well as a genetic risk factor. A significant association between the minor allele at rs11136000 (MAF=0.37) and better cognitive scores was identified in cognitively normal elderly subjects (Mengel-From et al, 2011), a finding replicated by Thambisetty et al (2013). Despite an increase in total *CLU* mRNA in AD tissue, no effect of genotype at *CLU* SNPs on *CLU* expression was identified (Thambisetty et al, 2010). Further studies investigated whether risk variants in *CLU* are associated with brain gene expression changes, amyloidosis, and tauopathy. In temporal cortex from autopsied AD patients, rs11136000 was shown to significantly affect *CLU* expression, with higher levels in minor allele carriers; additionally, other cis-variants were found to influence *CLU* brain expression (Allen et al, 2012). In non-demented individuals, AD risk genes, including *CLU*, were tested for association with grey matter morphology at the voxel level (Roshchupkin et al, 2016). *CLU* was found to be significantly expressed in voxel clusters compared to background expression in samples from the Allen Human Brain Atlas. Using amyloid PET data from control, MCI, and AD patients, *CLU* rs9331949 was found to be associated with right superior frontal gyrus amyloidosis in demented individuals (Apostolova et al, 2018). Additionally, Tan et al (2021) reported *CLU* rs11136000 to be associated with increased *CLU* expression in frontal, temporal, occipital, and hippocampal brain tissue, as well as intralobular white matter, with no effects on blood *CLU* expression. The minor allele at rs11136000 was also associated with decreased amyloid PET burden, although no effect was seen on CSF Aβ42 levels. More recently, a new *CLU* SNP (rs11787077) was shown to be a significant expression quantitative trait locus (eQTL) for *CLU* expression in the brain, with the T allele being associated with increased *CLU* levels (Bellenguez et al, 2022). Although many large GWAS have consistently identified *CLU* as a GWS locus when investigating genetic risk factors for AD (Lambert et al, 2009; Kunkle et al 2019), our understanding of molecular mechanisms underlying the effects of noncoding variants on AD remains poor. Many other studies have since been conducted to identify these

mechanisms more precisely and confirmed that SNPs in *CLU* not only influence *CLU* expression levels in the brain but are also associated with brain amyloidosis and cognitive scores. This chapter aims to determine whether SNPs in *CLU* identified through GWAS impact clusterin plasma levels in patients with early onset AD, late onset AD, and cognitively well controls, and identify the SNP likely to have the most significant effect on brain pathology.

The aims of this chapter are to 1) test whether GWAS significant SNPs in *CLU* influence clusterin or neurodegeneration markers (Aβ and pTau) levels in plasma samples from AD patients and controls; 2) determine whether any of the SNPs in LD with GWS SNPs exert independent effects; 3) assess whether SNPs in *CLU* are significantly associated with changes in plasma clusterin levels using an endophenotype-GWAS approach.

4.2. Methods

Genetic data available from genome-wide array genotyping (Illumina 610, Illumina 550, or global screening array) were used to extract SNPs of interest in *CLU* using PLINK v1.07. LD scores (r^2) were determined using PLINK v1.07 and plotted as a heatmap using the corrplot package in R v4.2.0. Conditional analyses were performed using PLINK.

Genotypes at GWAS significant SNPs (rs11136000, rs9331888, rs9331896, rs2279590, rs1532278 in *CLU*) were used to test whether SNPs had a significant effect on protein levels as measured in plasma. Subjects with AD or controls were grouped based on their genotype at rs11136000 (used as a surrogate for the other SNPs in high LD) or rs9331888, and plasma clusterin, Aβ, and pTau-181 levels from homozygotes for the minor allele, homozygotes for the major allele, and heterozygotes were compared using one-way ANOVAs with Tukey's post hoc test using IBM SPSS Statistics 26.

To explore whether SNPs in *CLU* influence plasma levels of clusterin, genome-wide SNP-based association analyses using clusterin levels as outcome measures were performed by Dr Joshua Stevenson-Hoare using linear regression modelling in PLINK on the whole sample set. Outliers were removed based on thresholds calculated using the Median Absolute Deviation. Association analyses of SNPs with the biomarkers

were adjusted for age and sex, five principal components (PCs) and case-control status. The GWAS significance level was set to the commonly accepted $p<5x10^{-8}$. This type of analysis was previously performed on the data set used in this chapter with plasma levels of pTau-181, NfL, GFAP, Aβ40, and Aβ42 as outcome measures to identify genetic loci associated with these biomarkers (Stevenson-Hoare et al, 2023). Full details of the methodology used to perform the GWAS are described in Stevenson-Hoare et al (2023). Manhattan plots were generated in R v4.2.0 using the qqman package, and association results for a particular gene/region were visualised using LocusZoom.

4.3. Results

4.3.1. SNPs in CLU are in strong LD and do not have significant independent effects

The majority of SNPs in *CLU* identified through GWAS are common variants inherited together. LD scores between SNPs were determined to estimate the degree to which an allele of a genetic variant is inherited together with an allele of a nearby genetic variant and are shown in Figure 4.1. With the exception of rs9331908 and rs9331931, r^2 scores were above 0.8, indicating strong co-inheritance.

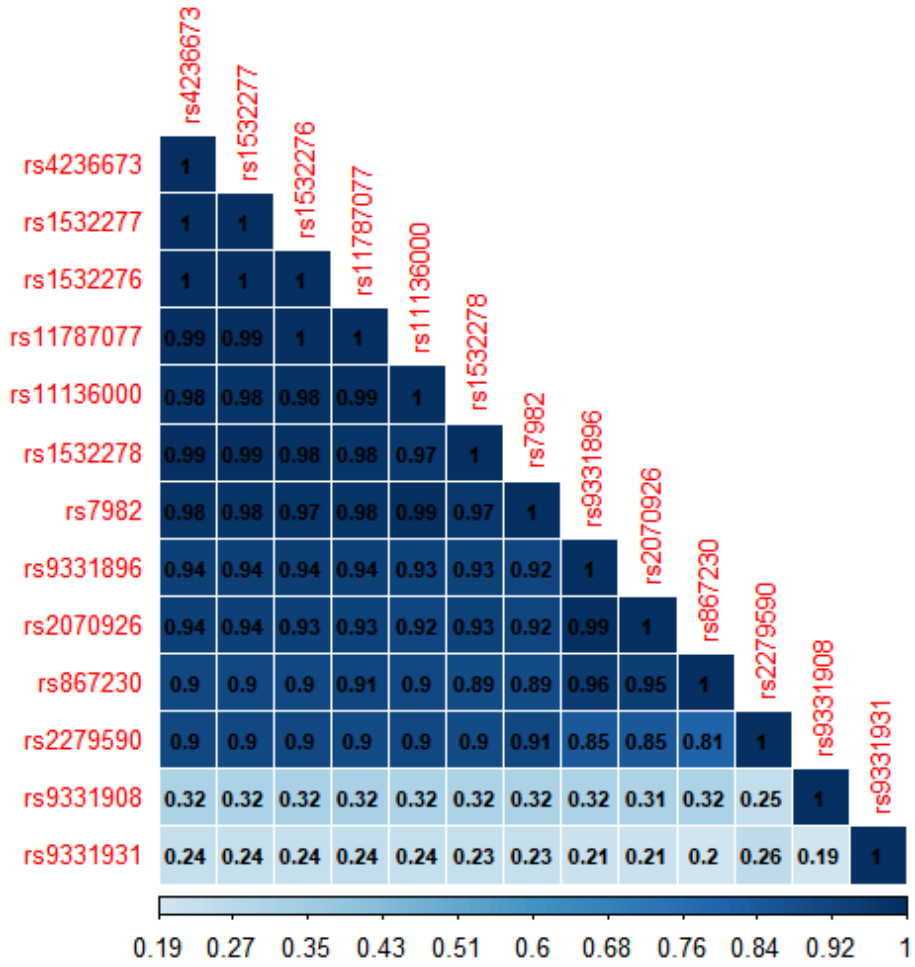

Figure 4.1 LD scores (r^2) between SNPs in *CLU*.

To determine whether rs9331888, a SNP outside the LD block significantly associated with AD risk, has independent effects, conditional haplotype-based association testing was performed on 1748 individuals (1320 AD cases and 438 controls) (Table 4.1). A basic omnibus test reported 8 common haplotypes (MHF>=0.01) out of 49 possible, based on 29 SNPs in *CLU*. To test for independent effects of rs9331888, the alternate and null models were compared using a chi-squared test, which showed no significant independent effects of rs9331888 (p=0.165) (Table 4.1). Due to strong LD among other SNPs (rs2279590, rs1532278, rs9331896, rs11787077), the test could not be performed for these SNPs as the null and alternate models were the same.

Table 4.1. Conditional haplotype testing for independent effects of rs9331888.

HAPLOTYPE	FREQ	OR(A)	OR(N)
TTGTGCGGGCCCCACTTATTTTAGCCCC	0.348	(-ref-)	(-ref-)
CTCGGAAAGCCGCGCCCGCCCCGCTGAC	0.27	1.231	1.235
CTGTGCGGCCACTGTTCGCCCCAGTGAG	0.202	1.166	1.164
CTGTGCGGCCACCGTTCGCCCCAGTGAG	0.0622	1.101	1.208
CTGTGCGGCCACCGTTCGCCCCAGTGAC	0.0156	1.86	|
CTGTGCGGCGACCGTTCGCCCCAGTGAC	0.0324	1.203	1.21
TCGTGCGGGCCCCACTTATTTTAGCCCC	0.0157	1.477	1.481
TTGTACGGCCACCGTTCGCCCCAGTGAG	0.02	1.153	1.162
Chi-squared test rs9331888	Chi-square	df	p
	1.93	1	0.165

4.3.2 SNPs in CLU do not significantly affect clusterin protein levels

SNPs in *CLU* previously identified in GWAS (rs11136000, rs1532278, rs9331896, rs2279590 in LD, and rs9331888) were tested for association with changes in clusterin protein levels by comparing plasma clusterin levels in carriers of the minor allele rs11136000 C/T (used as surrogate for the four SNPs in LD) and rs9331888 C/G with carriers of the major allele (Figure 4.2 A, B). Neither the SNP cluster defined by rs11136000 nor rs9331888 impacted clusterin levels whether assessed in the whole sample set, AD alone or control alone (Figure 4.2 A, B). No significant effects of rs11136000 on plasma levels of clusterin were observed in subjects with Down Syndrome either (Figure 4.2C).

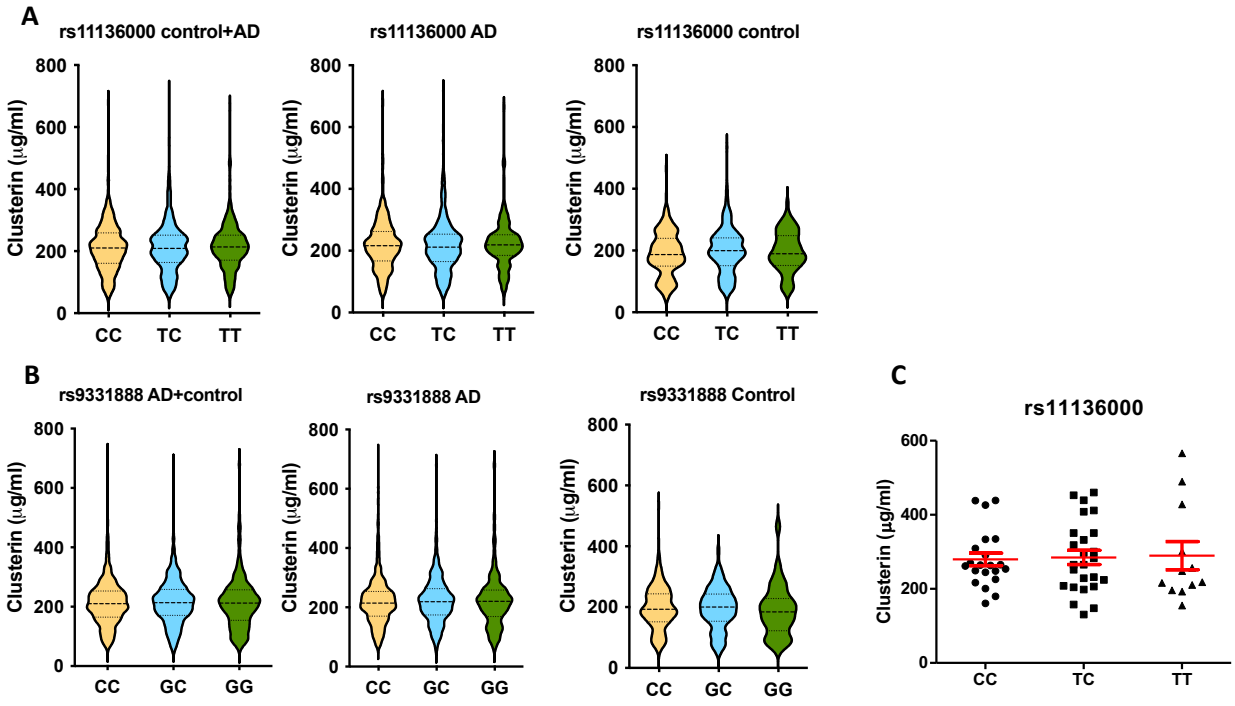

Figure 4.2. Effects of genotype at rs11136000 and rs9331888 on clusterin plasma levels. Neither rs11136000 (in strong LD with rs11787077) (**A**) nor rs9331888 (**B**) in *CLU* significantly impact plasma levels of clusterin. Data are shown as mean ± SD, analysed statistically by one-way ANOVA with Tukey's post-hoc test. rs11136000: n=746 CC, 880 TC, 273 TT control+AD; 574 CC, 638 TC, 191 TT AD; 172 CC, 242 TC, 82 TT control; rs9331888: n=952 CC, 751 GC, 155 GG control+AD; 698 CC, 550 GC, 120 GG AD; 254 CC, 201 GC, 35 GG control. No significant difference between carriers of the T or C allele at rs11136000 in DS was found either (**C**).

4.3.3. rs11136000 is associated with decreased Aβ and tau pathology in plasma of APOEε4 non-carriers

Effects of the T allele at rs11136000 on Aβ42 and pTau181 were investigated to determine whether a significant relationship between genetic variation in *CLU* and AD pathology measured in blood could be identified. Data were analysed separately on subjects carrying one or more *APOEε4* alleles and non-carriers, to eliminate effects of *APOEε4* on Aβ and tau pathology. In *APOEε4* non-carriers, late onset AD patients carrying the minor allele at rs11136000 had significantly higher levels of Aβ42 ($p<0.05$, Figure 4.3A) and significantly decreased pTau-181 levels ($p<0.05$, Figure 4.3B). These differences were not seen in *APOEε4* carrier patients or controls.

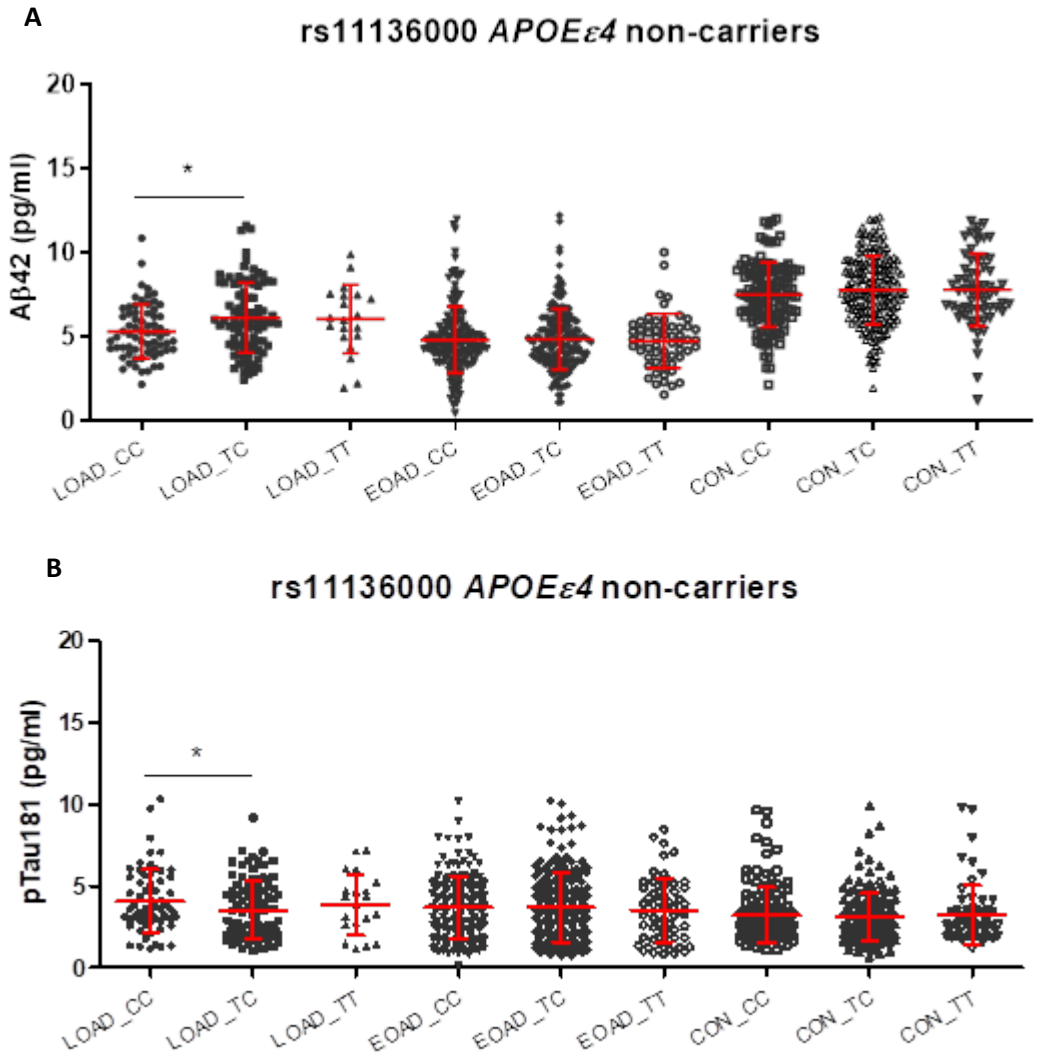

Figure 4.3. Plasma levels of Aβ42 (**A**) and pTau181 (**B**) in AD and control subjects non-carriers of *APOEε4.* LOAD carriers of the T allele at rs11136000 displayed higher levels of plasma Aβ42 and lower levels of pTau181.
LOAD = late onset AD; EOAD = early onset AD; CON = control. * p<0.05

4.3.4. GWAS using plasma clusterin levels as endophenotypes does not reveal significant associations with SNPs in CLU or other genes

When plasma clusterin levels were used as an outcome measure in GWAS on the whole sample set did not identify genome-wide significant SNPs in *CLU* or elsewhere in the genome associated with plasma clusterin changes (Figure 4.4A). The *CLU* gene was visualised using LocusZoom and the SNPs with the lowest p values within 200 kb of *CLU* were found upstream of *CLU*, in *SCARA3*, however these did not reach GWS ($p=2.14x10^{-2}$) (Figure 4.4B).

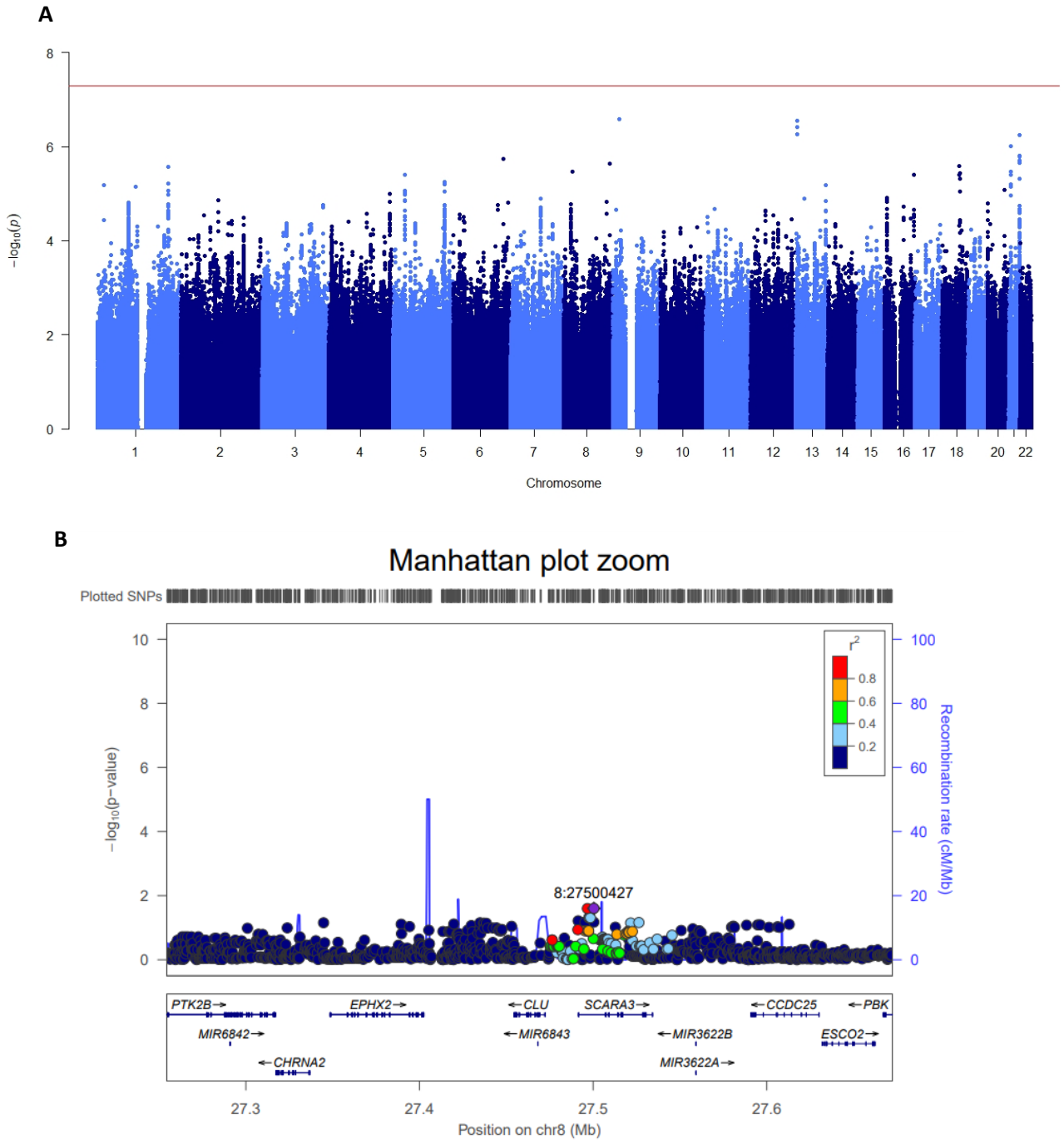

Figure 4.4. (**A**) Manhattan plot of GWAS performed on the whole sample set (n=1708) using clusterin plasma levels as endophenotypes does not show any significant SNPs. Red line indicates the commonly accepted genome-wide significant p-value ($5x10^{-8}$). (**B**) LocusZoom further analyses on the *CLU* locus ± 200 kb highlighted SNPs in *SCARA3*, but these did not reach GWS ($p=2.14x10^{-2}$).

4.4 Discussion

Clusterin has not only been investigated as a plasma biomarker for AD, but also as a genetic risk factor. So far, eleven non-coding SNPs in *CLU* have been identified through GWAS, most of which are found within a linkage disequilibrium (LD) block. In this chapter, rs11136000 was used as a surrogate for the LD block formed by rs2279590, rs1532278, rs9331896, rs11787077, while rs9331888 was used as a SNP independent of the LD block (r^2<0.26). No significant associations were identified between genotypes at either rs11136000 or rs9331888 on clusterin levels in AD or control subjects. This is consistent with previous studies reporting no effects of genetic variation in *CLU* on clusterin levels in plasma, CSF, or brain tissue (Mullan et al, 2013; Thambisetty et al, 2010). A few studies confirmed an association between the minor and protective T allele at rs11136000 and better cognitive scores (Cruz-Sanabria et al, 2021; Thambisetty et al, 2013), however no association with higher MMSE score was found in subjects carrying the T allele in this study. To test whether SNPs in *CLU* impacted AD pathology reflected through plasma Aβ and pTau-181 levels instead, levels of these biomarkers were compared in subjects with LOAD, EOAD, and controls carrying the T/T, T/C, or C/C genotypes at rs11136000. In *APOEε4* non-carrier LOAD patients, a significant difference was found between T allele and C allele carriers, as T allele carriers had lower pTau-181 and higher Aβ42 levels, indicating a protective effect of this SNP over AD pathology. Similar findings were previously reported, with lower brain amyloid burden in individuals carrying the T allele (Tan et al, 2021), and lower tau CSF levels in AD patients carrying the T allele (Zhou et al, 2014), suggesting a possible role of clusterin in both amyloid and tau pathology. As non-coding SNPs, these common variants in *CLU* are unlikely to influence protein structure and function, but may, however, sit within regulatory regions and influence gene expression levels, as shown by Allen et al (2012) and Bellenguez et al (2022) in brain tissue.

While previous large genetic studies have performed GWAS to identify new loci associated with AD, GWAS using an intermediate phenotype (including plasma or CSF protein levels, imaging data, or any other quantifiable trait) allow a deeper analysis of uncharacterised mechanisms of effect (Kauwe et al, 2014; Shen et al, 2013; Cruchaga et al, 2013). Using plasma clusterin concentrations as an endophenotype permits interpretation of the role of GWAS-implicated intronic SNPs by linking them directly to a change in plasma levels. This approach can also identify

novel SNPs that influence the expression of clusterin and increase statistical power by focusing on a single quantitative trait. For these reasons, this type of GWAS was used to further interrogate the relationship between SNPs in *CLU* and the increase in clusterin protein levels seen in AD. The GWAS revealed no significant associations between plasma clusterin levels and variants in *CLU* or elsewhere in the genome, indicating that mutations in *CLU* are not responsible for changes in plasma protein levels; however given the underpowered nature of the study, these findings should be replicated using a larger sample size. Using the same cohort and type of GWAS, Stevenson-Hoare et al (2023) used plasma levels of Aβ40, Aβ42, NfL, and GFAP to identify SNPs which might influence levels of these AD biomarkers. The authors did not identify any novel SNPs in a case-control analysis, but found significant associations between the Aβ40/Aβ42 ratio and SNPs in *WWOX* and *COPG2*, highlighting the usefulness of this method in discovering SNPs that are implicated in modulating levels of proteins involved in AD, despite being located in genes that do not code for these proteins.

As SNPs in *CLU* are not functional variants, determining how much they contribute to AD risk is difficult, since they may act as part of a complex polygenic effect. Additionally, as this is not a longitudinal study, it is not possible to identify when changes in plasma protein levels occurred, and whether in AD these were driven by risk SNPs. If CSF measurements of clusterin and AT(N) markers were available for the study participants, together with MRI scans, amyloid/tau PET, and post-mortem Braak staging, more in-depth analyses could be performed to determine the relationship between disease stage or severity with genotype at *CLU* SNPs and clusterin protein levels in brain tissue, offering more comprehensive insight into CLU-mediated disease mechanisms.

CHAPTER 5: Differentiation of astrocytes from human iPSCs to study the effects of SNPs in *CLU* on clusterin production and function

5.1 Introduction

Astrocytes, the second most abundant cell type in the brain, comprise a diverse family of supportive glia responsible for various roles in normal brain physiology, including mopping up excess glutamate and maintaining blood brain barrier integrity and function (Barres, 2008). Additionally, they have been shown to play important roles in neuroinflammation in pathological conditions such as AD, where astrocytes enter a reactive state and release pro-inflammatory cytokines (Li et al, 2019). Critically for this project, they are the major source of secreted clusterin in the brain, responsible for approximately 50% brain clusterin production; the remainder is made by GABAergic neurons, endothelial cells, glutamatergic neurons, oligodendrocytes and microglia (Bellenguez et al, 2022). For these reasons, astrocytes were selected as the most relevant brain cell type to study in this project. However, access to human brain cells, including astrocytes, is very limited, and maintaining these cells alive ex vivo can be especially difficult. Advances in iPSC technology have made reprogramming somatic cells into pluripotent cells a relatively straightforward process which now utilises viral vectors to express pluripotency genes without integration of the vectors into the genome (Fusaki et al, 2009). Human peripheral blood mononuclear cells (PBMCs) or skin fibroblasts can be reprogrammed to induce a pluripotent state, which can be further exploited to generate a vast array of cell types. To differentiate iPSCs into astrocytes, several protocols can be implemented, as described in Chapter 1. For this study, human iPSCs were first directed to a neural lineage through dual SMAD inhibition, a well-known method for deriving neural precursor cells (NPCs) (Chambers et al, 2009). This type of differentiation involves exposing cells to inhibitors of the BMP (LDN193189), WNT (IWR-1-endo), and ALK (SB431542) signalling pathways, forcing them to become NPCs within 8 days (Figure 5.1). The cells then grow as a dense neuro-epithelial sheet and proliferate rapidly, allowing large stocks to be accumulated and cryopreserved. NPCs can then be differentiated into neurons, or directed towards the astrocytic lineage by growing in the presence of leukaemia inhibitory factor (LIF), which maintains them in an undifferentiated state and allows cells with a high gliogenic potential to proliferate. Moreover, it has been shown that CD44 positive NPCs are

more likely to become committed to generating astrocytes (Liu et al, 2004), and these cells can be selected though fluorescence activated cell sorting (FACS) to generate a pure population of astrocyte precursors cells (APCs) for terminal differentiation through exposure to ciliary neurotrophic factor (CNTF). A summary of the astrocyte differentiation process is provided as a timeline in Figure 5.1.

During the astrocyte maturation process, the expression of various proteins changes to reflect the mature phenotype or specialised astrocyte function. GFAP is the most commonly used marker as it is a major component of intermediate filaments. However, its expression is variable in the healthy CNS depending on the region and activation state of the cells (Khakh et al, 2015), which makes its use as a general astrocytic marker questionable. Other astrocyte markers include vimentin, expressed in some specialised glial cells and predominantly found in immature astrocytes, with decreased expression during brain development (Luo et al, 2017). CD44 marks astrocyte precursor cells committed to the astrocytic lineage early in development (Liu et al, 2004). Excitatory amino acid transporter 1 (EAAT1) is an essential transporter for glutamate, aiding in clearing up excess glutamate from the synaptic cleft to prevent toxic effects, while S100ß is a cytosolic marker which labels bodies of small astrocytes with less extensive branching (Regan et al, 2007). These markers will be used in this chapter to assess the maturity of the iPSC-derived astrocytes.

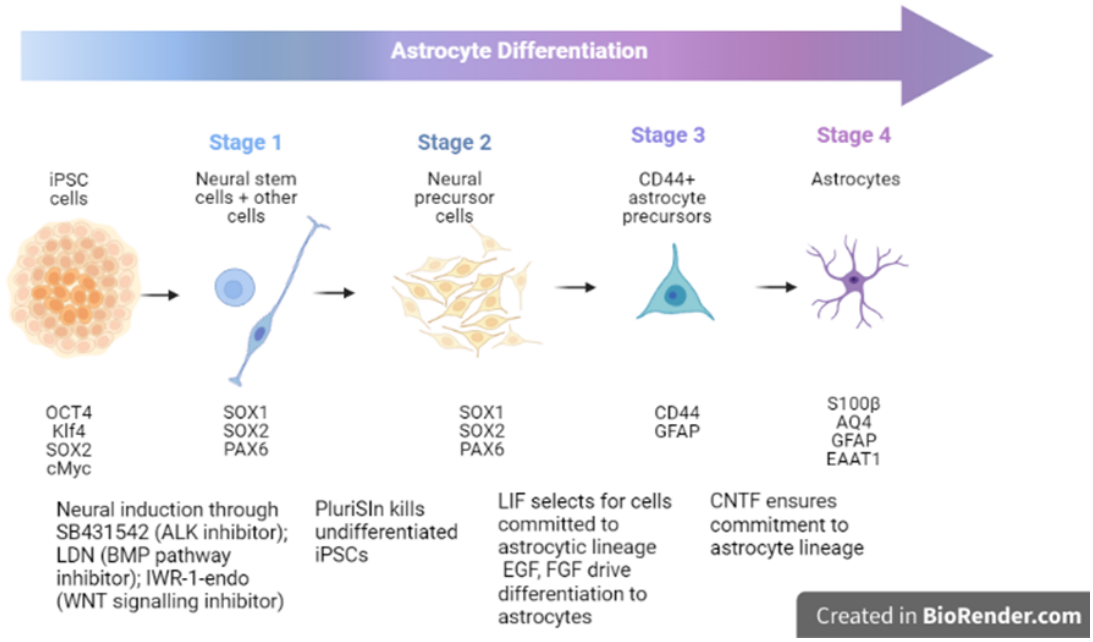

Figure 5.1. Stages of astrocyte differentiation from iPSC. iPSCs undergo neural induction, with a pure NPC population obtained after treatment with PluriSIn. NPCs are then exposed to LIF to allow selection of cells with highest gliogenic potential, which can be terminally differentiated into astrocytes.

The iPSC lines chosen for this study carried different genotypes at rs11136000 and rs11787077 (2 homozygous for the C allele (F1 and HPSI1213i-babk_2), 2 homozygous for the T allele (B1 and KOLF2), and 2 heterozygous (A1 and H1); all homozygous for the *APOE* ε3 allele), two of the most significant SNPs identified in GWAS and discussed in Chapters 1 and 4. Rs11787077 is the most significant eQTL for *CLU* expression in the brain, where the T allele is associated with increased *CLU* expression, and it overlaps with an astrocyte-specific enhancer and super enhancer (Bellenguez et al, 2022; Nott et al, 2019). Previous studies have found increased clusterin mRNA levels in subjects with high AD brain pathology compared to those with low pathology, however only nCLU mRNA was influenced by genotype at rs11136000 (Ling et al, 2012). Other studies have investigated changes in sCLU and nCLU in iPSC-derived neurons; neurons stimulated with Aβ for 48h produced significantly more nCLU, while sCLU levels remained unchanged (Robbins et al, 2018). These findings make rs11136000 and rs11787077 interesting candidates in the study of the role of non-coding variants in *CLU* on clusterin protein production and function in brain cells. Therefore, the aims of this chapter were to differentiate into astrocytes iPSCs from donors carrying different genotypes at these SNPs and quantify levels of secreted and intracellular clusterin at protein and mRNA levels from C allele carriers compared to T allele carriers.

5.2 Methods

5.2.1. Culture and maintenance of stem cells

All work involving iPSCs was carried out under sterile conditions in a class II type A2 biosafety cabinet (ThermoFisher Scientific MaxiSafe2020), using sterile tissue culture plastics and reagents. All contact surfaces were regularly disinfected using 70% EtOH to prevent cell contamination.

iPSCs banked in cryovials at 1-2 million cells/500 µl Cryostor (Merck Millipore #C2874) in LN2 were thawed by immersing the vial in a 37°C water bath for 1 minute. Cells were added to 10 ml DMEM warmed to RT drop-wise to avoid osmotic shock, and centrifuged at 300xg for 5 mins. Supernatant was aspirated and cells were gently resuspended in 1 ml Essential 8 flex medium (Thermo Scientific #A2858501) or mTeSR Plus medium (Stemcell technologies #100-0276) containing 10 µM Rho-kinase inhibitor, pipetting 2-3 times to avoid dissociating cells. Cells were seeded in a

final volume of 2 ml/well in one well of a 6-well plate precoated with 1% Geltrex in DMEM for 1h at 37°C, and placed in an incubator set to 37°C, 5% CO_2 and 18% O_2. Medium was changed daily, and cells were visually inspected for colony growth and spontaneous differentiation under a microscope. When cells reached 80% confluency, they were passaged at 1:3-1:6 ratios. Medium was aspirated and 1 ml ReLeSR (Stemcell technologies #05872) was added to each well for 1 minute at RT. ReLeSR was then aspirated and the plates were incubated at 37°C for 3-7 mins. 1 ml fresh medium warmed to RT was added to each well and large cell colonies were gently broken up by pipetting. Cells were then split at the desired ratio in 6-well plates precoated with Geltrex.

5.2.2. iPSC differentiation into NPCs

iPSC lines were obtained from the Dementia Research Institute (lines A1, B1, F1, H1, reprogrammed by Dr Nikoleta Daskoulidou from PBMCs) or purchased from the Sanger Institute (lines KOLF2.c1 and HPSI1213i-babk_2, reprogrammed from fibroblasts). Each iPSC line was maintained in 6 well Nunc cell culture treated plates (Table 5.1) using mTeSR or Essential 8 flex medium in an incubator set to 37°C (5% CO_2, 18% O_2) (Table 5.2). Details regarding volumes used for each type of culture vessel are listed in Table 5.3, and all reagents and growth factors are listed in Table 6.4. At 80% confluency, for each cell line, cells from 3 wells of a 6 well plate were treated with 10 μM Y-27632 Rho kinase inhibitor (RI) for 1 hour. Treated cells were washed with 2 ml/well DPBS and dissociated into single cells with 1 ml/well Accutase for 10 minutes at 37°C. mTeSR medium (1 ml/well) was added to inhibit the reaction and cells were collected in a 15 ml tube, centrifuged at 300xg for 5 minutes, and supernatant aspirated. The cell pellet was resuspended in 12 ml mTeSR with 10 μM RI and 1 ml/well cell suspension was added to wells of a 12-well plate precoated with Geltrex (1:100) for 1 hour at 37°C. Untreated cells in the remaining wells were harvested for RNA extraction, resuspended in 600 μl RLT buffer with 1% β-mercaptoethanol, and frozen at -80°C. The following day, cells were washed 3 times with 1 ml/well DPBS, and 1 ml SLI medium (Table 5.5) was added to each well. SLI medium was changed every day for 7 days. On day 8, cells were treated with 10 μM RI for 1 hour, washed with DPBS and dissociated with 250 μl/well Accutase for 10 minutes at 37°C. Cells from 3 wells were harvested for RNA extraction, while cells from 9 wells were centrifuged at 300xg for 5 minutes and resuspended in 36 ml NB

medium with 10 µM RI. Cells were split 1:4 in 3 12-well plates precoated with Geltrex (1:100). NB medium was changed every day until day 16. On days 14 and 15, NB medium with 20 µM PluriSIn-1 was used to select for NPCs and remove undifferentiated cells. The neural induction process is summarised in Figure 5.2.

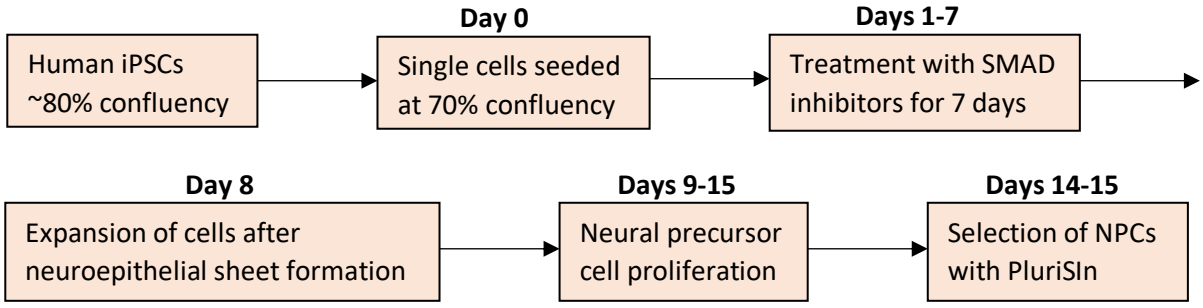

Figure 5.2. Flowchart of neural induction, from day 0 to day 16.

5.2.3. NPC differentiation into astrocytes

On day 16, NPCs in the 3 12-well plates were washed with DPBS and dissociated with Accutase for 10 minutes at 37°C. Cells from all wells (0.5 ml/well) were pooled in a 50 ml tube, 1.5 ml were set aside for RNA extraction, and 2 ml were set aside for passaging. Cells were centrifuged at 300xg for 5 minutes, and cells to be passaged were resuspended in 5 ml NB medium with 20 µM PluriSIn-1 and added to a T25 flask precoated with Geltrex (1:100). The following day, medium was changed to 5 ml NEL (Table 5.5). The remaining cells were counted using the Countess II FL automated cell counter, centrifuged at 300xg for 5 minutes, and resuspended in Cryostor with 10 µM RI to be frozen as 6 million cells per cryovial. Cells were grown in T25 flasks in NEL medium for 12-37 days, passaging them at least three times (1:3 split ratio) when they reached 90-100% confluency, and freezing excess cells. After 4 passages, when cells reached 90% confluency, they were sorted by FACS to select for APCs. Medium was aspirated from flasks and cells washed with 5 ml DPBS, then dissociated using 2 ml Accutase for 2 mins at 37°C. Approximately 1-2 million cells were transferred in 15 ml tubes for CD44 staining or isotype control staining, and remaining cells were frozen using Cryostor. Cells were centrifuged at 300xg for 5 minutes, supernatant was aspirated, and cells were resuspended in 98 µl NEL medium with either 2 µl anti-CD44 antibody (Miltenyi Biotec #130-113-896) or 2 µl isotype control antibody (Miltenyi

Biotec #130-113-199) and incubated on ice for 10 minutes. Cells were then centrifuged at 300xg for 5 minutes and resuspended in 1 ml PBS with 0.1% BSA and 1% Pen/Strep. FACS sorting was performed by qualified staff using a FACS Aria Fusion automated cell sorter. Cells positive for CD44 signal were collected in 1 ml NEF medium and seeded in Geltrex pre-coated plates of appropriate dimension for the number of cells obtained. Cells were grown in NEF medium and expanded in larger culture plates, up to three T75 flasks. Medium was changed every 4-5 days or upon passage. When cells reached 70% confluency in three T75 flasks, medium was changed to CNTF medium (Table 5.5) for terminal differentiation. Cells were grown in CNTF for 2 weeks, with one passage at day 4-5, when cells became 90% confluent, then cultured in NBA medium for an additional 2-3 weeks. The differentiation process from NPC to astrocytes is summarised in Figure 5.3.

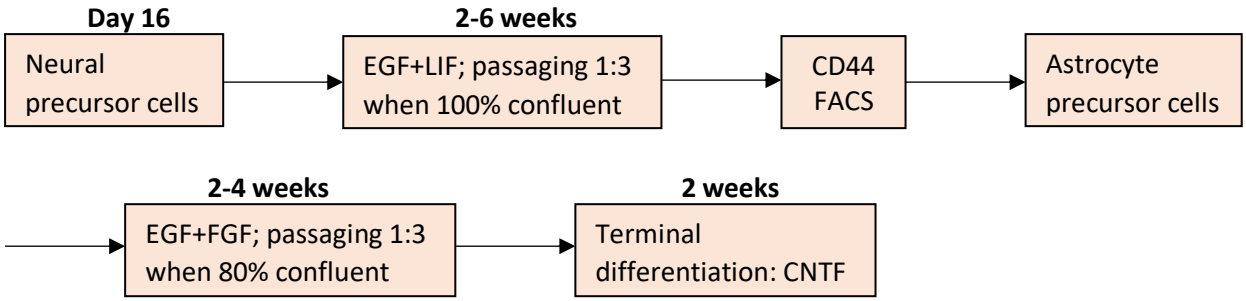

Figure 5.3. Flowchart of neural induction, from neural precursor cells to astrocytes.

Table 5.1. Cell culture plastics.

	Supplier	**Catalogue number**
96-well plates	ThermoFisher	167008
12-well plates	Greiner	665970
6-well plates	Greiner	657160
T25 flasks	Sarstedt	83.3910.002
T75 flasks	Sarstedt	83.3911.002
Cryovials	Greiner	126263

Table 5.2. Equipment used for maintenance and analysis of cells.

Equipment	Manufacturer	Model
Incubator	Thermo Fisher Scientific	Heracell 150i
Water bath	Grant Instruments	SUB Aqua Pro
Microscope	Olympus Life Science	CKX41
FACS instrument	BD Biosciences	BD FACSAria Fusion
Cell counter	Thermo Fisher Scientific	Countess II FL

Table 5.3. Volumes per culture vessel size.

Plate Size	Medium	Geltrex (1:100)	ReLeSR	Accutase	D-PBS Wash
T75 flask	15 ml	6 ml	6 ml	6 ml	10 ml
T25 flask	5 ml	2 ml	2 ml	2 ml	5 ml
6-well	2 ml	1 ml	1 ml	1 ml	2 ml
12-well	1 ml	0.5 ml	0.5 ml	0.5 ml	1 ml
24-well	0.5 ml	250 µl	250 µl	250 µl	0.5 ml
48-well	250 µl	125 µl	125 µl	125 µl	0.25 ml
96-well	100 µl	50 µl	50 µl	50 µl	0.1 ml

Table 5.4. Reagents, supplements and growth factors used for differentiation of iPSCs into astrocytes.

Reagent/supplement/growth factor	Supplier	Catalogue number
Pen/Strep (10,000 U/ml)	Gibco	15070063
Glutamax 100X	Thermo Scientific	35050038
Geltrex hESC qualified matrix, LDEV-free	Fisher Scientific	11612149
Accutase	Thermo Scientific	A1110501
ReLeSR	Stemcell technologies	05872
CryoStor	Merck Millipore	C2874
Y-27632 dihydrochloride	Tocris Bio-Techne	1254
NeuroBrew 50X	Miltenyi Biotech	130-093-566
NeuroBrew without vitamin A 50X	Miltenyi Biotech	130-097-263
SB431542	Stratech	S1067-SEL
LDN193189	Merck Millipore	SML0559
IWR-1-endo	Santa Cruz	Sc-295215

EGF	Sigma Aldrich	SRP3027
FGF-2	Peprotech	100-18B
CNTF	Thermo Fisher	PHC7015
LIF	Peprotech	300-05
PluriSIn-1	Stemcell technologies	72822

Table 5.5. Media composition.

Basal medium	**Supplier**	**Catalogue number**
Essential 8 flex	Thermo Scientific	A2858501
mTeSR Plus	Stemcell technologies	100-0276
Advanced DMEM/F-12	Gibco	12634010
Neurobasal A	Thermo Scientific	10888022
Specific medium	**Basal medium**	**Additives**
ADF-PSG	Advanced DMEM/F-12	100 U/ml Pen/Strep, 1X Glutamax
SLI	ADF-PSG	0.5X NeuroBrew without Vitamin A, 10 µM SB431542, 200 nM LDN193189, 1.5 µM IWR-1-endo
NB	ADF-PSG	1X NeuroBrew without Vitamin A
NEL	ADF-PSG	1X NeuroBrew, 20 ng/ml EGF, 20 ng/ml LIF
NEF	ADF-PSG	1X NeuroBrew, 20 ng/ml EGF, 20 ng/ml FGF-2
CNTF	Neurobasal-A	100 U/ml Pen/Strep, 1X Glutamax, 1X NeuroBrew, 10 ng/ml CNTF
NBA	ADF-PSG	1X NeuroBrew

5.2.4. Immunocytochemistry of astrocytes

Immunocytochemistry was performed on cells seeded at ~70% confluency in black 96-well half area plates with transparent bottom (Fisher Scientific #165305) precoated with Geltrex (1:100). Cells were washed three times with Dulbecco's PBS (DPBS, Gibco #14190-094), fixed using 50 µl/well 4% PFA for 5 mins at RT, permeabilised with 50 µl 0.05% Saponin for 20 mins at RT and blocked with 100 µl/well 10% normal goat serum in PBS for 30 mins at RT. Primary antibody incubation was performed overnight at 4°C in PBS containing 0.1% Tween-20 and 1% goat serum using the following primary antibodies: polyclonal rabbit anti-GFAP (Agilent Dako #GA524) at

1:500, monoclonal mouse anti-S100β (Sigma-Aldrich #S2532) at 1:200, polyclonal rabbit anti-Vimentin (Cell Signaling Technology #3932) at 1:500, monoclonal mouse anti-clusterin (4C7, in-house) at 1:200. AlexaFluor-conjugated secondary antibodies (anti-mouse AlexaFluor594 and anti-rabbit AlexaFluor488 at 1:1000), and the nuclear stain Hoechst (1:500) were incubated for 1 hour at RT in PBS with 0.1% Tween-20. Negative control staining was performed by omitting the primary antibody step, or using an isotype control at the same concentration as the corresponding primary antibody (mouse IgG1 Biolegend #406601, mouse IgG2a Biolegend #401501; rabbit IgG Invitrogen #02-6102). Three PBS washes were performed between each step. Images were captured using Leica SP8 confocal microscope and Z stacks were analysed using the LASX software.

5.2.5. qPCR for astrocytic genes expression

RNA extractions were performed at days 0 (iPSC; from cells in 3 wells of a 6-well plate) and day 14 (astrocytes; from half of 3 T125 flasks) of terminal differentiation using the RNeasy Plus Mini kit (Qiagen #74134) according to the manufacturer's instructions. A Dnase digestion step (80 µl/sample Dnase I, Qiagen #79254) was incorporated after the sample was passed through the Rneasy spin column to remove genomic DNA, followed by two wash steps with 350 and 700 µl buffer RW1, respectively. RNA purity and concentration were determined using a spectrophotometer (DeNovix), and RNA samples were stored at -80°C.

cDNA synthesis was performed using the High-Capacity RNA-to-cDNA kit (ThermoFisher #4387406), using 182 ng RNA per sample and following the manufacturer's instructions. Reactions were performed either with or without reverse transcriptase (RT) using a thermal cycler for 1 hour at 37°C, 5 min at 95°C, and held at 4°C. cDNA was stored at -20°C. qPCR was performed in 384-well reaction plates, with 10 µl reactions/well (Table 5.6) for samples with or without RT, and negative controls with H_2O replacing cDNA. All reactions were performed in triplicate using the QuantStudio 7 Flex instrument (Thermo Fisher Scientific), with the following protocol for comparative ΔΔCt: hold at 50°C 2 min, 95°C 10 min; 40 cycles at 95°C 15 sec, 60°C 1 min; hold at 95°C 15 sec, 60°C 1 min, 95°C 15 sec. Primers were purchased from Thermo Fisher Invitrogen as 50 nM desalted custom DNA oligos, in liquid form (100 µM in water). Their sequences are shown in Table 5.7.

Table 5.6. qPCR reaction components.

Component	Volume
SYBR Green (Thermo Fisher Scientific #A25742)	5 µl
Forward primer (10 µM stock)	0.5 µl
Reverse primer (10 µM stock)	0.5 µl
Nuclease-free water	3.5 µl
cDNA	0.5 µl

Table 5.7. Primer sequences used for qPCR.

Gene	Forward primer 5'-3'	Reverse primer 5'-3'
total *CLU*	CTATCTGCGGGTCACCAC (exon 7)	CTCAGTGACACCGGAAGGAAC (exon 8)
***CLU* v1 (sCLU)**	ACAGGGTGCCGCTGACC (exon 1a)	CAGCAGAGTCTTCATCATGCC (exon 2)
***CLU* v1 Δ exon 2 (nCLU)**	GGGTGCCGCTGACCGAAAT (exon 1a/exon 3)	GAGTCTTTATCTGTTTCACCCCG (exon 3)
VIM	TGGACCAGCTAACCAACGAC	GCCAGAGACGCATTGTCAAC
GFAP	GAGCAGGAGGAGCGGCAC	TAGTCGTTGGCTTCGTGCTT
S100B	ATGTCTGAGCTGGAGAAGGC	TTCAAAGAACTCGTGGCAGG
EAAT1	CGAAGCCATCATGAGACTGGTA	TCCCAGCAATCAGGAAGAGAA
CD44	AGCATCGGATTTGAGACCTG	GTTGTTTGCTGCACAGATGG
ACTB	ACCATGGATGATGATATCGC	TCATTGTAGAAGGTGTGGTG
GAPDH	TGCACCACCAACTGCTTAGC	GGCATGGACTGTGGTCATGAG

5.2.6. Supernatant protein precipitation and cell lysis

Supernatant was collected from 3 T125 flasks of 80% confluent astrocytes on day 7 during terminal differentiation in serum-free medium (Neurobasal A with 2% NeuroBrew), filtered through 0.2 µm filter units and stored at -20°C. To increase the amount of clusterin in supernatant, 4x1.8 ml samples from each flask for each cell line were subjected to trichloroacetic acid (TCA) precipitation and the pellet resolubilised in 90 µl (20-fold concentration increase). Medium only was also concentrated by TCA precipitation as a negative control. For each sample, 200 µl 100% TCA were added to 1.8 ml supernatant, vortexed and incubated on ice for 30 minutes. The sample was

centrifuged at 10000xg for 10 minutes at 4°C, supernatant was discarded, the pellet washed with 500 µl ice-cold acetone, and centrifuged at 10000xg for 5 minutes at 4°C. The pellet was washed again, air dried, resuspended in 100 µl PBS with Tris pH 8 and stored at -20°C. For Western blotting, the pellet was resuspended in 50 µl SDS-PAGE gel loading buffer and boiled at 100°C for 10 minutes before loading onto the gel.

Astrocytes were harvested from 3 T125 flasks using Accutase as described above (Section 5.2.1), half of each pellet was washed with PBS, resuspended in 0.2-1 ml RIPA buffer (Thermo Fisher #89900) with protease inhibitors (Thermo Fisher #A32955) for 5 minutes on ice, centrifuged at 14000xg for 15 minutes at 4°C, and supernatant was collected and stored at -20°C prior to analysis by ELISA.

Total protein in supernatant and cell lysate samples was measured using the BCA kit (Thermo Fisher #23225). Cell lysate samples (diluted 1:2 in sterile PBS), concentrated supernatant (diluted 1:30 in sterile PBS), and albumin standard (from 2 µg/ml serially diluted 1:2) were added to a 96 well plate in duplicate (25 µl/well). Working reagent (49 parts A, 1 part B) was then added to each well (200 µl/well) and the plate was incubated at 37°C for 30 mins. Absorbance was read at 592 nm, a standard curve was constructed using GraphPad Prism 5, raw values interpolated on the curve and quantified by multiplying results by the dilution factor.

5.2.7. Western Blotting

Western blotting was performed as described in Section 2.3.2. Samples used were cell lysate (neat, 25 µl), conditioned medium following TCA precipitation (neat, 25 µl), pure human clusterin (1 µg) as positive control, medium only as negative control. Clusterin was detected using 4C7 anti-clusterin mAb at 2 µg/ml O/N at 4°C, followed by donkey anti-mouse IgG 2nd HRP-labelled antibody at 1:10000. Signal was visualised by electrochemiluminescence.

5.2.8. Quantification of secreted and intracellular clusterin by ELISA

The ELISA described in Section 3.3.6.3 was used to quantify intracellular clusterin (in cell lysate) and secreted clusterin (in concentrated supernatant). Samples were used undiluted (50 µl/well) in duplicate. After quantification, values were reported as ng/mg total protein.

5.2.9. Phagocytosis assays

Phagocytosis assays were performed on terminally differentiated astrocytes to assess their phagocytic capacity for pHrodo E. coli bioparticles. Cells were seeded at 80% confluency in 100 µl/well in a 96-well plate precoated with Geltrex and tested for phagocytosis 6 days later. Cells to be used in conditions including Cytochalasin D (CytoD; Cayman Chemicals #CAYM11330-1) were treated with 10 µM CytoD for 1 hour at 37°C before starting the experiments. All wells were washed once with live imaging solution (LIS, Invitrogen #A14291DJ) and the plate was scanned using IncuCyte (Sartorius) to obtain a baseline image of the cells. pHrodo bioparticles (Invitrogen #P35361) were sonicated for 15 cycles of 90 seconds on, 30 seconds off, then vortexed for 20 minutes. All reagents were diluted in LIS and incubated at 37°C for 10 minutes before addition to the wells. The following conditions were then tested for 8 wells/condition (100 µl/well): LIS only, CytoD only (10 µM), bioparticles only (10 µg/ml), bioparticles (10 µg/ml) with human serum (50 µl), bioparticles (10 µg/ml) with CytoD (10 µM), bioparticles (10 µg/ml) with CytoD (10 µM) and serum (50 µl). The wells were imaged every 20 minutes for the first 4 hours, then every 4 hours for 1 day.

5.3 Results

5.3.1 iPSCs undergo morphological changes during astrocyte differentiation

Human iPSCs were first differentiated into NPCs by neural induction. Cells were observed under an inverted phase contrast microscope every day and imaged using a PixeLINK digital integrated camera (Table 5.2). iPSCs were seeded as single cells to be 60-70% confluent on day 1 (Figure 5.4A). By day 8, the cells formed a dense neuroepithelial sheet, appearing tightly packed with smaller nuclei (Figure 5.4B). At day 14, neural rosettes were formed (Figure 5.4C). After 16 days of neural induction and proliferation of NPCs, cells showed substantial changes in morphology (Figure 5.4D). Cells of neuronal appearance were also observed at this stage, with no neurons observed after FACS selection of APCs (Figure 5.4E, F). APCs adopted an astrocyte-like morphology during exposure to FGF2 and EGF (Figure 5.4G), and terminally differentiated astrocytes after culture in the presence of CNTF had diverse morphologies (Figure 5.4H).

A. iPSCs under neural induction – day 1

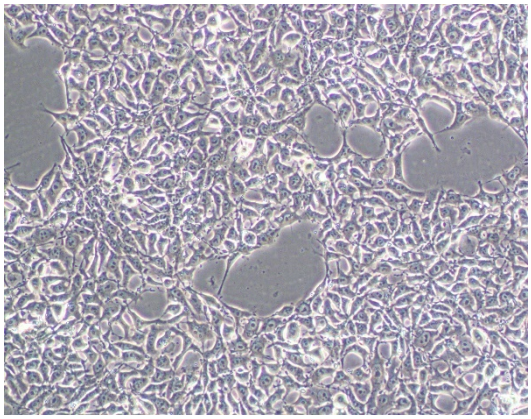

B. iPSCs under neural induction – day 7

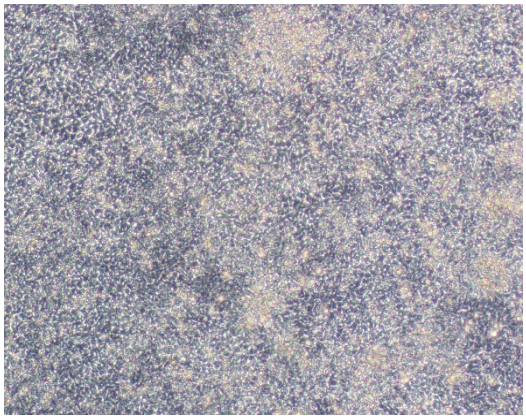

C. Neural rosettes – day 14

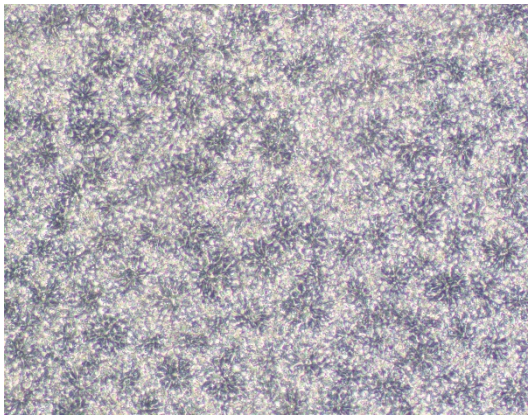

D. Neural precursor cells – P2

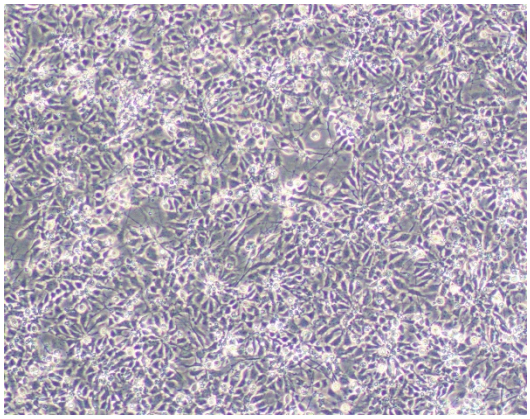

E. Neural precursor cells – before FACS

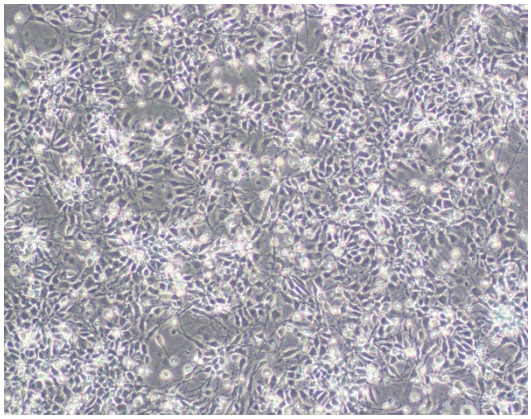

F. Astrocyte precursor cells – P1

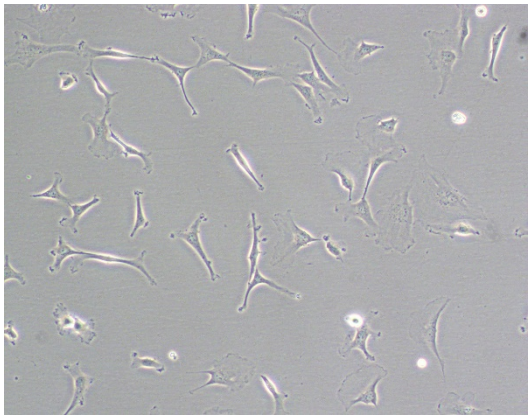

G. Astrocyte precursor cells – P7

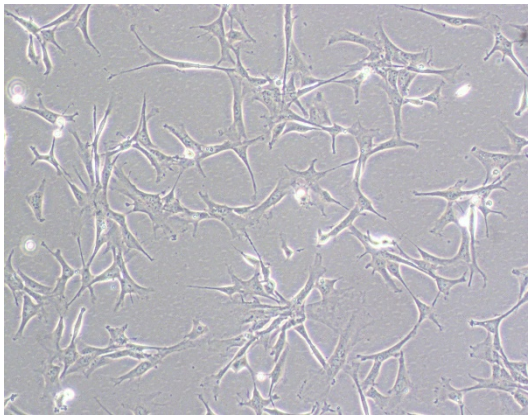

H. Astrocytes (2 week old)

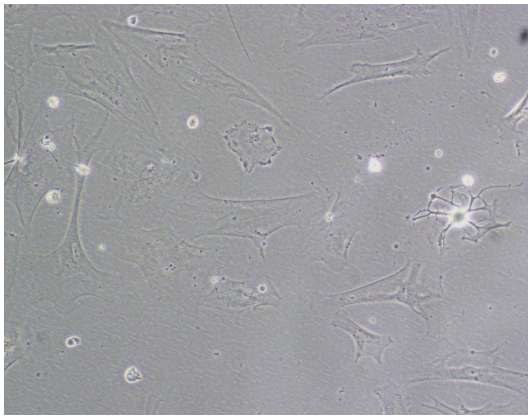

Figure 5.4. Morphological changes in KOLF2 cells at various time points during astrocyte differentiation. **A.** iPSCs seeded as single cells at the start of neural induction (day 1). **B.** iPSCs at the end of neural induction (day 7). **C.** Neural rosettes appeared during expansion of neural precursor cells. **D.** Neural precursor cells at P2, during selection for cells with high gliogenic potential. **E.** Neural precursor cells at P5, before FACS sorting of CD44-positive cells. **F.** Astrocyte precursor cells 10 days post-FACS. **G.** Astrocyte precursor cells at P7, before terminal differentiation. **H.** Terminally differentiated astrocytes (14 days post terminal differentiation). Images were taken under 10x magnification.

5.3.2 iPSC lines respond differently to neural induction

Following neural induction, at day 16, there was little variability between the morphology of NPCs derived from independent cell lines, and only NPCs and immature neurons were observed in culture (Figure 5.4D). However, one cell line (HPSI1213i-babk_2) did not respond to neural induction and formed very few NPCs and neurons, while >90% of cells appeared to be of a different, unknown identity (Figure 5.5). The neural induction was attempted 3 times and despite treatment of NPCs with neural rosette selection reagent (Stemcell technologies #05832) to selectively detach the few small rosettes, other spontaneously differentiated cells proliferated rapidly, contaminating the NPC culture. These cells were not used for further experiments.

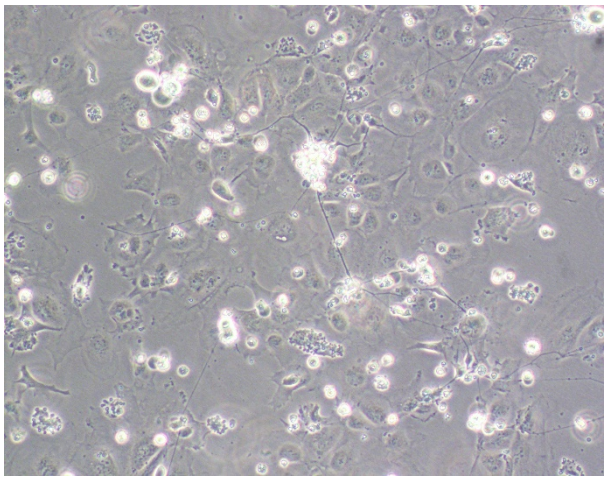

Figure 5.5. Morphology of cells which failed to produce NPCs.

5.3.3 iPSC-derived astrocytes from different lines display diverse morphologies

During terminal differentiation, cells typically started showing changes in morphology after day 4-5. Following terminal differentiation, at day 14, astrocytes from 5 different iPSC lines had distinct morphologies (Figure 5.6).

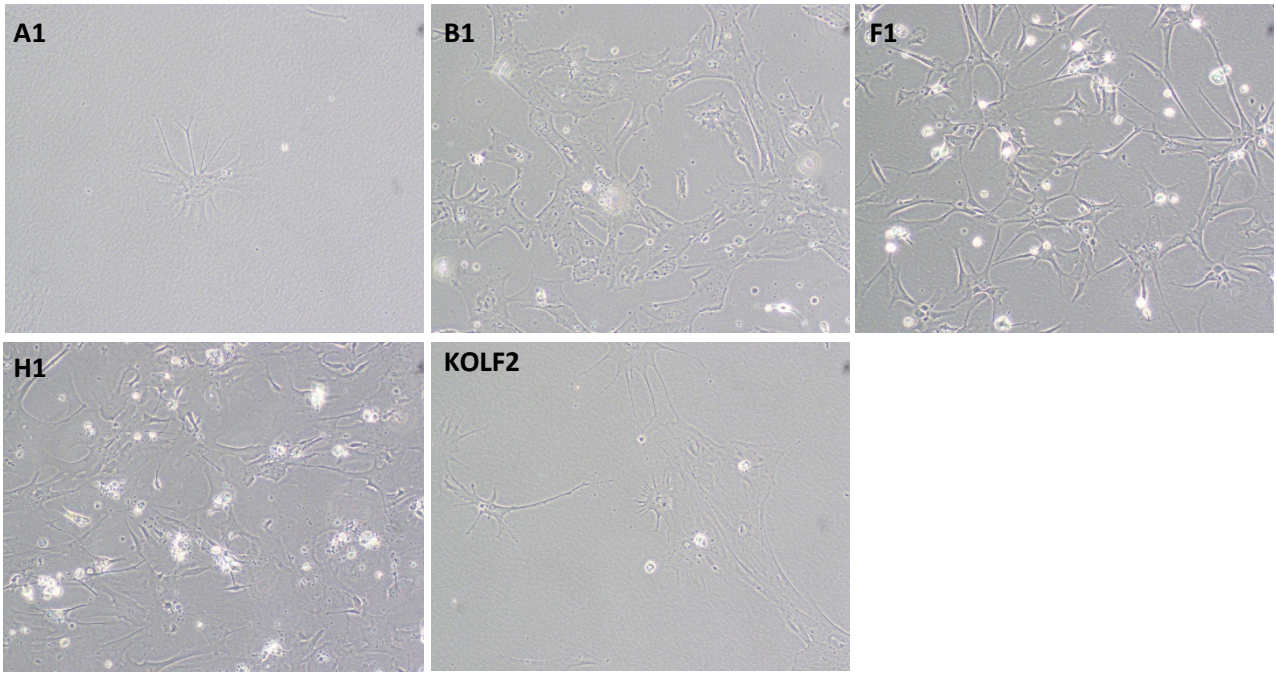

Figure 5.6. Morphology of terminally differentiated astrocytes from 5 iPSC lines. After APCs were seeded for terminal differentiation, cells from independent lines proliferated at different rates and adopted different morphologies.

5.3.4 CD44⁺ cells can be isolated by FACS

FACS was performed on NPCs to select cells expressing CD44. NPCs were incubated with an anti-CD44 antibody as described above (Section 5.2.3) and sorted using a FACS Aria Fusion automated cell sorter. Cell numbers obtained varied between 790 – 120,000, depending on passage number and length of time the cells were exposed to LIF. Figure 5.7 shows plots of CD44 positive signal intensity for A1 line, which was sorted at P5 after 4 weeks of growing the cells in NEL medium. A large peak of positive CD44 signal was observed (P3), and those cells were selected for sorting.

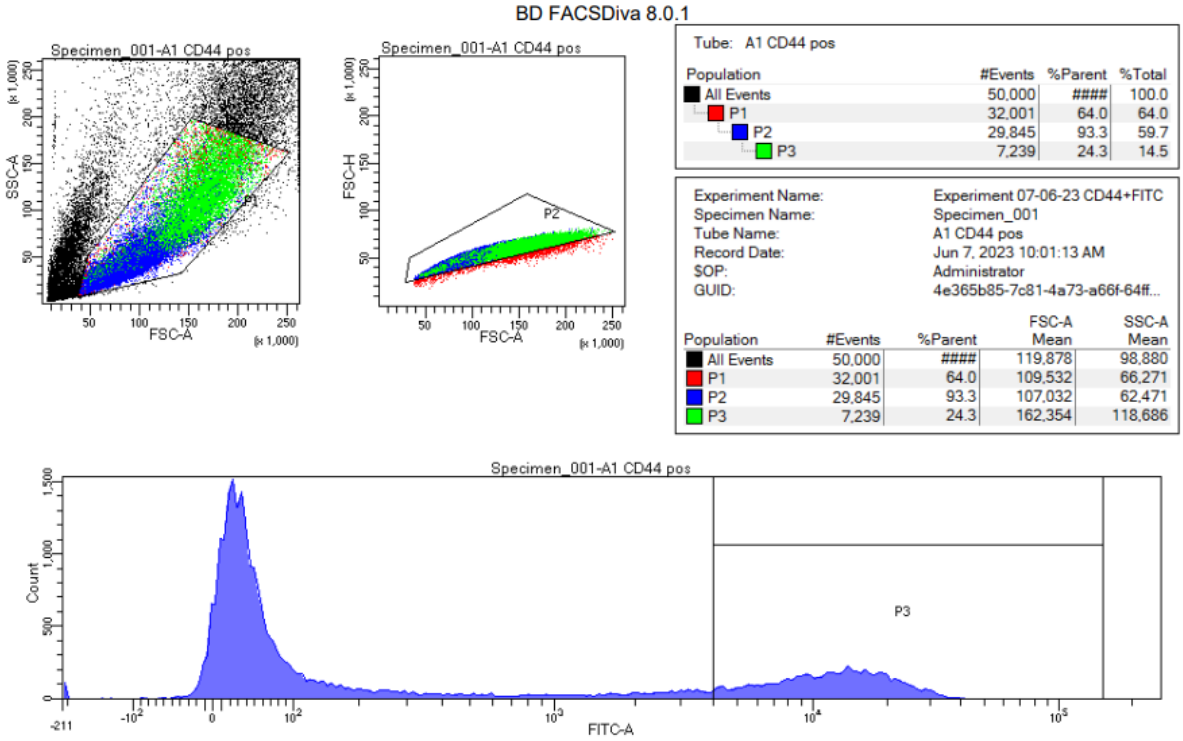

Figure 5.7. FACS on A1 NPCs stained with anti-CD44 antibody. After gating, 24.3% of cells (~120,000) were positive for CD44-FITC signal (green population) and were sorted.

5.3.5. iPSC-derived astrocytes expression of astrocytic proteins and clusterin confirmed by ICC

Immunocytochemistry was used to verify that differentiated KOLF2 astrocytes express astrocytic markers (GFAP, S100β, vimentin) at the protein level. The cells displayed fluorescence signal for all four markers tested, with no signal observed for negative control samples (Figure 5.8, Figure 5.9). iPSC-astrocytes also expressed clusterin, which was found to colocalise with GFAP (Figure 5.9B).

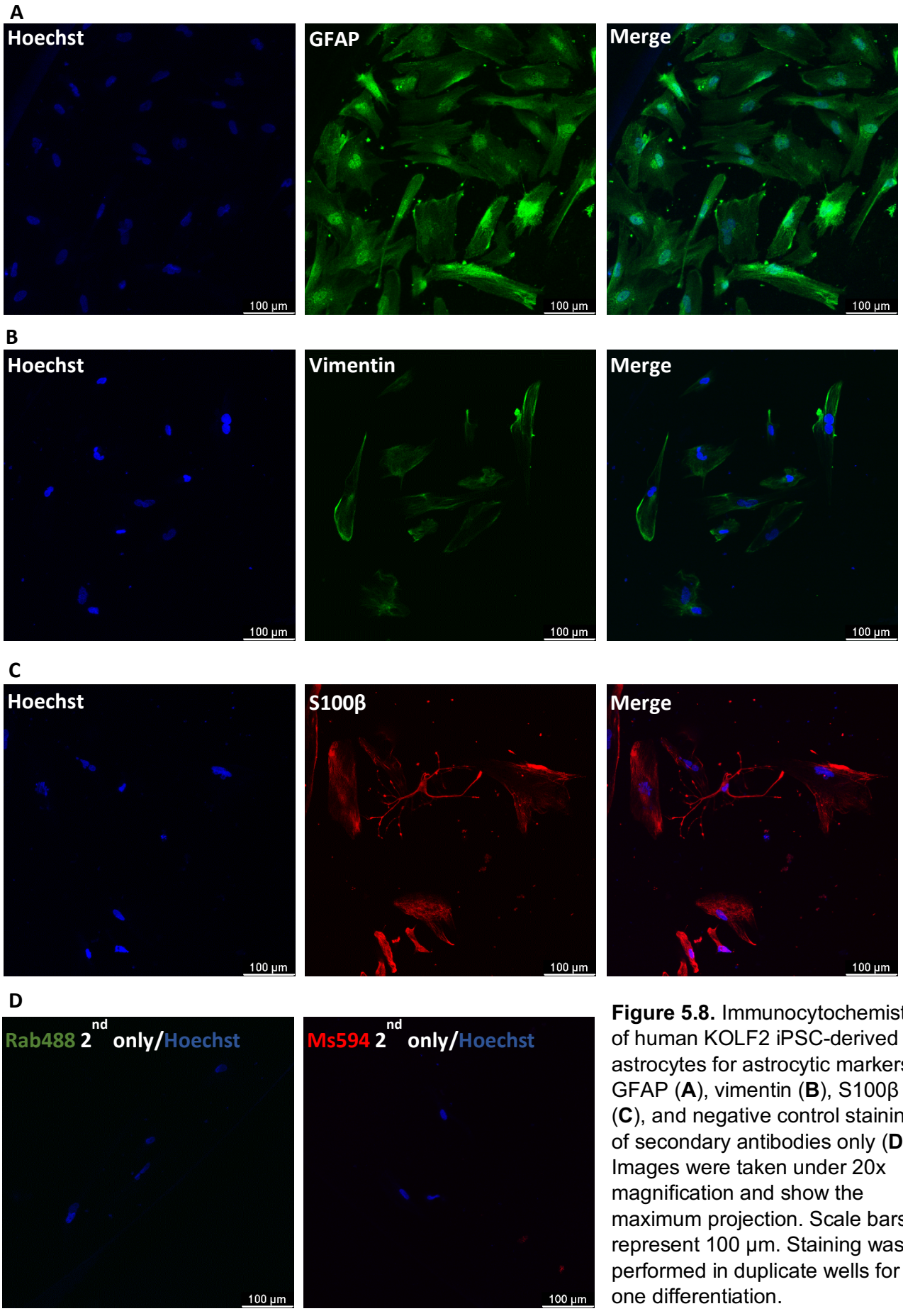

Figure 5.8. Immunocytochemistry of human KOLF2 iPSC-derived astrocytes for astrocytic markers GFAP (**A**), vimentin (**B**), S100β (**C**), and negative control staining of secondary antibodies only (**D**). Images were taken under 20x magnification and show the maximum projection. Scale bars represent 100 µm. Staining was performed in duplicate wells for one differentiation.

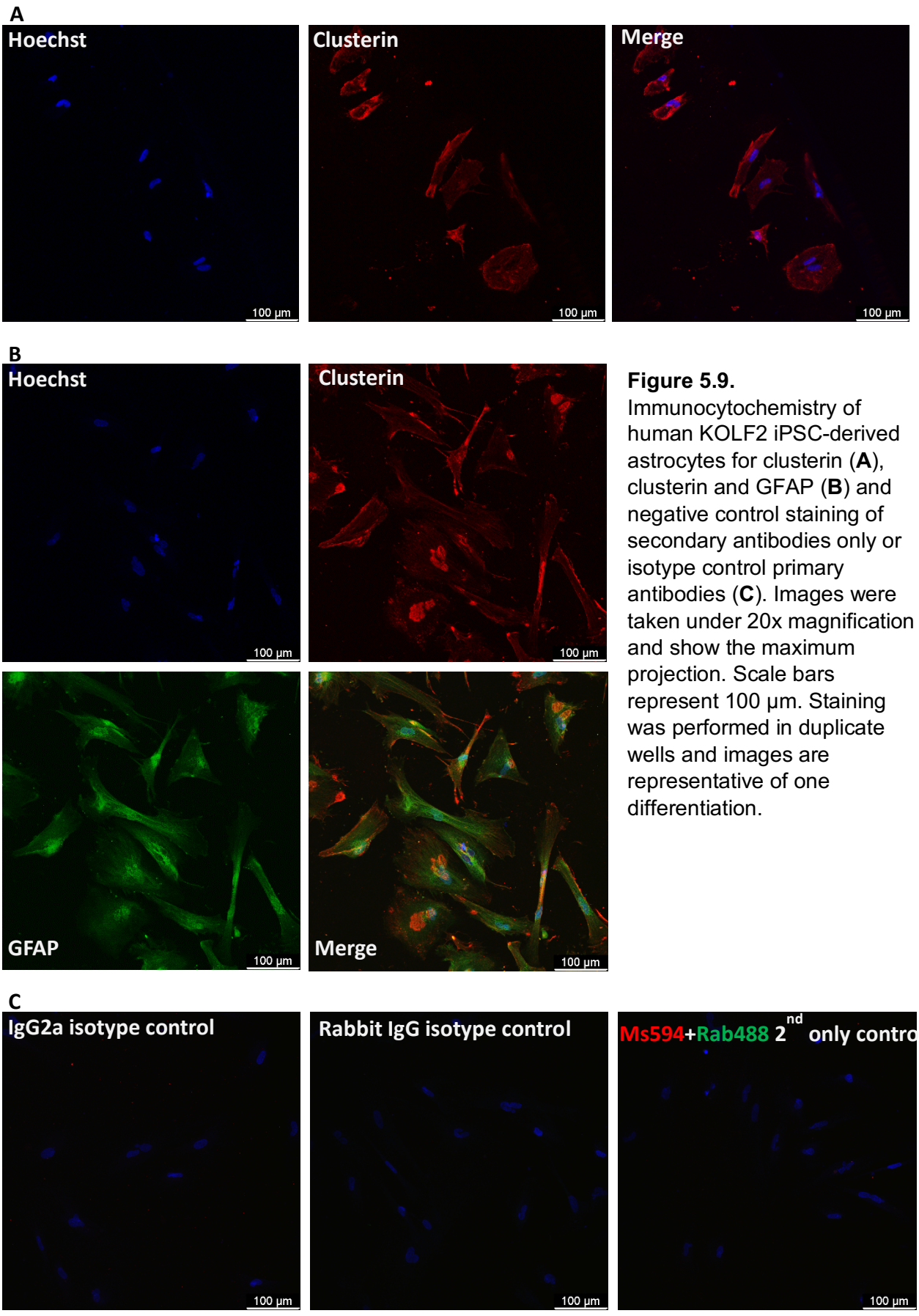

Figure 5.9. Immunocytochemistry of human KOLF2 iPSC-derived astrocytes for clusterin (**A**), clusterin and GFAP (**B**) and negative control staining of secondary antibodies only or isotype control primary antibodies (**C**). Images were taken under 20x magnification and show the maximum projection. Scale bars represent 100 µm. Staining was performed in duplicate wells and images are representative of one differentiation.

5.3.6. iPSC-derived astrocytes express astrocytic genes confirmed by qPCR

Gene expression of astrocytic markers (*GFAP, VIM, S100B, EAAT1, CD44)* and house-keeping control genes *(ACTB* and *GAPDH)* was quantified by RT-qPCR using cDNA from cells at day 0 (iPSC) and 14-day old astrocytes. Fold change expression was calculated relative to the day 0 sample. *VIM* and *CD44* expression was increased in all cell lines, while *GFAP, S100B* and *EAAT1* showed more variable expression across cell lines (Figure 5.10).

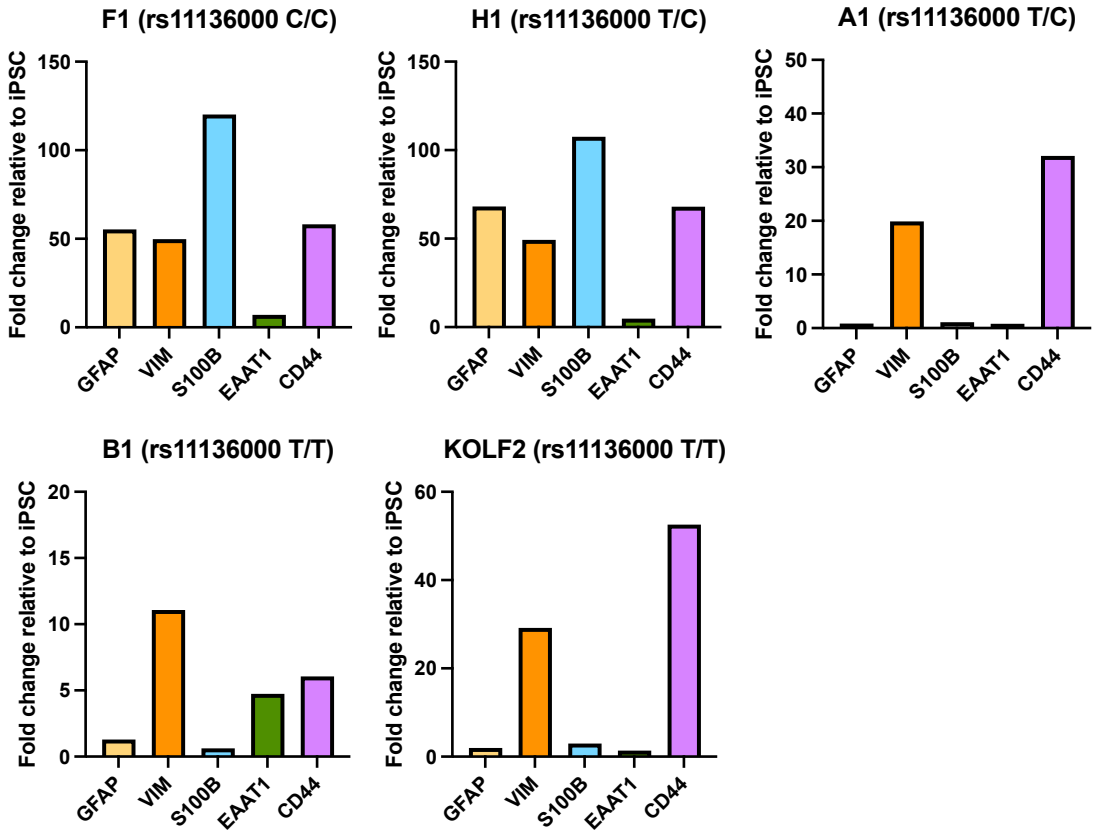

Figure 5.10. Fold change expression of astrocytic genes relative to iPSC. Gene expression of astrocytic markers was quantified by RT-qPCR in 14 day old astrocytes and compared to expression at iPSC stage. *VIM* and *CD44* were increased in all cell lines, while *GFAP, S100B* and *EAAT1* were only increased in F1 and H1 lines.

All iPSC-derived astrocytes were found to express astrocytic markers at the gene level, although expression varied across lines. Given that expression of *VIM* and *CD44*, two markers of immature astrocytes, was highest, this may indicate that astrocytes had not reached a fully mature state.

5.3.7. iPSC-derived astrocytes express intracellular and secreted forms of clusterin confirmed by Western blotting

To confirm that astrocytes express clusterin protein, cell lysate and concentrated supernatant were tested in Western blot. Clusterin in cell lysate appeared as two intracellular isoforms of approximately 55 and 60 kDa bands (Figure 5.11A, 7.5% gel), while secreted mature clusterin appeared as a 100 kDa band (Figure 5.11B, 10% gel). Clusterin was not detectable in non-concentrated supernatant (Figure 5.11A).

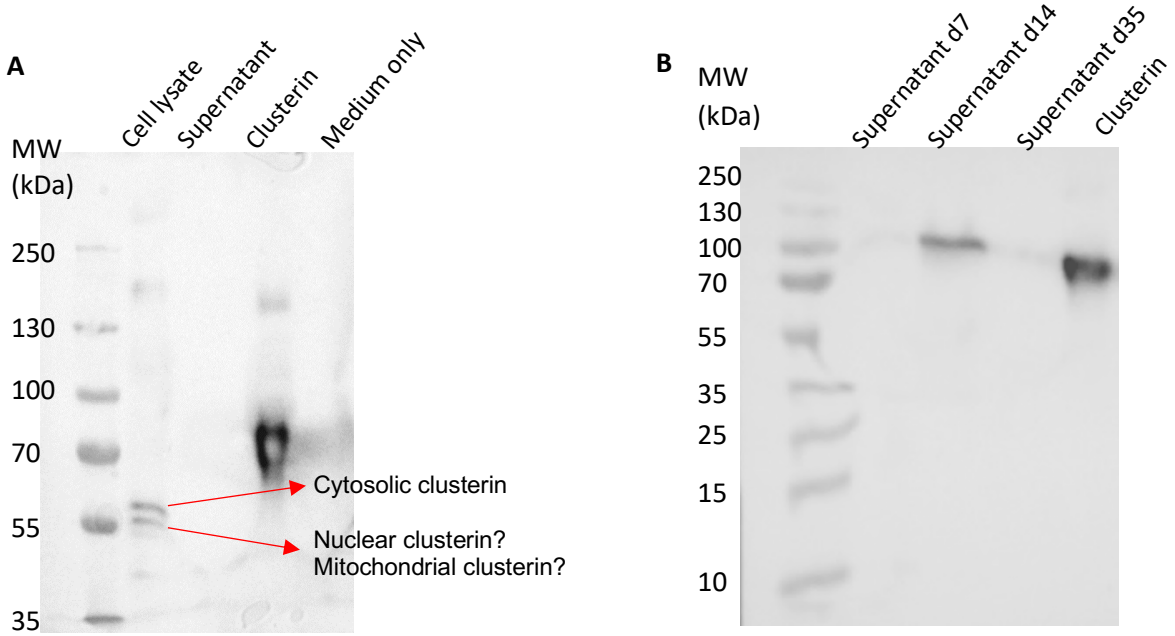

Figure 5.11. Western blot for clusterin in astrocyte cell lysate (**A**) and supernatant (**B**). Supernatant was collected at days 7 and 14 during terminal differentiation, and at day 35, and in B was concentrated by TCA precipitation. Samples were analysed under non-reducing conditions. N=1 experimental repeat.

Western blotting demonstrated that clusterin is present in astrocytes, as well as secreted in supernatant. In day 14 supernatant samples, clusterin appeared as a higher molecular weight band, possibly due to concentration of the sample which could result in clusterin forming high molecular weight aggregates. The lack of secondary antibody only negative controls is a limitation of this experiment.

5.3.8 Intracellular clusterin is increased at the protein and gene level in rs11136000 C/C astrocytes

Expression of intracellular and extracellular isoforms of clusterin were quantified at mRNA (RT-qPCR) and protein (ELISA) levels. mRNA levels of intracellular clusterin were detected using primers for transcripts lacking exon 2 (*CLU* variant 1 Δ exon 2)

and protein levels were determined by ELISA in cell lysates. Extracellular, mature clusterin was quantified at mRNA levels using primers spanning exons 1 and 2, and exons 7 and 8 for total *CLU* expression (secreted and intracellular isoforms), and by ELISA in concentrated supernatant samples. Three independent samples from one differentiation of each cell line were obtained, and all measurements were performed in duplicate (in ELISA) or triplicate (in qPCR) for each sample. Intracellular clusterin levels were significantly elevated at both protein and mRNA level in line F1, homozygous for the major allele at rs11136000 (Figure 5.12A). Extracellular clusterin levels were significantly elevated in lines KOLF2 (T/T) and H1 (T/C), however this only corresponded to a significant increase at mRNA level in line H1, but not KOLF2 (Figure 5.12B). Expression of total *CLU* mRNA followed a very similar pattern to expression of secreted *CLU* (Figure 5.12C). Expression of housekeeping genes *ACTB* and *GAPDH* was consistent across all cell lines (Figure 5.12D).

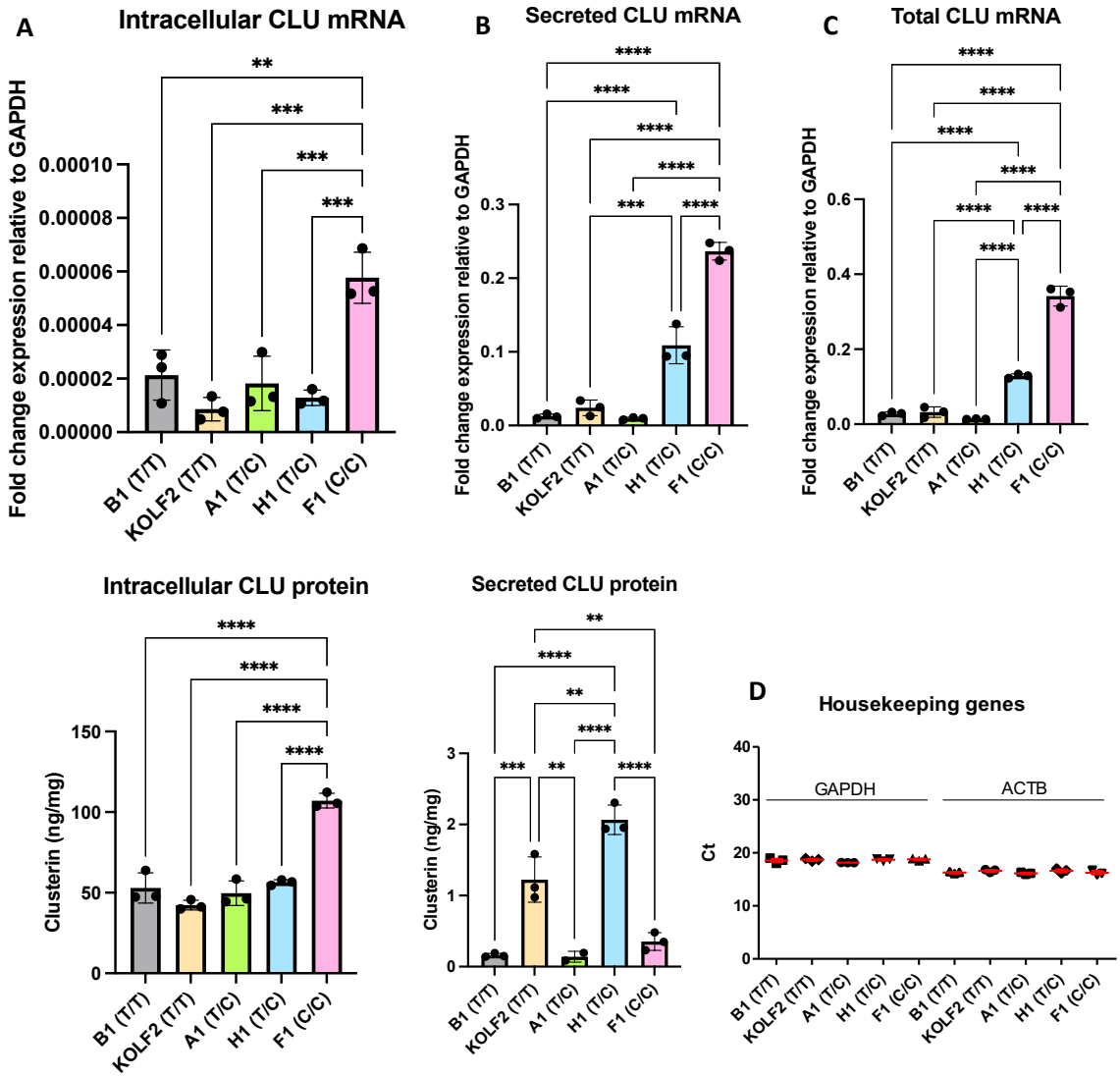

Figure 5.12. Quantification of intracellular and secreted clusterin isoforms. Intracellular clusterin was quantified in astrocyte lysate (**A**). Extracellular clusterin was quantified in concentrated supernatant (**B**). Total *CLU* mRNA was quantified in astrocytes and reflects mRNA levels of all *CLU* isoforms (**C**). Housekeeping genes *GAPDH* and *ACTB* were used to ensure equal amounts of mRNA for each sample were used (**D**). Data were analysed using one-way ANOVA with Tukey's post-hoc test. Ct=cycle threshold. ** p<0.01, *** p<0.001, *** p<0.0001.

5.3.9. iPSC-derived astrocytes phagocytose opsonised pHrodo bioparticles in vitro

Astrocytes were assessed for phagocytic capacity by incubating with pH sensitive E. coli bioparticles and monitoring changes in bioparticle uptake. Several conditions were tested including CytoD treatment, bioparticles alone, opsonised or non-opsonised bioparticles with or without CytoD (Figure 5.13). After 22h30min, cells only displayed phagocytic activity for serum-opsonised bioparticles as indicated by intracellular red fluorescence (Figure 5.13E, F). Morphological changes were also observed; cells treated with the actin disruptor CytoD were more ramified (Figure 5.13C, D), while cells treated with CytoD and opsonised bioparticles appeared to have damaged membranes (Figure 5.13F).

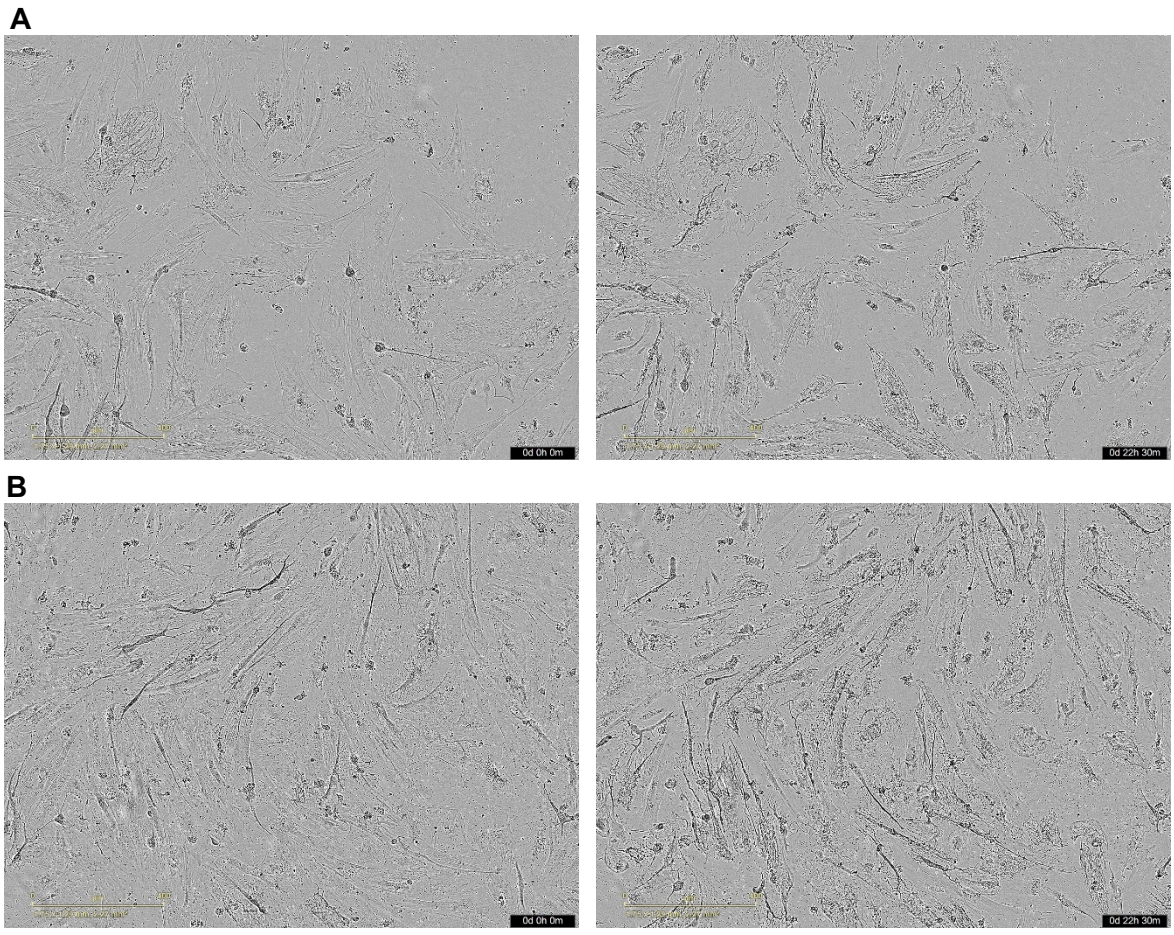

C

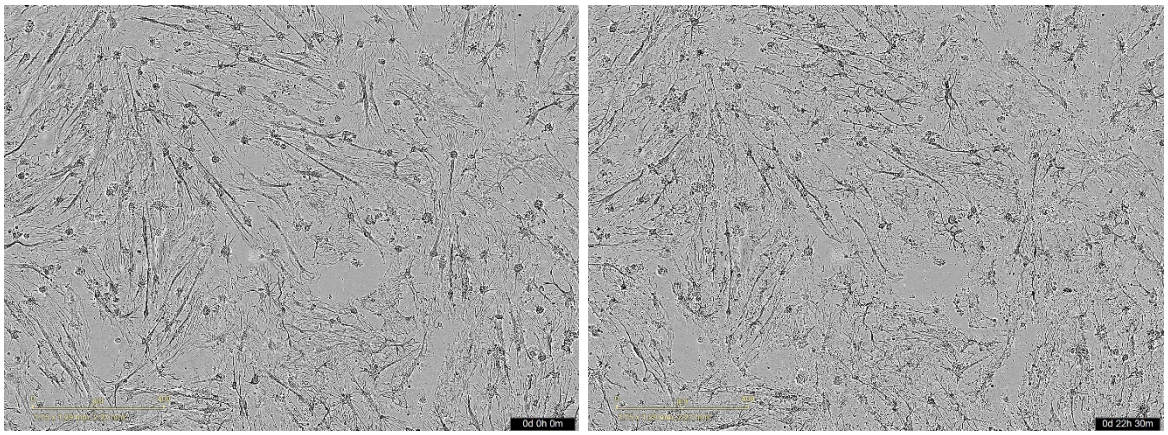
0d 0h 0m
0d 22h 30m

D

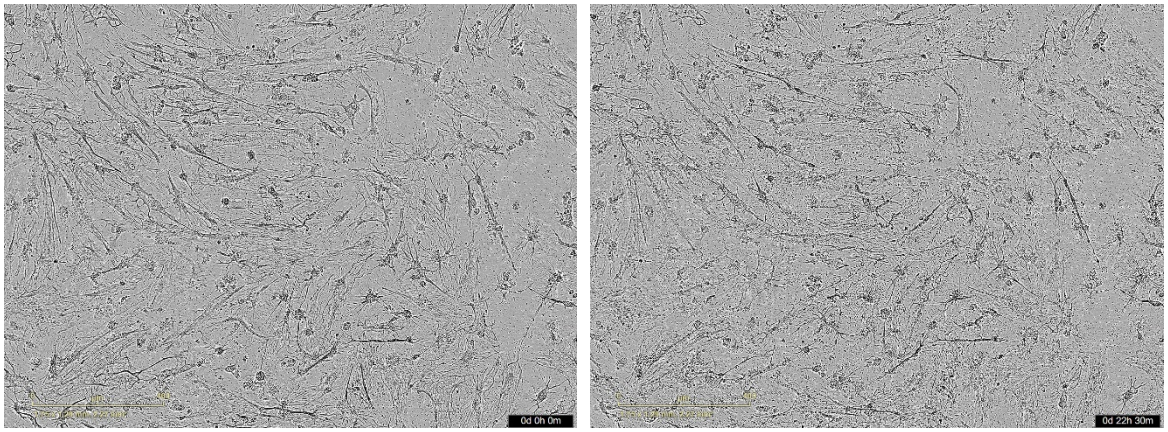
0d 0h 0m
0d 22h 30m

E

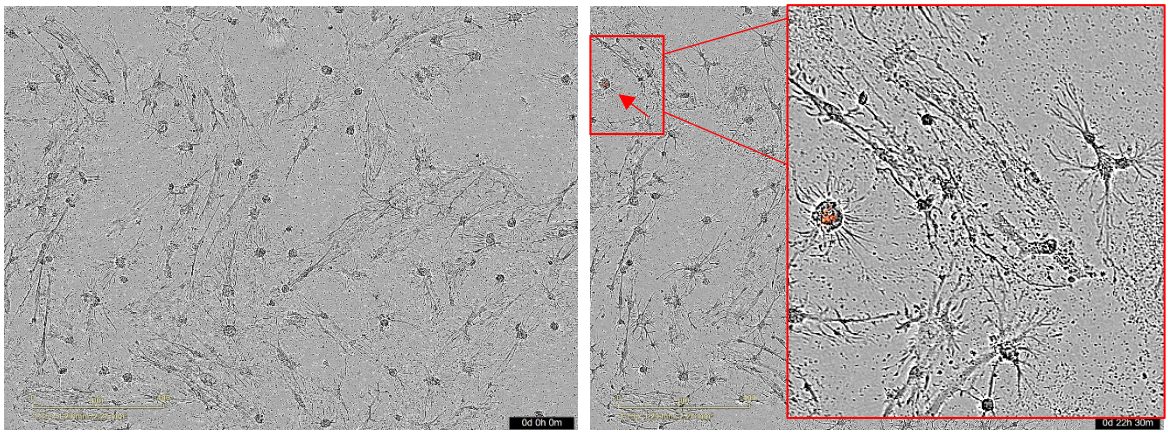
0d 0h 0m
0d 22h 30m

F

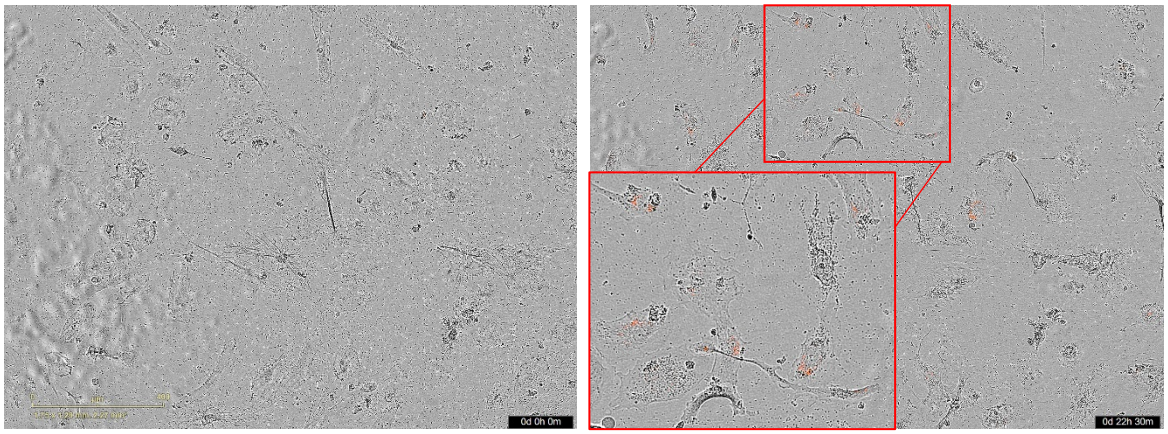
0d 0h 0m
0d 22h 30m

Figure 5.13. Phagocytosis of pHrodo tagged bioparticles by hiPSC-derived astrocytes at timepoint 0 (left) and 22h (right). (**A**) Cells (no stimulus). (**B**) Bioparticles. (**C**) CytoD. (**D**) Bioparticles + CytoD. (**E**) Opsonised bioparticles. (**F**) Opsonised bioparticles + CytoD. Enlarged red panels and arrow in (**E**) and (**F**) indicate cells which display red fluorescence signal following phagocytosis of bioparticles. Images were taken under 10x magnification. Scale bars represent 400 μm.

5.3 Discussion

Astrocytes are the second most abundant cell type in the CNS after neurons and fulfil many essential roles to provide support to neurons and efficient synaptic transmission. Moreover, they secrete clusterin, a key player in AD pathology which transports cholesterol between neurons and interacts with Aβ to clear it across the blood brain barrier (Bell et al, 2007). Since clusterin production was shown to be impacted by SNPs in *CLU* (Ling et al, 2012), some of which are found in an astrocyte-specific enhancer and super enhancer (Bellenguez et al, 2022; Nott et al, 2019), identifying the mechanisms through which these SNPs contribute to changes in the secretion of extracellular clusterin or production of cytosolic clusterin is the major aim of this chapter.

Astrocyte differentiation from human iPSCs led to gradual morphological changes throughout the differentiation process, typical of cells undergoing neural induction, becoming larger and more ramified, and exhibiting morphology resembling mature human astrocytes. Although some neurons were observed in cultures, a pure population of astrocyte progenitors was obtained by FACS, ensuring no contamination from other cell types, essential for future experiments investigating clusterin secretion. Mature astrocytes expressed astrocyte-specific proteins (vimentin, S100β, GFAP) and genes (*VIM, S100B, GFAP, CD44, EAAT1*), validating the efficacy of the differentiation method. Importantly, the cells also expressed clusterin isoforms normally found in the human brain as demonstrated by Western blotting: mature, secreted clusterin in cell supernatant (~80 kDa), and two intracellular clusterin protein isoforms in cell lysate (~50 kDa), which may be nuclear, mitochondrial, or cytosolic. By using primers specific for each isoform, secreted and intracellular clusterin was also quantifiable at the mRNA level. Previously, it was reported that quantification of *CLU* mRNA in human brain tissue separately for intracellular and secreted isoforms revealed significantly

elevated expression of the intracellular, but not secreted, isoforms in carriers of the T allele at rs11136000 (Ling et al, 2012). In the present study in iPSC astrocytes the opposite effect was seen, where homozygous C allele carriers at rs11136000 and rs11787077 had significantly elevated intracellular clusterin levels at both mRNA and protein levels. Since brain tissue contains many different cell types, it is difficult to determine the contribution of each cell type to clusterin production. More recently, Liu et al (2023) reported that iPSC-derived astrocytes carrying the C/C genotype had significantly elevated clusterin levels at both mRNA and protein level, supporting my findings. Moreover, by knocking out rs11136000 and surrounding SNPs in LD, they showed that clusterin expression was significantly reduced, providing evidence for a functional role of intronic GWS SNPs (Liu et al, 2023). Together, these findings suggest that the risk alleles in *CLU* SNPs influence clusterin expression in astrocytes, albeit in the opposite direction to that previously reported in whole brain homogenate.

While astrocytes play many and diverse roles in the brain, their contribution to clearance of debris, protein aggregates, and dead cells has not been extensively studied, in contrast to microglia, the chief scavengers of the brain. Since clusterin is a molecular chaperone in the brain aiding in the uptake and clearance of misfolded and aggregated proteins, and astrocytes secrete it in abundance, an interesting question was raised regarding their ability to phagocytose in vitro. When hiPSC-derived astrocytes from the KOLF2 line were tested for phagocytic capacity of pHrodo E.coli bioparticles, phagocytosis only occurred when bioparticles were serum opsonised and was very slow (>24 hours); in contrast, microglia showed phagocytosis of opsonised bioparticles within minutes (Levtova et al, 2017). This inefficiency of phagocytosis might be because astrocytes are poor at degrading phagocytosed material due to low acidity of endocytic compartments (Loov et al, 2015), causing them to store the intracellular load of phagocytosed material for long periods of time (Sollvander et al, 2016). For these reasons, further cell lines were not tested in phagocytosis experiments.

In summary, in this chapter astrocytes were differentiated from five human iPSC lines homozygous or heterozygous for rs11136000 and rs11787077 in *CLU*, and were shown to express astrocyte-specific markers, as well as clusterin. Clusterin levels were significantly elevated in C/C carriers, consistent with other recent findings in iPSC-astrocytes (Liu et al, 2023), but not with studies using brain tissue (Thambisetty

et al, 2012). It is important that future studies investigate the functional effects of these SNPs in other iPSC-derived brain cells, to identify which cells contribute to the increase in clusterin in brains of T/T carriers.

Some limitations of the work described in this chapter relate to the differentiation protocol, which could not be successfully implemented for all 6 cell lines initially planned, resulting in data only being available for 5 lines; additionally, the findings could not be replicated for a second and third independent differentiation due to neural precursors contaminating the astrocyte progenitor culture for 2 of the cell lines used, which led to few or no astrocytes observed in culture at the end of terminal differentiation. Despite these challenges, astrocyte differentiation from iPSCs was successful for 5 lines and resulted in novel and interesting findings regarding clusterin expression at the protein and gene level in cells carrying different genotypes at *CLU* GWAS significant SNPs.

CHAPTER 6: Discussion

This project set out to identify the mechanisms of interaction between SNPs in *CLU* and risk for AD by establishing an assay to quantify clusterin in plasma and CSF from AD and control subjects, linking clusterin protein levels to genotype at genome-wide significant SNPs in *CLU*, and measuring clusterin protein and mRNA levels in iPSC-derived astrocytes. To address these research aims, antibodies were necessary for a variety of experiments (protein purification, ELISA, Western blot, ICC, IHC). Antibodies have been an essential tool in biomedical research for decades and will continue to be used widely due to their extensive applications.

Good antibodies are also required for fluid biomarker studies, and good biomarkers are still being sought to aid early diagnosis of AD. There is now ample evidence that the AT(N) framework is a reliable measure to predict not only which individuals are more likely to develop dementia (Palmqvist et al, 2021), but also specifically distinguish between neurodegenerative diseases (Chouliaras et al, 2022). Moreover, longitudinal studies measuring plasma levels of Aβ and tau biomarkers can inform on disease progression or treatment effectiveness in clinical trials investigating anti-Aβ therapies. Since clusterin was found to colocalise with Aβ plaques, and later was identified as a significant genetic risk factor for AD, this prompted the investigation of clusterin as a biomarker for AD. Due to a lack of good quality monoclonal antibodies against human clusterin, generating a panel of antibodies was a crucial aim of this project. This was successfully accomplished following a standard protocol already developed by the group, and 2 of the resulting antibodies were used to build a sandwich ELISA which is now commercially available from Hycult Biotech (#HM2435, #HM2436), demonstrating its high quality and utility for the scientific community.

A major finding of this study was the demonstration that clusterin was significantly elevated in AD compared to controls in a cohort comprising 1907 subjects, replicating results from other studies using smaller sample sizes (Mullan et al, 2013; Hakobyan et al, 2016). Clusterin was also significantly increased in plasma from subjects with DS compared to healthy controls, a novel finding now published in Alzheimer's and Dementia: The Journal of the Alzheimer's Association (Veteleanu et al, 2022). Since clusterin is expressed in numerous tissue types and is predominantly produced by liver cells, the relationship between elevated plasma levels and AD pathology is not

completely understood. Due to its ubiquitous expression, clusterin supports various roles spanning lipid homeostasis, apoptosis, and complement regulation, making it difficult to establish which of these roles are impacted in the context of AD risk and which ones become dysregulated to increase in peripheral clusterin protein. Moreover, it has been shown that most people with AD have at least two comorbidities, further complicating matters when trying to identify the precise mechanism behind roles of clusterin role in AD (Bunn et al, 2014). To address this it would be necessary to conduct longitudinal biomarker studies, monitoring changes in both physical and cognitive health. Nevertheless, it is becoming increasingly clear that AD pathology can be detected in the periphery, and this is an important clue not only for diagnosis but also for drug development purposes.

Despite the significant increase in clusterin levels in AD and a well-known association between SNPs in *CLU* and risk of AD, no genetic variants in *CLU* were found that influenced plasma clusterin protein levels, a finding consistent with previous studies (Jongbloed et al, 2015; Thambisetty et al, 2010; Mullan et al, 2013; Haight et al, 2018; Trindade et al, 2023). As discussed previously, the observed increase could be attributed to other functions clusterin performs in the periphery, and may not necessarily be influenced by genetics. Through other studies using brain tissue, it has become apparent that SNPs in *CLU* are associated with changes in clusterin expression in the brain only, and not in the periphery, which is not unexpected given that AD affects the brain (Bellenguez et al, 2022). Additionally, SNPs in *CLU* were shown to be associated with entorhinal atrophy in AD and MCI (Thambisetty et al, 2010) and cerebral amyloid angiopathy (Bonaterra-Pastra et al, 2023). These findings prompted my study of clusterin synthesis in astrocytes, the brain cells responsible for producing the majority of clusterin in the brain, which may offer a window into how SNPs in *CLU* modulate the expression of clusterin protein in a cell type relevant to AD.

A substantial part of this project was dedicated to the use of human iPSCs from donors with different genotypes at GWAS-significant SNPs in *CLU*; these were used to generate astrocytes and study the effect of the SNPs on secreted and intracellular clusterin levels. This is a relatively novel approach, as the majority of previous studies have investigated roles of clusterin in AD using mouse models, human brain tissue, or simply as a biomarker in plasma or CSF (Wojtas et al, 2020; Thambisetty et al, 2010). iPSCs are an extremely useful tool with many advantages in neuroscience research:

they can be obtained using minimally invasive techniques from subjects suffering from a disease or carrying a risk mutation, are a much more relevant model than rodent cells while helping minimise the use of animals in research, and can be used for high-throughput compound screening after differentiating into relevant cell types. For the purpose of this project, iPSCs were differentiated into astrocytes, a cell type that is now recognised to play an important role in AD (Monterey et al, 2021).

There are numerous approaches to obtaining astrocytes from iPSCs, including traditional approaches relying on growth factors that signal through pathways which switch on transcription factors for astrocytic genes, commercial kits which simplify the differentiation process by providing proprietary ready-made reagent mixes for culturing the cells, and forward reprogramming approaches, where cells can be directly differentiated into the cell type of interest. The latter approach started with Yamanaka's discovery of the 4 transcription factors (*SOX2, NANOG, OCT4, c-MYC*) that were sufficient and necessary to reprogram somatic cells back to a pluripotent state (Takahashi and Yamanaka, 2006). Since then, numerous direct reprogramming strategies have been developed to obtain neurons or astrocytes, two cell types which are otherwise difficult to differentiate from iPSCs, with relatively good efficiencies (Tian et al, 2021; Caiazzo et al, 2015). There are certain advantages and disadvantages to each method and researchers must choose and design their approach carefully before attempting to differentiate iPSCs, to maximise the likelihood of obtaining the cells of interest. An ideal differentiation protocol would generate mature astrocytes in a short period of time (under one month) utilising reagents that are widely available and inexpensive, be reproducible among different users and for different cell lines, and result in a highly pure cell population (>90%). In-house developed protocols using traditional methods to differentiate astrocytes have the advantage of flexibility in designing and optimising each step, tend to be less expensive than commercial approaches, and can generate 100% pure astrocyte populations following a cell sorting step. However, they also have major disadvantages, including length of time needed to obtain mature cells (>2 months), and lack of reproducibility. In comparison, commercial kits offer the advantage of convenience, faster results, and better reproducibility, albeit at a higher cost. Direct reprogramming methods are much faster (~2 weeks) as they do not depend on the time needed by the cells to respond to the growth factors that signal to activate transcription of astrocytic genes. By transfecting

iPSCs with lentiviral vectors containing pro-astrocytic transcription factors (*NFIA, NFIB, SOX9*) and overexpressing them in genomic safe harbour sites, the cells can be quickly, precisely, and consistently differentiated into astrocytes, making this approach highly advantageous. Some disadvantages include difficulties in identifying the right combination of transcription factors, and variability in the purity of the cell populations obtained.

The protocol used in this project was adapted from previously published methods (Shi et al, 2012; Serio et al, 2013), and was modified to involve neural induction with cells as a monolayer rather than neurospheres. Although this protocol (described in Chapter 6) generated highly pure astrocyte progenitor populations that could be cryopreserved following cell sorting, was reproducible when repeated on the same cell lines, and delivered mature astrocytes expressing astrocytic markers at the protein and gene level, several issues were identified while attempting to differentiate iPSCs using this method. 1) The protocol is expensive and very time consuming. 2) Not all cell lines responded to neural induction using LDN193189, SB431542, IWR-1-endo, failing to produce neural precursor cells, an essential intermediate step between iPSCs and astrocytes. 3) The time needed for each cell line to respond to astrocyte gene expression induction through LIF was very variable, anything between 2 and 6 weeks, therefore making optimisation of the protocol very challenging. 3) A sorting step is required to isolate a pure population of astrocyte progenitors, which involves an expensive instrument and specialist skills. 5) Astrocyte progenitors proliferated at different rates and mature astrocyte populations were very heterogenous between different lines, which may have consequences for functional assays. For these reasons, and considering the advantages and disadvantages of other methods described above, if I were to do this project again, I would opt for a direct reprogramming approach. Although this approach is not guaranteed to generate astrocytes, its short experimental timeline would offer the possibility to quickly troubleshoot and optimise a protocol capable of efficiently generating astrocytes from any iPSC line.

Although research involving iPS-derived cells has undoubtedly helped advance our understanding of neurodegenerative diseases by providing insight into the role of protein aggregates in neuronal death, how different brain cells react during pathological events, and the effect of genetic mutations on cell behaviour, it has its

limitations. The iPS cell lines need to be of high quality and periodically tested for chromosomal abnormalities and other genetic defects acquired during the reprogramming process and during passaging; iPSC maintenance and differentiation is an expensive and time-consuming process with varying degrees of success for obtaining cells of interest. Finally, no protocol is perfect because experimenters can influence or modify, but not control, the fate of iPSCs when attempting to differentiate them into CNS cells using various methods. It is important that future research aims to provide the scientific community with an optimal method that can be employed by researchers world-wide to reproducibly generate astrocytes from iPSCs.

Despite these challenges, I succeeded in generating iPSC-derived astrocytes as tools for exploring the roles of SNPs in *CLU* in risk for AD and generated novel data. The risk alleles at rs11136000 and rs11787077 were associated with increased levels of mRNA encoding intracellular and secreted clusterin isoforms; this corresponded to an increase at protein level for intracellular clusterin only, highlighting the importance of this isoform. Together with findings from recent studies showing that: 1) knockout of SNPs in the LD block containing rs11136000 by small-scale CRISPR-Cas9 screen led to a significant reduction in clusterin synthesis (Liu et al, 2023); 2) rs11787077 is a significant eQTL for brain clusterin expression and overlaps with an astrocyte-specific enhancer and super-enhancer (Bellenguez et al, 2022; Nott et al, 2019), these results provide compelling evidence that AD-associated intronic SNPs in *CLU* regulate clusterin expression in astrocytes, which may be implicated in AD pathogenesis.

Concluding remarks and future directions

To summarise the major findings of this work, clusterin was found to be significantly elevated in AD plasma, but not CSF, and this change was not attributed to known AD risk SNPs in *CLU*. For this reason, it is important to consider other genetic modifiers of protein expression, such as epigenetics, as well as non-genetic risk factors that may affect secretion of certain proteins when investigating a multifactorial disease such as AD. Future longitudinal studies should focus on the progression of AD from MCI to determine whether risk SNPs in *CLU*, alone or in combination with other genes associated with AD risk, lead to a faster cognitive decline. Future studies should also investigate changes in clusterin concentrations in larger CSF cohorts obtained following standardised collection methods, and post-mortem brain tissue homogenate,

to identify any correlations between plasma, CSF, and brain levels of clusterin as AD progresses.

Human iPSCs proved to be an invaluable resource in this project and, by differentiating them into astrocytes, led to novel findings showing increased clusterin synthesis at mRNA and protein levels in carriers of risk alleles at GWS SNPs in *CLU*. It is worth noting that results were derived from only one differentiation of the cells; these would need to be replicated at least twice to increase confidence in stating the outcome. Moreover, the number of cell lines used was small due to limited numbers of risk allele carriers available; at least 3 lines for each genotype should be used for future experiments to improve statistical power. Simulating *in vitro* an environment that more closely resembles AD pathology (Aβ fibrils, inflammation) using iPSC astrocytes alone or in co-culture with neurons and/or microglia could provide further insight into how clusterin synthesis changes in these conditions.

Overall, the findings described in this thesis contribute to our understanding of the mechanisms of interaction between SNPs in *CLU* and risk of AD, and highlight the role of non-coding variants in the gene encoding this important and versatile lipoprotein in brain homeostasis and disease.

References

Alcolea, D., Delaby, C., Munoz, L., Torres, S., Estelles, T., Zhu, N., et al. (2021). Use of plasma biomarkers for AT(N) classification of neurodegenerative dementias. *Journal of Neurology Neurosurgery and Psychiatry, 92*(11), 1206-1214.

Allen, M., Zou, F. G., Chai, H. S., Younkin, C. S., Crook, J., Pankratz, V. S., et al. (2012). Novel late-onset Alzheimer disease loci variants associate with brain gene expression. *Neurology, 79*(3), 221-228.

Andrade-Moraes, C. H., Oliveira-Pinto, A. V., Castro-Fonseca, E., da Silva, C. G., Guimaraes, D. M., Szczupak, D., et al. (2013). Cell number changes in Alzheimer's disease relate to dementia, not to plaques and tangles. *Brain, 136*, 3738-3752.

Apostolova, L. G., Risacher, S. L., Duran, T., Stage, E. C., Goukasian, N., West, J. D., et al. (2018). Associations of the Top 20 Alzheimer Disease Risk Variants with Brain Amyloidosis. *Jama Neurology, 75*(3), 328-341.

Bailey, R. W., Dunker, A. K., Brown, C. J., Garner, E. C., & Griswold, M. D. (2001). Clusterin, a binding protein with a molten globule-like region. *Biochemistry, 40*(39), 11828-11840.

Barres, B. A. (2008). The Mystery and Magic of Glia: A Perspective on Their Roles in Health and Disease. *Neuron, 60*(3), 430-440.

Bateman, R. J., Xiong, C. J., Benzinger, T. L. S., Fagan, A. M., Goate, A., Fox, N. C., et al. (2012). Clinical and Biomarker Changes in Dominantly Inherited Alzheimer's Disease. *New England Journal of Medicine, 367*(9), 795-804.

Beeg, M., Stravalaci, M., Romeo, M., Carra, A. D., Cagnotto, A., Rossi, A., et al. (2016). Clusterin Binds to A(1-42) Oligomers with High Affinity and Interferes with Peptide Aggregation by Inhibiting Primary and Secondary Nucleation. *Journal of Biological Chemistry, 291*(13), 6958-6966.

Bell, R. D., Sagare, A. P., Friedman, A. E., Bedi, G. S., Holtzman, D. M., Deane, R., et al. (2007). Transport pathways for clearance of human Alzheimer's amyloid beta-peptide and apolipoproteins E and J in the mouse central nervous system. *Journal of Cerebral Blood Flow and Metabolism, 27*(5), 909-918.

Bellenguez, C., Kucukali, F., Jansen, I. E., Kleineidam, L., Moreno-Grau, S., Amin, N., et al. (2022). New insights into the genetic etiology of Alzheimer's disease and related dementias. *Nature Genetics, 54*(4), 412-+.

Bettens, K., Vermeulen, S., Van Cauwenberghe, C., Heeman, B., Asselbergh, B., Robberecht, C., et al. (2015). Reduced secreted clusterin as a mechanism for Alzheimer-associated CLU mutations. *Molecular Neurodegeneration, 10*, 30.

Blaschuk, O., Burdzy, K., & Fritz, I. B. (1983). Purification and characterization of a cell-aggregating factor (clusterin), the major glycoprotein in ram rete testis fluid. *Journal of Biological Chemistry, 258*(12), 7714-7720.

Blennow, K., & Zetterberg, H. (2018). Biomarkers for Alzheimer's disease: current status and prospects for the future. *Journal of Internal Medicine, 284*(6), 643-663.

Bonaterra-Pastra, A., Benítez, S., Pancorbo, O., Rodríguez-Luna, D., Vert, C., Rovira, A., et al. (2023). Association of candidate genetic variants and circulating levels of ApoE/ApoJ with common neuroimaging features of cerebral amyloid angiopathy. *Frontiers in Aging Neuroscience, 15*, 1134399.

Bunn, F., Burn, A. M., Goodman, C., Rait, G., Norton, S., Robinson, L., et al. (2014). Comorbidity and dementia: a scoping review of the literature. *Bmc Medicine, 12*, 192.

Caiazzo, M., Giannelli, S., Valente, P., Lignani, G., Carissimo, A., Sessa, A., et al. (2015). Direct Conversion of Fibroblasts into Functional Astrocytes by Defined Transcription Factors. *Stem Cell Reports, 4*(1), 25-36.

Chambers, S. M., Fasano, C. A., Papapetrou, E. P., Tomishima, M., Sadelain, M., & Studer, L. (2009). Highly efficient neural conversion of human ES and iPS cells by dual inhibition of SMAD signaling. *Nature Biotechnology, 27*(3), 275-280.

Chen, J. J., Wang, M. Y., & Turko, I. V. (2012). Mass spectrometry quantification of clusterin in the human brain. *Molecular Neurodegeneration, 7*, 41.

Chen, L. H., Mak, T. S. H., Fan, Y. H., Ho, D. T. Y., Sham, P. C., Chu, L. W., et al. (2020). Associations between CLU polymorphisms and memory performance: The role of serum lipids in Alzheimer's disease. *Journal of Psychiatric Research, 129*, 281-288.

Choimiura, N. H., Ihara, Y., Fukuchi, K., Takeda, M., Nakano, Y., Tobe, T., et al. (1992). SP-40,40 is a constituent of Alzheimers amyloid. *Acta Neuropathologica, 83*(3), 260-264.

Chouliaras, L., Thomas, A., Malpetti, M., Donaghy, P., Kane, J., Mak, E., et al. (2022). Differential levels of plasma biomarkers of neurodegeneration in Lewy body dementia, Alzheimer's disease, frontotemporal dementia and progressive supranuclear palsy. *Journal of Neurology Neurosurgery and Psychiatry*, *93*(6), 651–658.

Cirrito, J. R., Kang, J. E., Lee, J., Stewart, F. R., Verges, D. K., Silverio, L. M., et al. (2008). Endocytosis is required for synaptic activity-dependent release of amyloid-beta in vivo. *Neuron, 58*(1), 42-51.

Cruchaga, C., Kauwe, J. S. K., Harari, O., Jin, S. C., Cai, Y. F., Karch, C. M., et al. (2013). GWAS of Cerebrospinal Fluid Tau Levels Identifies Risk Variants for Alzheimer's Disease. *Neuron, 78*(2), 256-268.

Cruz-Sanabria, F., Bonilla-Vargas, K., Estrada, K., Mancera, O., Vega, E., Guerrero, E., et al. (2021). Analysis of cognitive performance and polymorphisms of SORL1, PVRL2, CR1, TOMM40, APOE, PICALM, GWAS_14q, CLU, and BIN1 in patients with mild cognitive impairment and cognitively healthy controls. *Neurologia, 36*(9), 681-691.

Cummings, D. M., Liu, W. F., Portelius, E., Bayram, S., Yasvoina, M., Ho, S. H., et al. (2015). First effects of rising amyloid-beta in transgenic mouse brain: synaptic transmission and gene expression. *Brain, 138*, 1992-2004.

Dai, J. T., Johnson, E. C. B., Dammer, E. B., Duong, D. M., Gearing, M., Lah, J. J., et al. (2018). Effects of APOE Genotype on Brain Proteomic Network and Cell Type Changes in Alzheimer's Disease. *Frontiers in Molecular Neuroscience, 11,* 454.

De Rojas, I., Moreno-Grau, S., Tesi, N., Grenier-Boley, B., Andrade, V., Jansen, I. E., et al. (2021). Common variants in Alzheimer's disease and risk stratification by polygenic risk scores. *Nature Communications, 12*(1), 3417.

DeMattos, R. B., O'Dell, M. A., Parsadanian, M., Taylor, J. W., Harmony, J. A. K., Bales, K. R., et al. (2002). Clusterin promotes amyloid plaque formation and is critical

for neuritic toxicity in a mouse model of Alzheimer's disease. *Proceedings of the National Academy of Sciences of the United States of America, 99*(16), 10843-10848.

Deming, Y., Xia, J., Cai, Y. F., Lord, J., Holmans, P., Bertelsen, S., et al. (2016). A potential endophenotype for Alzheimer's disease: cerebrospinal fluid clusterin. *Neurobiology of Aging, 37,* 208.e1-208.e9.

Desikan, R. S., Thompson, W. K., Holland, D., Hess, C. P., Brewer, J. B., Zetterberg, H., et al. (2014). The Role of Clusterin in Amyloid-beta-Associated Neurodegeneration. *Jama Neurology, 71*(2), 180-187.

Desilva, H. V., Harmony, J. A. K., Stuart, W. D., Gil, C. M., & Robbins, J. (1990). Apolipoprotein-j – structure and tissue distribution. *Biochemistry, 29*(22), 5380-5389.

Dourlen, P., Fernandez-Gomez, F. J., Dupont, C., Grenier-Boley, B., Bellenguez, C., Obriot, H., et al. (2017). Functional screening of Alzheimer risk loci identifies PTK2B as an in vivo modulator and early marker of Tau pathology. *Molecular Psychiatry, 22*(6), 874-883.

Dukic, L., Simundic, A. M., Martinic-Popovic, I., Kackov, S., Diamandis, A., Begcevic, I., et al. (2016). The role of human kallikrein 6, clusterin and adiponectin as potential blood biomarkers of dementia. *Clinical Biochemistry, 49*(3), 213-218.

Ertekin-Taner, N. (2007). Genetics of Alzheimer's Disease: A centennial review. *Neurologic Clinics, 25*(3), 611-+.

Farrer, L. A., Cupples, L. A., Haines, J. L., Hyman, B., Kukull, W. A., Mayeux, R., et al. (1997). Effects of age, sex, and ethnicity on the association between apolipoprotein E genotype and Alzheimer disease – A meta-analysis. *Jama-Journal of the American Medical Association, 278*(16), 1349-1356.

Fryer, J. D., & Holtzman, D. M. (2005). The bad seed in Alzheimer's disease. *Neuron, 47*(2), 167-168.

Fu, Y. X., Lai, Y. R., Wang, Q. J., Liu, X. Y., He, W. P., Zhang, H. H., et al. (2013). Overexpression of clusterin promotes angiogenesis via the vascular endothelial growth factor in primary ovarian cancer. *Molecular Medicine Reports, 7*(6), 1726-1732.

Fusaki, N., Ban, H., Nishiyama, A., Saeki, K., & Hasegawa, M. (2009). Efficient induction of transgene-free human pluripotent stem cells using a vector based on

Sendai virus, an RNA virus that does not integrate into the host genome. *Proceedings of the Japan Academy Series B-Physical and Biological Sciences, 85*(8), 348-362.

Gelissen, I. C., Hochgrebe, T., Wilson, M. R., Easterbrook-Smith, S. B., Jessup, W., Dean, R. T., et al. (1998). Apolipoprotein J (clusterin) induces cholesterol export from macrophage-foam cells: a potential anti-atherogenic function? *Biochemical Journal, 331*, 231-237.

Geraghty, N. J., Satapathy, S., Kelly, M., Cheng, F., Lee, A., & Wilson, M. R. (2021). Expanding the family of extracellular chaperones: Identification of human plasma proteins with chaperone activity. *Protein Science, 30*(11), 2272-2286.

Haight, T., Bryan, R. N., Meirelles, O., Tracy, R., Fornage, M., Richard, M., et al. (2018). Associations of plasma clusterin and Alzheimer's disease-related MRI markers in adults at mid-life: The CARDIA Brain MRI sub-study. *Plos One, 13*(1), e0190478.

Hakobyan, S., Harding, K., Aiyaz, M., Hye, A., Dobson, R., Baird, A., et al. (2016). Complement Biomarkers as Predictors of Disease Progression in Alzheimer's Disease. *Journal of Alzheimers Disease, 54*(2), 707-716.

Hardy, J., Guerreiro, R., & Lovestone, S. (2011). Clusterin as an Alzheimer Biomarker. *Archives of Neurology, 68*(11), 1459-1460.

Hardy, J., & Selkoe, D. J. (2002). Medicine – The amyloid hypothesis of Alzheimer's disease: Progress and problems on the road to therapeutics. *Science, 297*(5580), 353-356.

Harold, D., Abraham, R., Hollingworth, P., Sims, R., Gerrish, A., Hamshere, M. L., et al. (2009). Genome-wide association study identifies variants at CLU and PICALM associated with Alzheimer's disease. *Nature Genetics, 41*(10), 1088-U1061.

Herring, S. K., Moon, H. J., Rawal, P., Chhibber, A., & Zhao, L. Q. (2019). Brain clusterin protein isoforms and mitochondrial localization. *Elife, 8,* e48255.

Hollander, Z., Lazarova, M., Lam, K. K. Y., Ignaszewski, A., Oudit, G. Y., Dyck, J. R. B., et al. (2014). Proteomic biomarkers of recovered heart function. *European Journal of Heart Failure, 16*(5), 551-559.

Hollingworth, P., Harold, D., Sims, R., Gerrish, A., Lambert, J. C., Carrasquillo, M. M., et al. (2011). Common variants at ABCA7, MS4A6A/MS4A4E, EPHA1, CD33 and CD2AP are associated with Alzheimer's disease. *Nature Genetics, 43*(5), 429-+.

Hsu, J. L., Lee, W. J., Liao, Y. C., Wang, S. J., & Fuh, J. L. (2017). The clinical significance of plasma clusterin and A beta in the longitudinal follow-up of patients with Alzheimer's disease. *Alzheimers Research & Therapy, 9*(1), 91.

Jack, C. R., Bennett, D. A., Blennow, K., Carrillo, M. C., Dunn, B., Haeberlein, S. B., et al. (2018). NIA-AA Research Framework: Toward a biological definition of Alzheimer's disease. *Alzheimers & Dementia, 14*(4), 535-562.

Jack, C. R., & Holtzman, D. M. (2013). Biomarker Modeling of Alzheimer's Disease. *Neuron, 80*(6), 1347-1358.

Jackson, R. J., Rose, J., Tulloch, J., Henstridge, C., Smith, C., & Spires-Jones, T. L. (2019). Clusterin accumulates in synapses in Alzheimer's disease and is increased in apolipoprotein E4 carriers. *Brain Communications, 1*(1), fcz003.

Jansen, I. E., Savage, J. E., Watanabe, K., Bryois, J., Williams, D. M., Steinberg, S., et al. (2019). Genome-wide meta-analysis identifies new loci and functional pathways influencing Alzheimer's disease risk. *Nature Genetics, 51*(3), 404-+.

Jenne, D. E., & Tschopp, J. (1989). Molecular-structure and functional-characterization of a human-complement cytolysis inhibitor found in blood and seminal plasma – identity to 123ulphated glycoprotein-2, a constituent of rat testis fluid. *Proceedings of the National Academy of Sciences of the United States of America, 86*(18), 7123-7127.

Jervis, G. A. (1948). Early senile dementia in mongoloid idiocy. *American Journal of Psychiatry, 105*(2), 102-+.

Jongbloed, W., Herrebout, M. A. C., Blankenstein, M. A., & Veerhuis, R. (2014). Quantification of clusterin in paired cerebrospinal fluid and plasma samples. *Annals of Clinical Biochemistry, 51*(5), 557-567.

Jongbloed, W., van Dijk, K. D., Mulder, S. D., van de Berg, W. D. J., Blankenstein, M. A., van der Flier, W., et al. (2015). Clusterin Levels in Plasma Predict Cognitive Decline

and Progression to Alzheimer's Disease. *Journal of Alzheimers Disease, 46*(4), 1103-1110.

T.C.W., J., Wang, M. H., Pimenova, A. A., Bowles, K. R., Hartley, B. J., Lacin, E., et al. (2017). An Efficient Platform for Astrocyte Differentiation from Human Induced Pluripotent Stem Cells. *Stem Cell Reports, 9*(2), 600-614.

Jun, G., Ibrahim-Verbaas, C. A., Vronskaya, M., Lambert, J. C., Chung, J., Naj, A., et al. (2016). A novel Alzheimer disease locus located near the gene encoding tau protein. *Molecular Psychiatry, 21*(1), 108-117.

Jun, G., Naj, A. C., Beecham, G. W., Wang, L. S., Buros, J., Gallins, P. J., et al. (2010). Meta-analysis Confirms CR1, CLU, and PICALM as Alzheimer Disease Risk Loci and Reveals Interactions With APOE Genotypes. *Archives of Neurology, 67*(12), 1473-1484.

Jun, H. O., Kim, D. H., Lee, S. W., Lee, H. S., Seo, J. H., Kim, J. H., et al. (2011). Clusterin protects H9c2 cardiomyocytes from oxidative stress-induced apoptosis via Akt/GSK-3 beta signaling pathway. *Experimental and Molecular Medicine, 43*(1), 53-61.

Kang, S. S., Kurti, A., Wojtas, A., Baker, K. E., Liu, C. C., Kanekiyo, T., et al. (2016). Identification of plexin A4 as a novel clusterin receptor links two Alzheimer's disease risk genes. *Human Molecular Genetics, 25*(16), 3467-3475.

Kato, S., Gondo, T., Hoshii, Y., Takahashi, M., Yamada, M., & Ishihara, T. (1998). Confocal observation of senile plaques in Alzheimer's disease: Senile plaque morphology and relationship between senile plaques and astrocytes. *Pathology International, 48*(5), 332-340.

Kauwe, J. S. K., Bailey, M. H., Ridge, P. G., Perry, R., Wadsworth, M. E., Hoyt, K. L., et al. (2014). Genome-Wide Association Study of CSF Levels of 59 Alzheimer's Disease Candidate Proteins: Significant Associations with Proteins Involved in Amyloid Processing and Inflammation. *Plos Genetics, 10*(10), e1004758.

Khakh, B.S., Sofroniew, M.V. (2015) Diversity of astrocyte functions and phenotypes in neural circuits. *Nat Neurosci, 18*, 942– 952

Kohler, G., & Milstein, C. (1975). Continuous cultures of fused cells secreting antibody of predefined specificity. *Nature, 256*(5517), 495-497.

Krencik, R., & Zhang, S. C. (2011). Directed differentiation of functional astroglial subtypes from human pluripotent stem cells. *Nature Protocols, 6*(11), 1710-1717.

Kunkle, B. W., Grenier-Boley, B., Sims, R., Bis, J. C., Damotte, V., Naj, A. C., et al. (2019). Genetic meta-analysis of diagnosed Alzheimer's disease identifies new risk loci and implicates A beta, tau, immunity and lipid processing. *Nature Genetics, 51*(3), 414-+.

Lambert, J. C., Heath, S., Even, G., Campion, D., Sleegers, K., Hiltunen, M., et al. (2009). Genome-wide association study identifies variants at CLU and CR1 associated with Alzheimer's disease. *Nature Genetics, 41*(10), 1094-U1068.

Lambert, J. C., Ibrahim-Verbaas, C. A., Harold, D., Naj, A. C., Sims, R., Bellenguez, C., et al. (2013). Meta-analysis of 74,046 individuals identifies 11 new susceptibility loci for Alzheimer's disease. *Nature Genetics, 45*(12), 1452-U1206.

Leskov, K. S., Klokov, D. Y., Li, J., Kinsella, T. J., & Boothman, D. A. (2003). Synthesis and functional analyses of nuclear clusterin, a cell death protein. *Journal of Biological Chemistry, 278*(13), 11590-11600.

Levtova, N., Healy, L. M., Marysol, C., Gonczi, C., Stopnicki, B., Blain, M., et al. (2017). Comparative morphology and phagocytic capacity of primary human adult microglia with time-lapse imaging. *Journal of Neuroimmunology, 310*, 143-149.

Li, K. Y., Li, J. T., Zheng, J. L., & Qin, S. (2019). Reactive Astrocytes in Neurodegenerative Diseases. *Aging and Disease, 10*(3), 664-675.

Li, Z. H., Shue, F., Zhao, N., Shinohara, M., & Bu, G. J. (2020). APOE2: protective mechanism and therapeutic implications for Alzheimer's disease. *Molecular Neurodegeneration, 15*(1), 63.

Liao, P. C., Yu, L., Kuo, C. C., Lin, C. J., & Kuo, Y. M. (2007). Proteomics analysis of plasma for potential biomarkers in the diagnosis of Alzheimer's disease. *Proteomics Clinical Applications, 1*(5), 506-512.

Lidstrom, A. M., Bogdanovic, N., Hesse, C., Volkman, I., Davidsson, P., & Blennow, K. (1998). Clusterin (apolipoprotein J) protein levels are increased in hippocampus and in frontal cortex in Alzheimer's disease. *Experimental Neurology, 154*(2), 511-521.

Lidstrom, A. M., Hesse, C., Rosengren, L., Fredman, P., Davidsson, P., & Blennow, K. (2001). Normal levels of clusterin in cerebrospinal fluid in Alzheimer's disease, and no change after acute ischemic stroke. *Journal of Alzheimers Disease, 3*(5), 435-442.

Lin, Y. L., Chen, S. Y., Lai, L. C., Chen, J. H., Yang, S. Y., Huang, Y. L., et al. (2012). Genetic polymorphisms of clusterin gene are associated with a decreased risk of Alzheimer's disease. *European Journal of Epidemiology, 27*(1), 73-75.

Ling, I. F., Bhongsatiern, J., Simpson, J. F., Fardo, D. W., & Estus, S. (2012). Genetics of Clusterin Isoform Expression and Alzheimer's Disease Risk. *Plos One, 7*(4), e33923.

Liu, C. C., Yamazaki, Y., Heckman, M. G., Martens, Y. A., Jia, L., Yamazaki, A., et al. (2020). Tau and apolipoprotein E modulate cerebrovascular tight junction integrity independent of cerebral amyloid angiopathy in Alzheimer's disease. *Alzheimers & Dementia, 16*(10), 1372-1383.

Liu, Y., Han, S. S. W., Wu, Y. Y., Tuohy, T. M. F., Xue, H. P., Cai, J. L., et al. (2004). CD44 expression identifies astrocyte-restricted precursor cells. *Developmental Biology, 276*(1), 31-46.

Liu, Z. Q., Chao, J. F., Wang, C., Sun, G. H., Roeth, D., Liu, W., et al. (2023). Astrocytic response mediated by the CLU risk allele inhibits OPC proliferation and myelination in a human iPSC model. *Cell Reports, 42*(8), 112841.

Lööv, C., Mitchell, C. H., Simonsson, M., & Erlandsson, A. (2015). Slow degradation in phagocytic astrocytes can be enhanced by lysosomal acidification. *Glia, 63*(11), 1997-2009.

Luo, H., Wu, X.-Q., Zhao, M., Wang, Q., Jiang, G.-P., Cai, W.-J., Luo, M.-Y. (2017). Expression of vimentin and glial fibrillary acidic protein in central nervous system development of rats. *Asian Pac. J. Trop. Med. 10*:1185–1189.

Mahley, R. W., & Rall, S. C. (2000). Apolipoprotein E: Far more than a lipid transport protein. *Annual Review of Genomics and Human Genetics, 1*, 507-537.

Mahmoud, S. A., Lowery-Nordberg, M., Chen, H., Thurmon, T., Ursin, S., & Bahna, S. L. (2005). Immune defects in subjects with dysmorphic disorders. *Allergy and Asthma Proceedings, 26*(5), 373-381.

Marioni, R. E., Harris, S. E., Zhang, Q., McRae, A. F., Hagenaars, S. P., Hill, W. D., et al. (2018). GWAS on family history of Alzheimer's disease. *Translational Psychiatry, 8*(1), 99.

Martin-Rehrmann, M. D., Hoe, H. S., Capuani, E. M., & Rebeck, G. W. (2005). Association of apolipoprotein J-positive beta-amyloid plaques with dystrophic neurites in Alzheimer's disease brain. *Neurotoxicity Research, 7*(3), 231-241.

McCarron, M., McCallion, P., Reilly, E., Dunne, P., Carroll, R., & Mulryan, N. (2017). A prospective 20-year longitudinal follow-up of dementia in persons with Down syndrome. *Journal of Intellectual Disability Research, 61*(9), 843-852.

McGeer, P. L., Kawamata, T., & Walker, D. G. (1992). Distribution of clusterin in alzheimer brain-tissue. *Brain Research, 579*(2), 337-341.

McKhann, G. M., Knopman, D. S., Chertkow, H., Hyman, B. T., Jack, C. R., Kawas, C. H., et al. (2011). The diagnosis of dementia due to Alzheimer's disease: Recommendations from the National Institute on Aging-Alzheimer's Association workgroups on diagnostic guidelines for Alzheimer's disease. *Alzheimers & Dementia, 7*(3), 263-269.

Mengel-From, J., Christensen, K., McGue, M., & Christiansen, L. (2011). Genetic variations in the CLU and PICALM genes are associated with cognitive function in the oldest old. *Neurobiology of Aging, 32*(3), 554.e7–554.e11.

Miners, J. S., Clarke, P., & Love, S. (2017). Clusterin levels are increased in Alzheimer's disease and influence the regional distribution of A beta. *Brain Pathology, 27*(3), 305-313.

Monterey, M. D., Wei, H. C., Wu, X. Z., & Wu, J. Q. (2021). The Many Faces of Astrocytes in Alzheimer's Disease. *Frontiers in Neurology, 12,* 619626.

Mullan, G. M., McEneny, J., Fuchs, M., McMaster, C., Todd, S., McGuinness, B., et al. (2013). Plasma Clusterin Levels and the rs11136000 Genotype in Individuals with

Mild Cognitive Impairment and Alzheimer's Disease. *Current Alzheimer Research, 10*(9), 973-978.

Murphy, B. F., Kirszbaum, L., Walker, I. D., & Dapice, A. J. F. (1988). SP-40,40, a newly identified normal human-serum protein found in the sc5b-9 complex of complement and in the immune deposits in glomerulonephritis. *Journal of Clinical Investigation, 81*(6), 1858-1864.

Naj, A. C., Jun, G., Beecham, G. W., Wang, L. S., Vardarajan, B. N., Buros, J., et al. (2011). Common variants at MS4A4/MS4A6E, CD2AP, CD33 and EPHA1 are associated with late-onset Alzheimer's disease. *Nature Genetics, 43*(5), 436-+.

Narayan, P., Orte, A., Clarke, R. W., Bolognesi, B., Hook, S., Ganzinger, K. A., et al. (2012). The extracellular chaperone clusterin sequesters oligomeric forms of the amyloid-beta(1-40) peptide. *Nature Structural & Molecular Biology, 19*(1), 79-U97.

Nichols, E., Steinmetz, J. D., Vollset, S. E., Fukutaki, K., Chalek, J., Abd-Allah, F., et al. (2022). Estimation of the global prevalence of dementia in 2019 and forecasted prevalence in 2050: an analysis for the Global Burden of Disease 2019. *Lancet Public Health, 7*(2), E105-E125.

Nilselid, A. M., Davidsson, P., Nagga, K., Andreasen, N., Fredman, P., & Blennow, K. (2006). Clusterin in cerebrospinal fluid: Analysis of carbohydrates and quantification of native and glycosylated forms. *Neurochemistry International, 48*(8), 718-728.

Nott, A., Holtman, I. R., Coufal, N. G., Schlachetzki, J. C. M., Yu, M., Hu, R., et al. (2019). Brain cell type-specific enhancer-promoter interactome maps and disease-risk association. *Science, 366*(6469), 1134-+.

Nuutinen, T., Huuskonen, J., Suuronen, T., Ojala, J., Miettinen, R., & Salminen, A. (2007). Amyloid-beta 1-42 induced endocytosis and clusterin/apoJ protein accumulation in cultured human astrocytes. *Neurochemistry International, 50*(3), 540-547.

Padhy, B., Hayat, B., Nanda, G. G., Mohanty, P. P., & Alone, D. P. (2017). Pseudoexfoliation and Alzheimer's associated CLU risk variant, rs2279590, lies within an enhancer element and regulates CLU, EPHX2 and PTK2B gene expression. *Human Molecular Genetics, 26*(22), 4519-4529.

Palmqvist, S., Tideman, P., Cullen, N., Zetterberg, H., Blennow, K., Dage, J. L., et al. (2021). Prediction of future Alzheimer's disease dementia using plasma phospho-tau combined with other accessible measures. *Nature Medicine, 27*(6), 1034-+.

Peng, M., Deng, J., Zhou, S. C., Tao, T., Su, Q. L., Yang, X., et al. (2019). The role of Clusterin in cancer metastasis. *Cancer Management and Research, 11*, 2405-2414.

Perriot, S., Mathias, A., Perriard, G., Canales, M., Jonkmans, N., Merienne, N., et al. (2018). Human Induced Pluripotent Stem Cell-Derived Astrocytes Are Differentially Activated by Multiple Sclerosis-Associated Cytokines. *Stem Cell Reports, 11*(5), 1199-1210.

Poon, S., Rybchyn, M. S., Easterbrook-Smith, S. B., Carver, J. A., Pankhurst, G. J., & Wilson, M. R. (2002). Mildly acidic pH activates the extracellular molecular chaperone clusterin. *Journal of Biological Chemistry, 277*(42), 39532-39540.

Potokar, M., Morita, M., Wiche, G., & Jorgacevski, J. (2020). The Diversity of Intermediate Filaments in Astrocytes. *Cells, 9*(7), 1604.

Prochnow, H., Gollan, R., Rohne, P., Hassemer, M., Koch-Brandt, C., & Baiersdorfer, M. (2013). Non-Secreted Clusterin Isoforms Are Translated in Rare Amounts from Distinct Human mRNA Variants and Do Not Affect Bax-Mediated Apoptosis or the NF-kappa B Signaling Pathway. *Plos One, 8*(9), e75303.

Qi, X. M., Wang, C., Chu, X. K., Li, G., & Ma, J. F. (2018). Intraventricular infusion of clusterin ameliorated cognition and pathology in Tg6799 model of Alzheimer's disease. *Bmc Neuroscience, 19*(1), 2.

Redondo, M., Tellez, T., Roldan, M. J., Serrano, A., Garcia-Aranda, M., Gleave, M. E., et al. (2007). Anticlusterin treatment of breast cancer cells increases the sensitivities of chemotherapy and tamoxifen and counteracts the inhibitory action of dexamethasone on chemotherapy-induced cytotoxicity. *Breast Cancer Research, 9*(6), R86.

Regan, M.R., Huang, Y., Kim, Y.S., Dykes-Hoberg M.I., Jin L., Watkins, A.M., Bergles, D.E., Rothstein J.D. (2007). Variations in Promoter Activity Reveal a Differential Expression and Physiology of Glutamate Transporters by Glia in the Developing and Mature CNS. *J. Neurosci, 27*:6607–6619.

Ricklin, D., & Lambris, J. D. (2013). Complement in Immune and Inflammatory Disorders: Pathophysiological Mechanisms. *Journal of Immunology, 190*(8), 3831-3838.

Robbins, J. P., Perfect, L., Ribe, E. M., Maresca, M., Dangla-Valls, A., Foster, E. M., et al. (2018). Clusterin Is Required for β-Amyloid Toxicity in Human iPSC-Derived Neurons. *Frontiers in Neuroscience, 12,* 504.

Rohne, P., Prochnow, H., Wolf, S., Renner, B., & Koch-Brandt, C. (2014). The Chaperone Activity of Clusterin is Dependent on Glycosylation and Redox Environment. *Cellular Physiology and Biochemistry, 34*(5), 1626-1639.

Roshchupkin, G. V., Adams, H. H., van der Lee, S. J., Vernooij, M. W., van Duijn, C. M., Uitterlinden, A. G., et al. (2016). Fine-mapping the effects of Alzheimer's disease risk loci on brain morphology. *Neurobiology of Aging, 48*, 204-211.

Satapathy, S., Dabbs, R. A., & Wilson, M. R. (2020). Rapid high-yield expression and purification of fully post-translationally modified recombinant clusterin and mutants. *Scientific Reports, 10*(1), 14243.

Schurmann, B., Wiese, B., Bickel, H., Weyerer, S., Riedel-Heller, S. G., Pentzek, M., et al. (2011). Association of the Alzheimer's Disease Clusterin Risk Allele with Plasma Clusterin Concentration. *Journal of Alzheimers Disease, 25*(3), 421-424.

Schwartzentruber, J., Cooper, S., Liu, J. Z., Barrio-Hernandez, I., Bello, E., Kumasaka, N., et al. (2021). Genome-wide meta-analysis, fine-mapping and integrative prioritization implicate new Alzheimer's disease risk genes. *Nature Genetics, 53*(3), 392-+.

Serio, A., Bilican, B., Barmada, S. J., Ando, D. M., Zhao, C., Siller, R., et al. (2013). Astrocyte pathology and the absence of non-cell autonomy in an induced pluripotent stem cell model of TDP-43 proteinopathy. *Proceedings of the National Academy of Sciences of the United States of America, 110*(12), 4697-4702.

Seshadri, S., Fitzpatrick, A. L., Ikram, M. A., DeStefano, A. L., Gudnason, V., Boada, M., et al. (2010). Genome-wide Analysis of Genetic Loci Associated With Alzheimer Disease. *Jama-Journal of the American Medical Association, 303*(18), 1832-1840.

Sevigny, J., Chiao, P., Bussiere, T., Weinreb, P. H., Williams, L., Maier, M., et al. (2016). The antibody aducanumab reduces Aβ plaques in Alzheimer's disease. *Nature, 537*(7618), 50-56.

Shaltouki, A., Peng, J., Liu, Q. Y., Rao, M. S., & Zeng, X. M. (2013). Efficient Generation of Astrocytes from Human Pluripotent Stem Cells in Defined Conditions. *Stem Cells, 31*(5), 941-952.

Shen, L., Thompson, P. M., Potkin, S. G., Bertram, L., Farrer, L. A., Foroud, T. M., et al. (2014). Genetic analysis of quantitative phenotypes in AD and MCI: imaging, cognition and biomarkers. *Brain Imaging and Behavior, 8*(2), 183-207.

Shepherd, C. E., Affleck, A. J., Bahar, A. Y., Carew-Jones, F., & Halliday, G. M. (2020). Intracellular and secreted forms of clusterin are elevated early in Alzheimer's disease and associate with both A beta and tau pathology. *Neurobiology of Aging, 89*, 129-131.

Shi, X. R., Xie, B. J., Xing, Y., & Tang, Y. (2019). Plasma Clusterin as a Potential Biomarker for Alzheimer's Disease-A Systematic Review and Meta-analysis. *Current Alzheimer Research, 16*(11), 1018-1027.

Shi, Y. C., Kirwan, P., & Livesey, F. J. (2012). Directed differentiation of human pluripotent stem cells to cerebral cortex neurons and neural networks. *Nature Protocols, 7*(10), 1836-1846.

Sihlbom, C., Davidsson, P., Sjogren, M., Wahlund, L. O., & Nilsson, C. L. (2008). Structural and quantitative comparison of cerebrospinal fluid glycoproteins in Alzheimer's disease patients and healthy individuals. *Neurochemical Research, 33*(7), 1332-1340.

Silajdzic, E., Minthon, L., Bjorkqvist, M., & Hansson, O. (2012). No Diagnostic Value of Plasma Clusterin in Alzheimer's Disease. *Plos One, 7*(11), e50237.

Sims, R., Hill, M., & Williams, J. (2020). The multiplex model of the genetics of Alzheimer's disease. *Nature Neuroscience, 23*(3), 311-322.

Sollvander, S., Nikitidou, E., Brolin, R., Soderberg, L., Sehlin, D., Lannfelt, L., et al. (2016). Accumulation of amyloid-beta by astrocytes result in enlarged endosomes and microvesicle-induced apoptosis of neurons. *Molecular Neurodegeneration, 11*(1), 38.

Startin, C. M., D'Souza, H., Ball, G., Hamburg, S., Hithersay, R., Hughes, K. M. O., et al. (2020). Health comorbidities and cognitive abilities across the lifespan in Down syndrome. *Journal of Neurodevelopmental Disorders, 12*(1), 4.

Steiner, H., & Haass, C. (2000). Intramembrane proteolysis by presenilins. *Nature Reviews Molecular Cell Biology, 1*(3), 217-224.

Stevenson-Hoare, J., Heslegrave, A., Leonenko, G., Fathalla, D., Bellou, E., Luckcuck, L., Marshall, R., Sims, R., Morgan, B. P., Hardy, J., de Strooper, B., Williams, J., Zetterberg, H., & Escott-Price, V. (2023). Plasma biomarkers and genetics in the diagnosis and prediction of Alzheimer's disease. *Brain : a journal of neurology*, *146*(2), 690–699.

Stewart, E. M., Aquilina, J. A., Easterbrook-Smith, S. B., Murphy-Durland, D., Jacobsen, C., Moestrup, S., et al. (2007). Effects of glycosylation on the structure and function of the extracellular chaperone clusterin. *Biochemistry, 46*(5), 1412-1422.

Stoltzner, S. E., Grenfell, T. J., Mori, C., Wisniewski, K. E., Wisniewski, T. M., Selkoe, D. J., et al. (2000). Temporal accrual of complement proteins in amyloid plaques in Down's syndrome with Alzheimer's disease. *American Journal of Pathology, 156*(2), 489-499.

Takahashi, K., & Yamanaka, S. (2006). Induction of pluripotent stem cells from mouse embryonic and adult fibroblast cultures by defined factors. *Cell, 126*(4), 663-676.

Tan, L., Wang, H. F., Tan, M. S., Tan, C. C., Zhu, X. C., Miao, D., et al. (2016). Effect of CLU genetic variants on cerebrospinal fluid and neuroimaging markers in healthy, mild cognitive impairment and Alzheimer's disease cohorts. *Scientific Reports, 6,* 26027.

Tan, M. S., Yang, Y. X., Xu, W., Wang, H. F., Tan, L., Zuo, C. T., et al. (2021). Associations of Alzheimer's disease risk variants with gene expression, amyloidosis, tauopathy, and neurodegeneration. *Alzheimers Research & Therapy, 13*(1), 15.

Thambisetty, M., An, Y., Kinsey, A., Koka, D., Saleem, M., Guntert, A., et al. (2012). Plasma clusterin concentration is associated with longitudinal brain atrophy in mild cognitive impairment. *Neuroimage, 59*(1), 212-217.

Thambisetty, M., Simmons, A., Velayudhan, L., Hye, A., Campbell, J., Zhang, Y., et al. (2010). Association of Plasma Clusterin Concentration With Severity, Pathology, and Progression in Alzheimer Disease. *Archives of General Psychiatry, 67*(7), 739-748.

Tian, L. L., Al-Nusaif, M., Chen, X., Li, S., & Le, W. D. (2022). Roles of Transcription Factors in the Development and Reprogramming of the Dopaminergic Neurons. *International Journal of Molecular Sciences, 23*(2), 845.

van Dyck, C. H., Swanson, C. J., Aisen, P., Bateman, R. J., Chen, C., Gee, M., et al. (2023). Lecanemab in Early Alzheimer's Disease. *New England Journal of Medicine, 388*(1), 9-21.

Verbeek, M. M., Otte-Holler, I., Veerhuis, R., Ruiter, D. J., & De Waal, R. M. W. (1998). Distribution of A beta-associated proteins in cerebrovascular amyloid of Alzheimer's disease. *Acta Neuropathologica, 96*(6), 628-636.

Veteleanu, A., Pape, S., Davies, K., Kodosaki, E., Hye, A., Zelek, W. M., et al. (2023). Complement dysregulation and Alzheimer's disease in Down syndrome. *Alzheimers & Dementia, 19*(4), 1383-1392.

Vishnu, V. Y., Modi, M., Sharma, S., Mohanty, M., Goyal, M. K., Lal, V., et al. (2016). Role of Plasma Clusterin in Alzheimer's Disease-A Pilot Study in a Tertiary Hospital in Northern India. *Plos One, 11*(11), e0166369.

von Bartheld, C. S., Bahney, J., & Herculano-Houzel, S. (2016). The search for true numbers of neurons and glial cells in the human brain: A review of 150 years of cell counting. *Journal of Comparative Neurology, 524*(18), 3865-3895.

Weinstein, G., Beiser, A. S., Preis, S. R., Courchesne, P., Chouraki, V., Levy, D., et al. (2016). Plasma clusterin levels and risk of dementia, Alzheimer's disease, and stroke. *Alzheimers & Dementia, 3,* 103-9.

Wiseman, F.K., Pulford, L.J., Barkus, C., Liao, F., Portelius, E., Webb, R. et al. (2018). Trisomy of human chromosome 21 enhances amyloid-beta deposition independently of an extra copy of APP. *Brain, 141*, 2457–74.

Wightman, D. P., Jansen, I. E., Savage, J. E., Shadrin, A. A., Bahrami, S., Holland, D., et al. (2021). A genome-wide association study with 1,126,563 individuals identifies new risk loci for Alzheimer's disease. *Nature Genetics, 53*(9), 1276-+.

Wilson, M. R., & Easterbrooksmith, S. B. (1992). Clusterin binds by a multivalent mechanism to the Fc and Fab regions of IgG. *Biochimica Et Biophysica Acta, 1159*(3), 319-326.

Wojtas, A. M., Carlomagno, Y., Sens, J. P., Kang, S. S., Jensen, T. D., Kurti, A., et al. (2020). Clusterin ameliorates tau pathology in vivo by inhibiting fibril formation. *Acta Neuropathologica Communications, 8*(1), 210.

Wojtas, A. M., Sens, J. P., Kang, S. S., Baker, K. E., Berry, T. J., Kurti, A., et al. (2020). Astrocyte-derived clusterin suppresses amyloid formation in vivo. *Molecular Neurodegeneration, 15*(1), 71.

Wong, P., Pineault, J., Lakins, J., Putilina, T., Chader, G., & Tenniswood, M. (1993). Molecular characterization of the human trpm-2/clusterin gene - positional exclusion as a potential candidate gene for rp1. *Investigative Ophthalmology & Visual Science, 34*(4), 1460-1460.

Xing, Y. Y., Yu, J. T., Cui, W. Z., Zhong, X. L., Wu, Z. C., Zhang, Q., et al. (2012). Blood Clusterin Levels, rs9331888 Polymorphism, and the Risk of Alzheimer's Disease. *Journal of Alzheimers Disease, 29*(3), 515-519.

Yerbury, J. J., Poon, S., Meehan, S., Thompson, B., Kumita, J. R., Dobson, C. M., et al. (2007). The extracellular chaperone clusterin influences amyloid formation and toxicity by interacting with prefibrillar structures. *Faseb Journal, 21*(10), 2312-2322.

Zhao, N., Ren, Y. X., Yamazaki, Y., Qiao, W. H., Li, F. Y., Felton, L. M., et al. (2020). Alzheimer's Risk Factors Age, APOE Genotype, and Sex Drive Distinct Molecular Pathways. *Neuron, 106*(5), 727-+.

Zhou, Y., Hayashi, I., Wong, J., Tugusheva, K., Renger, J. J., & Zerbinatti, C. (2014). Intracellular Clusterin Interacts with Brain Isoforms of the Bridging Integrator 1 and with the Microtubule-Associated Protein Tau in Alzheimer's Disease. *Plos One, 9*(7), e103187.

Zolochevska, O., Bjorklund, N., Woltjer, R., Wiktorowicz, J. E., & Taglialatela, G. (2018). Postsynaptic Proteome of Non-Demented Individuals with Alzheimer's Disease Neuropathology. *Journal of Alzheimers Disease, 65*(2), 659-682.

Zwain, I. H., Grima, J., & Cheng, C. Y. (1994). Regulation of clusterin secretion and messenger-rna expression in astrocytes by cytokines. *Molecular and Cellular Neuroscience, 5*(3), 229-237.